Calhoun
Institutional Archive of the Naval Postgraduate School

Calhoun: The NPS Institutional Archive

DSpace Repository

Theses and Dissertations 1. Thesis and Dissertation Collection, all items

2004-06

Advanced thermophotovoltaic cells modeling, optimized for use in radioisotope thermoelectric generators (RTGS) for Mars and deep space missions

Davenport, Bradley P.

Monterey California. Naval Postgraduate School

http://hdl.handle.net/10945/1170

This publication is a work of the U.S. Government as defined in Title 17, United States Code, Section 101. Copyright protection is not available for this work in the United States.

Downloaded from NPS Archive: Calhoun

DUDLEY
KNOX
LIBRARY

Calhoun is the Naval Postgraduate School's public access digital repository for research materials and institutional publications created by the NPS community. Calhoun is named for Professor of Mathematics Guy K. Calhoun, NPS's first appointed -- and published -- scholarly author.

Dudley Knox Library / Naval Postgraduate School
411 Dyer Road / 1 University Circle
Monterey, California USA 93943

http://www.nps.edu/library

NAVAL POSTGRADUATE SCHOOL

MONTEREY, CALIFORNIA

THESIS

ADVANCED THERMOPHOTOVOLTAIC CELLS MODELING, OPTIMIZED FOR USE IN RADIOISOTOPE THERMOELECTRIC GENERATORS (RTGS) FOR MARS AND DEEP SPACE MISSIONS

by

Bradley P. Davenport

June 2004

Thesis Advisor:	Sherif Michael
Second Reader:	G. Karunasiri

Approved for public release; distribution is unlimited.

THIS PAGE INTENTIONALLY LEFT BLANK

REPORT DOCUMENTATION PAGE	*Form Approved OMB No. 0704-0188*

Public reporting burden for this collection of information is estimated to average 1 hour per response, including the time for reviewing instruction, searching existing data sources, gathering and maintaining the data needed, and completing and reviewing the collection of information. Send comments regarding this burden estimate or any other aspect of this collection of information, including suggestions for reducing this burden, to Washington headquarters Services, Directorate for Information Operations and Reports, 1215 Jefferson Davis Highway, Suite 1204, Arlington, VA 22202-4302, and to the Office of Management and Budget, Paperwork Reduction Project (0704-0188) Washington DC 20503.

1. AGENCY USE ONLY ***(Leave blank)***	**2. REPORT DATE** June 2003	**3. REPORT TYPE AND DATES COVERED** Master's Thesis

4. TITLE AND SUBTITLE: Advanced Thermophotovoltaic Cells Modeling, Optimized for Use in Radioisotope Thermoelectric Generators (RTGs) for Mars and Deep Space Missions	**5. FUNDING NUMBERS**
6. AUTHOR(S) Bradley P. Davenport	
7. PERFORMING ORGANIZATION NAME(S) AND ADDRESS(ES) Naval Postgraduate School Monterey, CA 93943-5000	**8. PERFORMING ORGANIZATION REPORT NUMBER**
9. SPONSORING /MONITORING AGENCY NAME(S) AND ADDRESS(ES) N/A	**10. SPONSORING/MONITORING AGENCY REPORT NUMBER**

11. SUPPLEMENTARY NOTES The views expressed in this thesis are those of the author and do not reflect the official policy or position of the Department of Defense or the U.S. Government.

12a. DISTRIBUTION / AVAILABILITY STATEMENT Approved for public release; distribution is unlimited.	**12b. DISTRIBUTION CODE**

13. ABSTRACT (maximum 200 words)

Thermophotovoltaic cells are a good candidate for use in high efficiency radioisotope thermoelectric generator (RTG) power devices for deep space missions. This thesis examines the use of Silvaco Virtual Wafer Fabrication Software as a tool for designing and optimizing TPV cells for different possible spectra. It gives results for GaSb and InGaAs cells optimized to the AM0 spectrum which closely match published data as well as hypothetical cells optimized to the spectrum of a 1300K blackbody.

14. SUBJECT TERMS Thermophotovoltaic cell, radioisotope thermoelectric generator, optimization, model, Silvaco, GaSb, InGaAs	**15. NUMBER OF PAGES** 131
	16. PRICE CODE

17. SECURITY CLASSIFICATION OF REPORT Unclassified	**18. SECURITY CLASSIFICATION OF THIS PAGE** Unclassified	**19. SECURITY CLASSIFICATION OF ABSTRACT** Unclassified	**20. LIMITATION OF ABSTRACT** UL

NSN 7540-01-280-5500

Standard Form 298 (Rev. 2-89)
Prescribed by ANSI Std. 239-18

THIS PAGE INTENTIONALLY LEFT BLANK

Approved for public release; distribution is unlimited.

ADVANCED THERMOPHOTOVOLTAIC CELLS MODELING, OPTIMIZED FOR USE IN RADIOISOTOPE THERMOELECTRIC GENERATORS (RTGS) FOR MARS AND DEEP SPACE MISSIONS

Bradley P. Davenport
Ensign, United States Navy
B.S., United States Naval Academy, 2003

Submitted in partial fulfillment of the
requirements for the degree of

MASTER OF SCIENCE IN
ELECTRICAL ENGINEERING

from the

NAVAL POSTGRADUATE SCHOOL
June 2004

Author:	Bradley P. Davenport
Approved by:	Sherif Michael Thesis Advisor
	Gamani Karunasiri Second Reader
	John P. Powers Chairman, Department of Electrical and Computer Engineering

THIS PAGE INTENTIONALLY LEFT BLANK

ABSTRACT

Thermophotovoltaic cells are a good candidate for use in high efficiency radioisotope thermoelectric generator (RTG) power devices for deep space missions. This thesis examines the use of Silvaco Virtual Wafer Fabrication Software as a tool for designing and optimizing TPV cells for different possible spectra. It gives results for GaSb and InGaAs cells optimized to the AM0 spectrum which closely match published data as well as hypothetical cells optimized to the spectrum of a 1300K blackbody.

THIS PAGE INTENTIONALLY LEFT BLANK

TABLE OF CONTENTS

I. INTRODUCTION 1

II. SOLAR CELLS 3
- A. HISTORY 3
- B. THE P-N JUNCTION 4
- C. PHOTOVOLTAIC CELL 8
- D. INCIDENT SPECTRUM 8
- E. POWER OUTPUT 11
- F. EFFICIENCY IMPROVEMENTS 13
  - 1. Reflection 13
  - 2. Low Energy Photons 14
  - 3. High Energy Photons 14
  - 4. Cell Resistance 14
  - 5. Material Defects 14
  - 6. Shading 15

III. THERMOPHOTOVOLTAIC CELLS 17
- A. HISTORY 17
- B. INCIDENT SPECTRUM 18
  - 1. Blackbody Radiation 18
  - 2. Radioisotope Thermoelectric Generator Spectrum 21
- C. THERMOPHOTOVOLTAIC SYSTEM 22
  - 1. Heat Source 23
  - 2. Selective Emitter 23
  - 3. Filter 23
  - 4. Photo-Electric Converter 25

IV. RADIOISIOTOPE THERMOELECTRIC GENERATOR 29
- A. HISTORY 29
- B. FUEL SUPPLY 32
- C. SAFETY 34
  - 1. Accident History 34
  - 2. Safety Measures 35
  - 3. Safety Testing 36
    - *a. Fire 36*
    - *b. Blast 36*
    - *c. Reentry 36*
    - *d. Earth Impact 37*
    - *e. Immersion in Water 37*
    - *f. Shrapnel 37*
    - *g. Large Fragments 37*
- D. FUTURE IMPROVEMENTS 38
  - 1. Dynamic Isotope Power Systems 38

    2. Alkaline Metal Thermal-to-Electric Conversion 40
    3. Thermophotovoltaic Cells 41

V. SIMULATION SOFTWARE 43
  A. SILVACO 43
  B. DEFINING A CELL 45
    1. Defining Constants 46
    2. Defining Mesh Boundaries 46
    3. Building the X- and Y- Meshes 47
    4. Defining Regions 48
    5. Placing Electrodes 50
    6. Defining Doping Levels 50
    7. Defining Material Properties 50
    8. Incident Spectrum 51
    9. Solving 52
    10. Source Code 53
  C. MATLAB 53
    1. Iterations 53
    2. Plotting 53

VI. MODELS AND RESULTS 55
  A. MODEL CONFIRMATION 55
    1. Gallium Arsenide 55
    2. Gallium Antimonide 58
    3. Indium Gallium Arsenide 60
  B. THERMOPHOTOVOLTAIC CELLS 62
    1. Gallium Antimonide 62
    2. Indium Gallium Arsenide 64

VII. CONCLUSIONS AND RECOMMENDATIONS 69

APPENDIX A: ATLAS CODE 71
  A. GALLIUM ARSENIDE 71
    1. *I-V* Curve 71
    2. Frequency Response 74
  B. GALLIUM ANTIMONIDE 80
    1. *I-V* Curve 80
    2. Frequency Response 84
  C. INDIUM GALLIUM ARSENIDE 87
    1. *I-V* Curve 87
    2. Frequency Response 92

APPENDIX B: MATLAB CODE 97
  A. ATLASARUN.M 97
  B. FILERW.M 99
  C. IVMAXP.M 99
  D. BLACKBODY.M 100
  E. FREQRESP.M 102

F. TIME.M 103

LIST OF REFERENCES 105

INITIAL DISTRIBUTION LIST...111

THIS PAGE INTENTIONALLY LEFT BLANK

LIST OF FIGURES

Figure 1. p-n Junction....4
Figure 2. Energy Band Model of a p-n Junction [From Ref. 2.]....5
Figure 3. Built-In Potential [After Ref. 2.]....5
Figure 4. p-n Junction Under Bias [After Ref. 2.]....7
Figure 5. Simple Solar Cell [After Ref. 3.]....8
Figure 6. AM0 Spectrum vs. Wavelength [Data for Plot is From Ref. 4.]....9
Figure 7. AM0 Spectrum vs. Photon Energy [Data for Plot is From Ref. 4.]....10
Figure 8. Current in a Solar Cell [After Ref. 5]....11
Figure 9. *I-V* Curve....12
Figure 10. Anti-Reflective Coating and Textured Cell Surface [From Ref. 6.]....13
Figure 11. AM0 vs. 5800K Blackbody Spectrum....20
Figure 12. 1300K Blackbody Spectrum....22
Figure 13. TPV System....22
Figure 14. Resonant Filter [After Ref. 11.]....24
Figure 15. Resonant Filter Frequency Response [From Ref. 11.]....24
Figure 16. RTG Module [From Ref. 16.]....32
Figure 17. Pu-238 Power Output [From Ref. 17.]....33
Figure 18. “President Shows Atom Generator” [From Ref. 17.]....34
Figure 19. RTG Safety Measures [From Ref. 19.]....35
Figure 20. Simplified Stirling Engine [From Ref. 20.]....38
Figure 21. 110 Watt Electric Stirling Generator [From Ref. 21.]....40
Figure 22. AMTEC Schematic [From Ref. 22.]....40
Figure 23. Simulator Block Diagram [From Ref. 23.]....45
Figure 24. Typical Mesh....48
Figure 25. Cell Regions....49
Figure 26. ‘GaSb.opt’ [Data for Plot is From Ref. 21]....51
Figure 27. GaAs Solar Cell....56
Figure 28. GaAs Cell Results....56
Figure 29. Spectral Response of GaAs....57
Figure 30. GaSb Solar Cell....58
Figure 31. GaSb Solar Cell *I-V* Characteristics....59
Figure 32. Spectral Response of GaSb....60
Figure 33. InGaAs Solar Cell....61
Figure 34. InGaAs Solar Cell *I-V* Characteristics....61
Figure 35. Spectral Response of InGaAs....62
Figure 36. GaSb TPV Cell....63
Figure 37. GaSb TPV Cell *I-V* Characteristics....63
Figure 38. GaSb Photogeneration Rate....64
Figure 39. InGaAs TPV Cell....65
Figure 40. InGaAs TPV Cell *I-V* Characteristics....65
Figure 41. InGaAs Photogeneration Rate....66

THIS PAGE INTENTIONALLY LEFT BLANK

LIST OF TABLES

Table 1. Temperature vs. Peak Wavelength....................21
Table 2. Maximum Frequency Response of Various Materials....................26
Table 3. RTG Missions [After Ref. 15.]....................31

THIS PAGE INTENTIONALLY LEFT BLANK

ACKNOWLEDGMENTS

I would like to thank Professor Sherif Michael Professor Karunasiri for their guidance on this thesis.

THIS PAGE INTENTIONALLY LEFT BLANK

EXECUTIVE SUMMARY

A major limitation in space exploration is the availability of power. While satellites stationed around Earth can produce an adequate supply of power using solar arrays, satellites farther from the Sun require unreasonably massive arrays to produce very little power. In order to accommodate the need for power on deep space missions, it is necessary for satellites to carry a source capable of providing adequate power for the life of the mission. This is currently done using radioisotope thermoelectric generators (RTGs). Current RTGs consist of a heat source, Pu-238, and a thermocouple that inefficiently converts heat into electricity.

In order to improve the overall efficiency of RTGs, a better thermoelectric converter is needed to replace the thermocouple. This thesis examines the possible use of thermophotovoltaic (TPV) cells in RTGs. Two cells were developed and optimized for the spectrum from a 1300K blackbody which simulates the spectrum of an RTG heat source.

Current TPV cells are optimized primarily using a trial-and-error method. Cells are built and tested with different thicknesses and doping levels in order to the most efficient design. This method is very expensive and time consuming. This thesis presents a model that can predict the output of a cell under various spectra. The model can easily be changed to simulate different cell thicknesses and doping levels. Additionally, with a comprehensive set of material parameters, the model can be changed to simulate cells of different materials.

The models presented in this thesis were built using the Silvaco Virtual Wafer Fabrication software package. This software package has been shown by other researchers as a capable tool for modeling advanced solar cell designs, but there is no record of any TPV models ever being designed.

In order to prove the capabilities of this software package, an initial cell was designed using a very well documented material, gallium arsenide (GaAs). Voltage-current characteristics and frequency response data were recorded from this model and compared with experimental data from a similar cell. Once the model was verified, more exotic materials could be examined. Gallium antimonide (GaSb) and indium gallium arsenide

(InGaAs) were examined for TPV cells because these are two of the most researched materials and, as such, there is a significant amount of experimental data to compare with.

As with the GaAs cell model, the GaSb and InGaAs models were first optimized for the AM0 spectrum and compared to experimental results. Again, the voltage-current relationship and frequency response of the cells were measured and found to be very close to available experimental data. Once these models were determined to be accurate, they could be optimized for a different spectrum.

Programs were written using Matlab to run iterations of Silvaco model changing layer thicknesses and doping levels in the cells. Other programs gathered data and calculated and recorded open-circuit voltage, short circuit current, maximum power, fill factor, and efficiency of each cell in order to determine the most efficient design. These results were also compared to experimental data on similar cells and found to be very close.

I. INTRODUCTION

As space-based-missions take both manned and unmanned vehicles farther from Earth, the need for a better source of power becomes more important. The intensity of light from the sun decreases with the square of the distance from it making solar cells an inadequate source of power on distant missions because the area of cells required would be tremendous. As an example, a $1\ \mathrm{m}^2$ solar panel at earth would have to be $25\ \mathrm{m}^2$ at Jupiter and almost $2000\ \mathrm{m}^2$ at Pluto to yield the same output power. Batteries, another common source of power on satellites are used primarily only as storage devices because they are only capable of providing a few hundred $\mathrm{watt} \cdot \mathrm{hr}/\mathrm{kg}$. This means that the amount of batteries required to provide primary power for a long mission would be too massive to even launch into space. Current deep space satellites use an alternative source of power known as a radioisotope thermoelectric generator or (RTG).

An RTG consists of a heat source and a means to convert that heat into electricity. Existing RTGs accomplish this using thermocouples. Although these are very simple and reliable thermoelectric converters, they operate at only a few percent efficiency. In order to improve overall efficiency of an RTG, the thermocouple will have to be replaced by a more capable thermoelectric converter.

The most attractive replacement for the thermocouple is currently the thermo-photovoltaic (TPV) cell. Research has been ongoing in this field since the 1950's, but the exotic materials necessary for high efficiency cells has only been recently available. Here, several models will be developed and optimized for both the sun's spectrum, AM0, and the spectrum from a 1300K blackbody which represents well the spectrum from an RTG heat source.

Due to the fact that TPV cells work on the same principles as solar cells, these are discussed in Chapter II. TPV cells are discussed in Chapter III. In Chapter IV, the entire RTG module is discussed including the safety precautions necessary when using a radio-active heat source. Chapter V discusses the software packages used in these models and Chapter VI gives the optimized cell characteristics along with results, and Chapter VII contains conclusions and recommendations for future work. ATLAS code used in this thesis is in Appendix A and Matlab code is in Appendix B.

THIS PAGE INTENTIONALLY LEFT BLANK

II. SOLAR CELLS

This chapter contains the basic principles of solar cells. This information is important to this thesis because thermophotovoltaic cells work on the same principles as solar cells.

A. HISTORY

The history of the solar cell, also known as a photovoltaic cell, can be traced all the way back to 1839 when the then nineteen-year-old French physicist Antoine-César Becquerel first discovered the photovoltaic effect [Ref. 1]. While experimenting with electrolytic cells containing two different metal electrodes in a solution, he found that some combinations of metal and solution would produce a small current when exposed to light.

The first actual solar cell was built in 1877 by Charles Fritts [Ref. 1]. He applied a very thin gold film to a piece of selenium. Although this cell operated with less than one percent efficiency, it was able to produce a measurable amount of power [Ref. 1]. A similar cell was constructed in 1927 consisting of a copper film on piece of copper oxide [Ref. 1]. This cell also operated with less than 1% efficiency [Ref. 1].

The next breakthrough came in 1941 when Russell Ohl built the first silicon solar cell [Ref. 4]. In 1954, Pearson, Chapin, and Fuller expanded on this design and were able to build a silicon cell with an efficiency of 6% [Ref. 1]. Since that time, there has been a great deal of progress in solar cell design. Gallium arsenide cell designs have been able to achieve efficiencies of over 20% and multijunction cells have been built with up to 37% efficiency [Ref. 1].

B. THE P-N JUNCTION

N-type materials have electrons as the majority carriers while p-type materials have holes as the majority carriers. What is important to semiconductor physics is what happens when these two types of materials come together [Ref. 2]. As can be seen from Figure 1 below, when the two materials come in contact, some electrons move across the junction to fill holes on the p-side and some holes move across the junction to the n-side [Ref. 2].

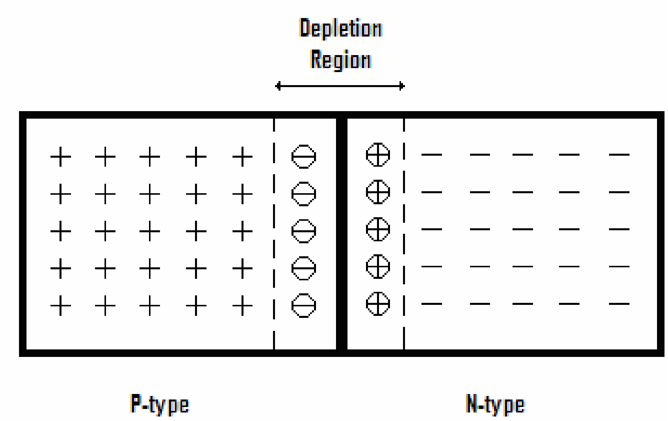

Figure 1. p-n Junction

When these electrons and holes migrate across the junction, an electric field forms. This area is referred to as the space charge region or depletion region, and it creates a built in potential in the material. The energy band diagram in Figure 2 [Ref. 2] helps to give a better idea what happens when n-type and p-type materials are brought together.

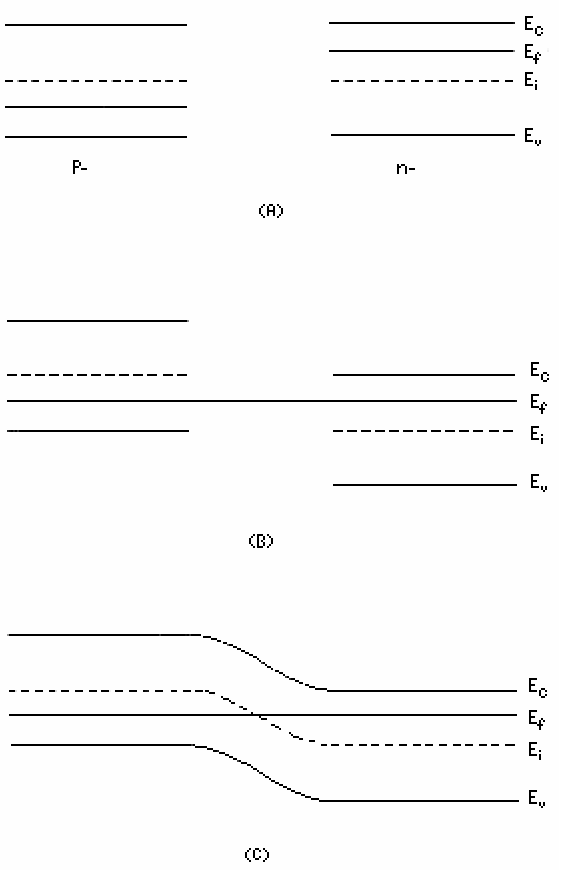

Figure 2. Energy Band Model of a p-n Junction [From Ref. 2.]

The Fermi level is constant throughout the material, so a straight line is drawn and the two band diagrams are shifted to match it. In order to have continuous conduction and valence bands in the material, the bands of the p- and n-type material must bend to meet each other [Ref. 2]. This bend in energy bands creates a built-in potential in the material equal to V_{bi} as seen in Figure 3 [Ref. 2]. It is this potential that causes the voltage drop across a diode [Ref. 2].

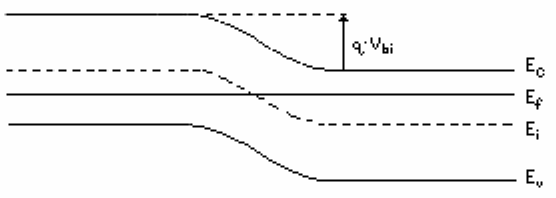

Figure 3. Built-In Potential [After Ref. 2.]

Figure 4 shows how the junction reacts when a bias is placed across it [Ref. 2]. Part (a) shows the band diagram under equilibrium conditions with no bias present. This diagram was previously explained.

Part (b) shows the junction under forward bias conditions. This is when the anode is held at a higher potential than the cathode. As more voltage is applied across the junction, it acts against the built in potential V_{bi}. Once the bias across the junction reaches a level that is equal to V_{bi}, current will begin to flow through the junction. The diode will then act like a short circuit with a constant voltage drop of V_{bi}.

Part (c) shows the band diagram of the p-n junction under reverse bias conditions. This occurs when the voltage at the cathode is higher than the voltage at the anode. In this case, the potential across the junction acts to increase the level between the energy bands of the two materials thereby preventing current from flowing.

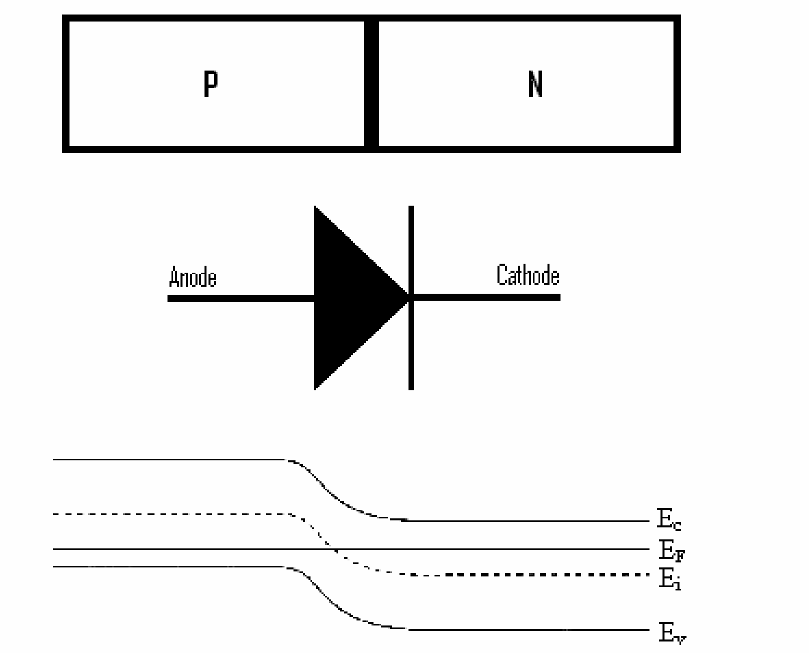

(a) Equilibrium (V_A=0)

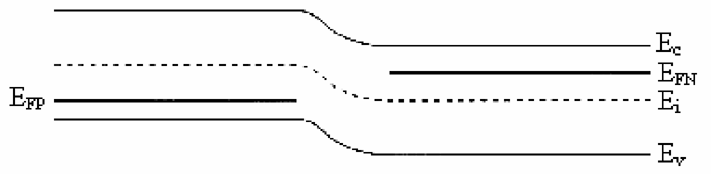

(b) Forward Bias (V_A>0)

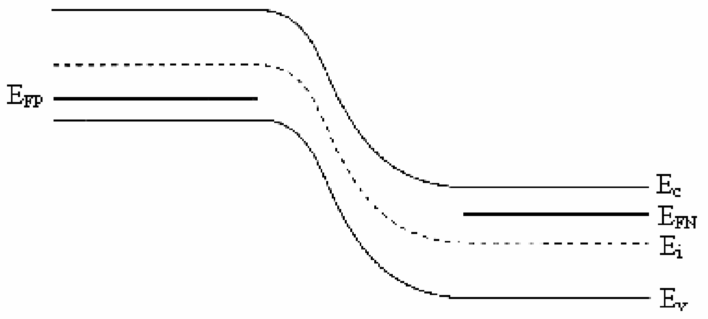

(c) Reverse Bias (V_A<0)

Figure 4. p-n Junction Under Bias [After Ref. 2.]

C. PHOTOVOLTAIC CELL

A photovoltaic cell [Ref. 3], shown in Figure 5, produces power using photogeneration. When a photon of light with energy higher than the bandgap energy strikes the material, an electron-hole pair is created. The cell itself is simply a p-n junction which was discussed in the previous section. The electric field in the depletion region at the junction attracts the free electrons towards the cathode, the top layer in the figure, and attracts the holes towards the anode, the bottom layer.

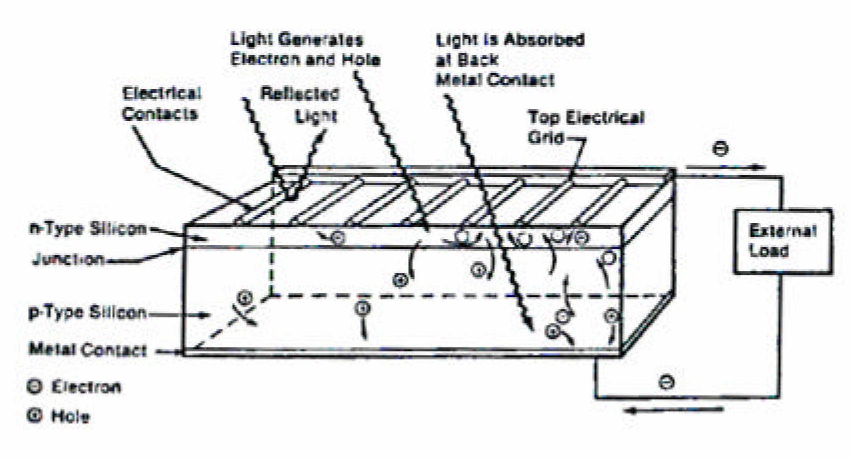

Figure 5. Simple Solar Cell [After Ref. 3.]

Current is carried away from the cell by contacts which are connected both on the top and bottom of the cell. The contact on the top of the cell is typically made up of a thin metal electrical grid to avoid shading the cell. The bottom metal contact, on the other hand, spans the entire surface of the cell. These contacts are connected to the external load.

D. INCIDENT SPECTRUM

Solar cells can be designed to be optimized for different spectra based on their intended use [Ref. 3]. Cells intended for outer space are designed to the spectrum of Air

Mass Zero (AM0). This is the spectrum from the sun measured just outside the earth's atmosphere. Figure 6 shows the AM0 spectrum in $\left[\mathrm{W/m^2/\mu m}\right]$. The data was measured by The National Renewable Energy Laboratory (NREL) [Ref. 4]. The total power in this spectrum is approximately $1367\ \mathrm{W/m^2}$.

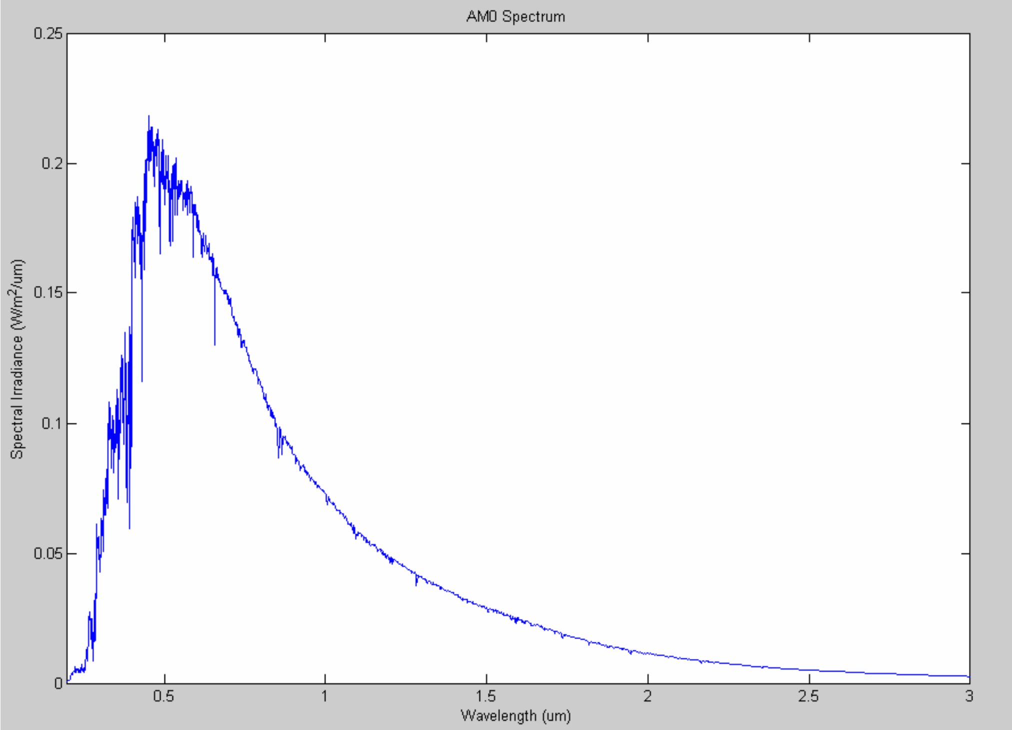

Figure 6. AM0 Spectrum vs. Wavelength [Data for Plot is From Ref. 4.]

As mentioned previously, the energy of a photon required to cause photogeneration in a material must be greater than the bandgap energy of the material. Because of this relationship, it is often useful to see the AM0 spectrum as a function of energy instead of wavelength. The relationship of photon energy to wavelength is expressed as

$$E = \frac{hc}{l}, \tag{2.1}$$

$$E\left[\mathrm{eV}\right] \approx \frac{1.24}{l\left[m\mathrm{m}\right]} \tag{2.2}$$

where h is Planck’s constant, c is the speed of light, and l is the wavelength of light [Ref. 3]. Figure 7 shows the AM0 spectrum [Ref. 4] as a function of energy.

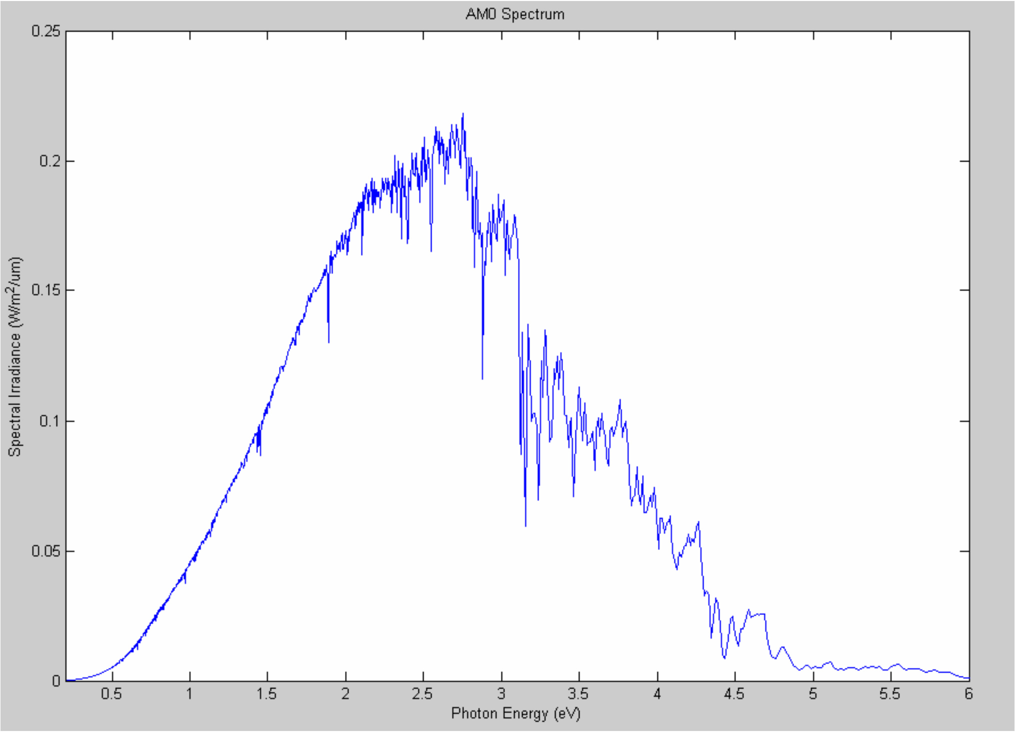

Figure 7. AM0 Spectrum vs. Photon Energy [Data for Plot is From Ref. 4.]

As the sun’s spectrum passes through the earth’s atmosphere some wavelengths are absorbed and others are reflected. This causes the radiance at the earth’s surface to be a subset of the AM0 spectrum. Other common spectra are Air Mass One (AM1) and Air Mass One Point Five (AM1.5). AM1 is the spectrum from the sun at earth’s surface on the equator when the sky is clear. Moving farther from the equator to higher latitudes and the presence of clouds and other weather conditions further reduces the radiance of the spectrum that reaches earth’s surface. AM1.5 is commonly used for testing terrestrial based solar cells [Ref. 3].

E. POWER OUTPUT

As discussed previously, a photovoltaic cell is simply a p-n junction. It therefore has associated with it the same current voltage relationship as a diode when there is no light incident on the cell.

Figure 8 shows currents that contribute to the total current from a solar cell [Ref. 5]. The curve in part (a) shows the photocurrent from the cell. This is a constant current level that is dependent on the amount power incident on the cell. The dark current curve in part (b) is an exponential curve that is a characteristic of the material. To find the current-voltage relationship of the solar cell, the dark current must be subtracted from the photocurrent. Part (c) of Figure 8 shows the resulting I-V curve of the cell.

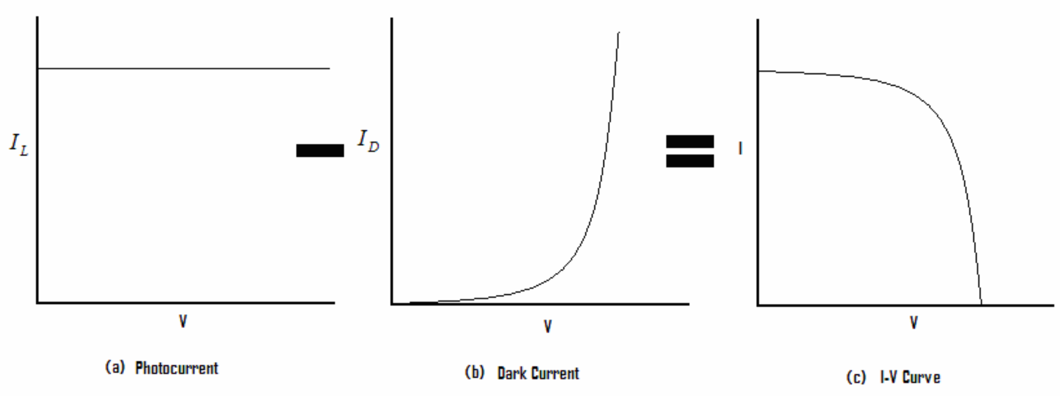

(a) Photocurrent (b) Dark Current (c) I-V Curve

Figure 8. Current in a Solar Cell [After Ref. 5]

Figure 9 shows an example of a solar cell I-V curve. The points on this curve of most importance are labeled. When the anode and cathode are shorted, the maximum current, called short circuit current, flows through the circuit [Ref. 3]. This is labeled as I_{sc} on the figure. If the circuit is opened, no current will flow; however the maximum voltage, called open-circuit voltage, can be measured across the cell [Ref. 3].

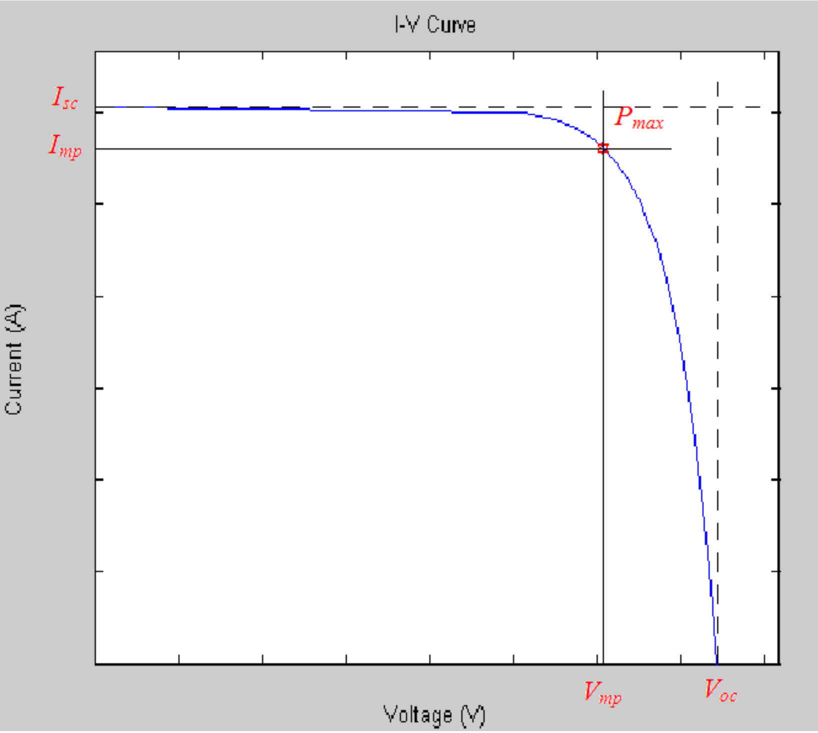

Figure 9. *I-V* Curve

While the cell can operate anywhere on this curve, it is most efficient when operated at the maximum power point, labeled P_{max} in the figure [Ref. 3]. This is the point on the curve where the product of the operating voltage and current is the highest. The efficiency of the cell is calculated as [Ref. 3]

$$h = \frac{P_{max}}{P_{in}}, \tag{2.3}$$

where P_{in} is the power in the incident spectrum; for AM0 this is $1367\ \mathrm{W/m^2}$ [Ref. 3]. Another important characteristic of a solar cell is the fill factor, which indicates the squareness of the *I-V* curve [Ref. 3]. This is calculated as [Ref. 3]

$$FF = \frac{V_{mp} I_{mp}}{V_{oc} I_{sc}}. \tag{2.4}$$

The dotted box that intersects I_{sc} and V_{oc} in the figure represents the optimal *I-V* curve with a fill factor of one. The fill factor is a measure of how much of this dotted box the actual *I-V* curve occupies [Ref. 3].

F. EFFICIENCY IMPROVEMENTS

There are many factors that can be changed to help improve the efficiency of solar cells.

1. Reflection

An untreated solar cell can reflect as much as 36% of the incident light [Ref. 3]. Anti-reflective coatings such as silicon nitride can reduce the reflectivity of the cell to as low 5% [Ref. 3]. In addition to adding antireflective coatings, texturing the cell surface also reduces the amount of light reflected at the surface of the cell [Ref. 3].

Figure 10 shows an example of surface texturing [Ref. 6]. This cell was able to operate at 24% efficiency which is very high for a silicon cell [Ref. 6]. The inverted pyramids labeled in the figure are at such an angle so that light that is reflected from the surface of the cell, is reflected in such a way that it will hit one of the other pyramids where it may be absorbed [Ref. 6]. The high absorption of this cell led to its record setting efficiency.

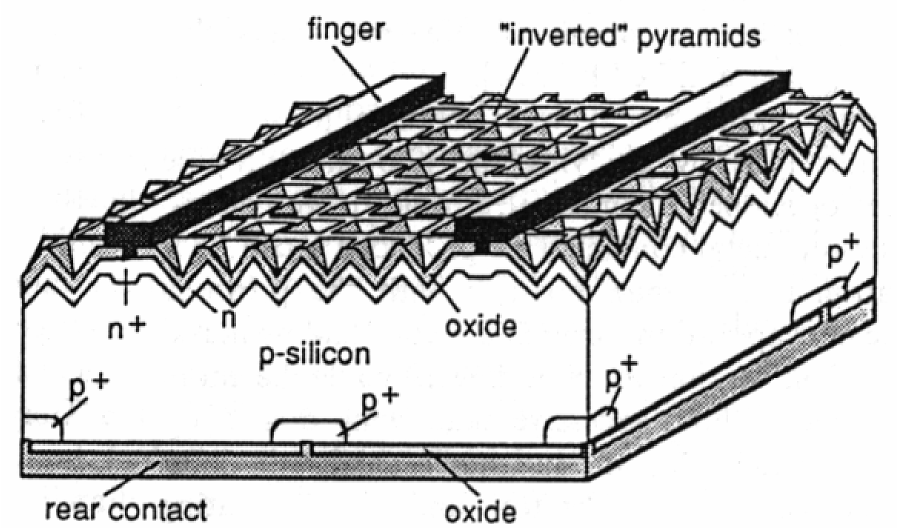

Figure 10. Anti-Reflective Coating and Textured Cell Surface [From Ref. 6.]

2. Low Energy Photons

Only photons with energy higher than the bandgap energy of the material can create an electron-hole pair in the cell. Photons with too little energy to create an electron-hole pair will be absorbed and increase the temperature of the cell [Ref. 3]. This in turn reduces the efficiency of the cell. Some designs utilize optical filters to block low energy photons to avoid this problem [Ref. 3].

3. High Energy Photons

Photons with energy significantly higher than the bandgap energy can still create an electron-hole pair, but the excess energy is given off as heat in the cell, thus reducing the efficiency [Ref. 3]. Some of these photons may simply pass through the cell without creating an electron-hole pair. A back surface reflector can reflect these high energy photons back through the cell where they once again have the opportunity to create an electron-hole pair [Ref. 3].

4. Cell Resistance

There are several sources of resistance in a solar cell. There is a resistance in the material itself that impedes the path of free electrons and holes to the contacts [Ref. 3]. There are also junction resistances where the electrical contacts are joined to the cell [Ref. 3]. Finally there is resistance in the contacts [Ref. 3]. All of these resistances cause losses which can be significant especially in high current applications.

5. Material Defects

Defects in the crystal structure aid in trap assisted recombination which reduces cell efficiency [Ref. 2]. This is a significant source of power loss in inexpensive polycrystalline and amorphous cells reducing efficiency by as much as 15% [Ref. 3]. There are also a significant number of material defects when lattice mismatch is a factor such as in multijunction cells. The effects of this in single junction cells can be reduced by using high quality crystals [Ref. 3]. The fewer the defects in the crystal structure, the higher the efficiency of the cell. In multijunction cells, a great deal of research has been done with ternary and quaternary compounds (compounds with three or four elements respectively) [Ref. 3]. By altering the molar concentrations of the elements in these compounds, the lattice constant can be set to a desired value reducing the amount of lattice mismatch.

6. Shading

In order to collect free carriers from the cell, there must be metal contacts on the surface. These contacts, while providing a necessary function, also shade the parts of the cell they cover from incident light [Ref. 3]. Larger and more closely spaced contacts have the benefit of being able to collect more generated carriers and having lower internal resistance [Ref. 3]. Conversely they shade more of the cell causing fewer carriers to be generated. Smaller and more loosely spaced carriers shade less of the cell, but also have higher resistance [Ref. 3]. In addition when contacts are more loosely spaced on the surface of the cell, carriers are more likely to recombine before they can be collected by the contacts [Ref. 3]. By trial and error, it has been found that the optimal contact arrangement consists of equally spaced contacts covering approximately 8% of the cell’s surface [Ref. 3].

This chapter reviewed the basic principles of solar cells. The input spectrum and output power were covered along with methods for improving the efficiency. The next chapter will introduce a related concept, the thermophotovoltaic cell.

THIS PAGE INTENTIONALLY LEFT BLANK

III. THERMOPHOTOVOLTAIC CELLS

This chapter discusses the basic principles of thermophotovoltaic (TPV) cells. Thermophotovoltaic cells are designed to convert the infrared (IR) region of the electromagnetic spectrum into electricity. The goal of this thesis is to model and optimize these cells, so it is important to know some background information on them.

A. HISTORY

Although the 'Father' of thermophotovoltaics is unknown, the field can be traced at least as far back as 1956 to Dr. Henry H. Kolm [Ref. 7]. While working at MIT's Lincoln Laboratory, Dr. Kolm built a primitive TPV device using a Coleman camping lantern as a radiator and silicon solar cells for photoconverters. Although his system only produced one watt of power, it was a start. Throughout the 1960's, researchers at MIT continued research on TPV devices focusing on germanium cells [Ref. 7.]. In the 1970's thermophotovoltaics was studied as a way to provide a portable power source for the U.S. Army [Ref. 7]. Early TPV generators consisted of standard silicon or germanium solar cells surrounding a heat source [Ref. 7]. Around 1980 a general interest in the area was lost because of the exceedingly low efficiency of these early TPV cells. With the recent advancements in III-V semiconductor technology (materials made of a combination of group III and group V elements from the periodic table), there was a possibility for significantly higher efficiency cells [Ref. 7]. Recent research has shown that gallium antimonide (GaSb) and indium gallium arsenide (InGaAs) are two of the most promising materials for new TPV cells.

B. INCIDENT SPECTRUM

1. Blackbody Radiation

Objects with a temperature above zero Kelvin radiate energy. In order to estimate the amount of energy radiated, it is convenient to introduce the concept of a blackbody. A blackbody is characterized by three key properties [Ref. 8]:

1. 100% absorption of all incident radiation
2. Maximum possible emission at any temperature and wavelength
3. Diffuse emitter, radiates energy equally in all directions

An ideal emitter, a blackbody, radiates energy over the whole electromagnetic spectrum as a function only of temperature and wavelength. A blackbody emitter radiates energy per wavelength into a unit solid angle in a distribution described by Planck's Law for spectral radiance as [Ref. 8]

$$L(T)\left[\frac{\mathrm{W}}{\mathrm{m}^2\cdot\mathrm{sr}\cdot\mu\mathrm{m}}\right]=\frac{2hc^2}{l^5\left(e^{\left(\frac{hc}{l kT}\right)}-1\right)}, \tag{3.1}$$

where h is Planck's constant, c is the speed of light in a vacuum, and k is Boltzmann's constant. T and l are the only two variables and refer to the blackbody temperature in Kelvin and the wavelength of energy emitted in meters. The units of spectral radiance are bracketed.

As can be seen from Planck's Law for spectral radiance, at a given temperature, the amount of radiation varies as function of wavelength. An important feature is that at any wavelength, the magnitude of radiant energy increases as temperature increases [Ref. 8]. This means that a hotter blackbody will emit more energy than a colder one.

Another important feature of Planck's Law is the distribution of radiant energy. More radiant energy is emitted at shorter wavelengths for hotter blackbodies [Ref. 8]. This phenomenon is described by Wien's Displacement Law [Ref. 8],

$$l_{\max}[\mu\text{m}] = \frac{2897.8}{T[\text{K}]}\,. \tag{3.2}$$

This equation gives the wavelength at which the maximum radiation is emitted from a blackbody at a given temperature. It can easily be seen that the location of this peak is inversely proportional to the temperature of the blackbody.

In order to find the total power emitted by a blackbody, it is necessary to integrate Planck's Law over all wavelengths. This calculation yields the Stefan-Boltzmann Law [Ref. 8],

$$E_b = s\,T^4\,. \tag{3.3}$$

where $s = 5.670\times10^{-8}\left[\text{W}/\text{m}^2/\text{K}^4\right]$. Here it can be seen that the total radiated power is dependent only on temperature.

When working with solar cells, the spectrum of interest is AM0. This spectrum corresponds to the radiation from blackbody at a temperature of 5800K. Because energy is radiated outward from a body at an average angle perpendicular to its surface, the magnitude of radiation in a given direction is equal to only one-fourth the total radiation [Ref. 8]. This corresponds to p steradians. With this information, the equation for the hemispherical spectral radiant flux in any direction from a flat surface emitter can be derived as [Ref. 8]

$$M(T)\left[\frac{\text{W}}{\text{m}^2\cdot\mu\text{m}}\right] = p\,L(T) = \frac{2p\,hc^2}{l^5\left(e^{\left(\frac{hc}{l\,kT}\right)}-1\right)}\,. \tag{3.4}$$

In order to find the AM0 spectrum, there is one more factor that must be considered. The magnitude of radiation emitted from a source is inversely proportional to the square of the distance from the source. The factor used to calculate the AM0 spectrum is found by taking the square of the ratio of the sun's radius to the mean distance between the earth and the sun. This factor, referred to as the dilution factor, comes out to 2.165×10^{-5} [Ref. 8]. The final equation for the AM0 spectrum can now be expressed as

$$AM0\left[\frac{\text{W}}{\text{m}^2\cdot\mu\text{m}}\right] = fM(T) = \frac{f\left(2p\,hc^2\right)}{l^5\left(e^{\left(\frac{hc}{l\,kT}\right)}-1\right)}, \tag{3.5}$$

where f is the dilution factor.

Using this equation, Figure 11 below shows the spectrum from a 5800K blackbody adjusted by the dilution factor. It is plotted on top of the actual AM0 spectrum as measured by NREL [Ref. 4]. It can be seen that the two spectra are very closely correlated in shape, magnitude, and area.

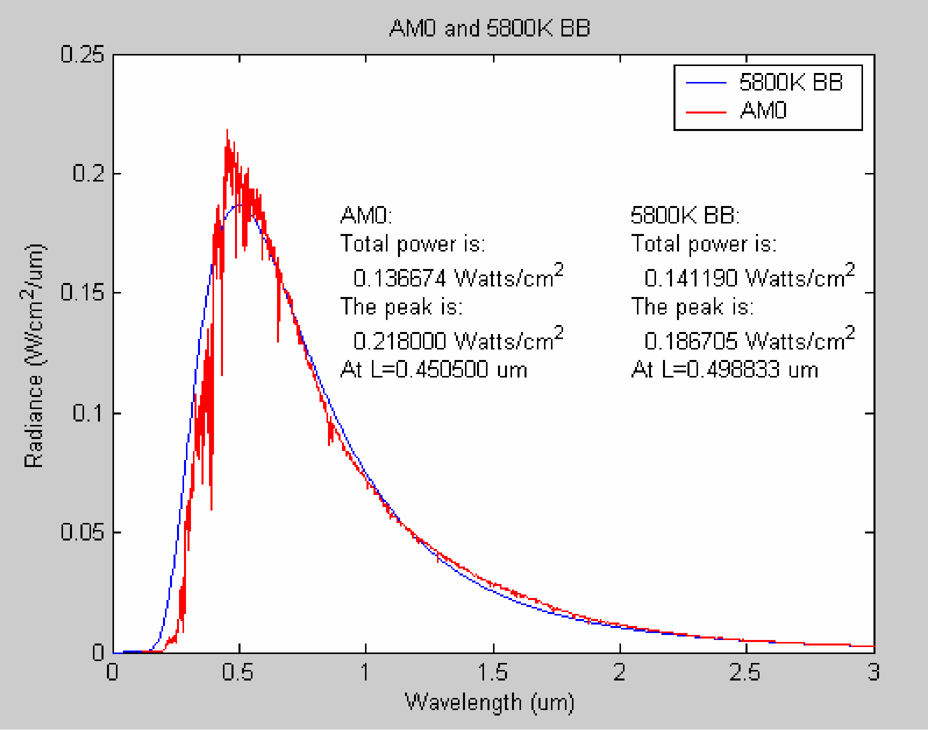

Figure 11. AM0 vs. 5800K Blackbody Spectrum

From Planck's distribution law, the magnitude of radiation at a given wavelength increases with temperature, so the magnitude of radiation from the sun is much larger than the magnitude of radiation from any heat source with a lower temperature. Unlike photovoltaics, however, where the radiant source, the sun, is millions of miles away, a heat source used for thermophotovoltaic applications can be placed in very close proximity to the cell. Although the sun radiates much more energy than a heat source, because of the distance between the source and the cell, the intensity of radiation at the cell is much higher for a heat source.

2. Radioisotope Thermoelectric Generator Spectrum

When dealing with solar cells, the input spectrum is a subset of the spectrum from the sun [Ref. 3]. With TPV cells, the input spectrum is dependent on the temperature of the radiator. Table 1 shows several temperatures and the wavelength at which their radiation spectrum is a maximum as calculated from Equation 3.2.

T (K)	**$?_{peak}$ (µm)**
300	9.66
1000	2.90
1300	2.23
2000	1.45
3000	0.97
5000	0.58
5800	0.50
7000	0.41
10000	0.29

Table 1. Temperature vs. Peak Wavelength

The previous section discussed blackbody radiation and compared a 5800K blackbody radiation curve to the AM0 spectrum in Figure 12. Because these two were so closely correlated, it was assumed that a blackbody curve would be a good best case approximation for the input spectrum from a radioisotope thermoelectric generator (RTG) heat source.

Current RTG's use Pu-238 as a heat source. In a pure form, Pu-238 can reach surface temperatures of 1300K [Ref. 9]. For simulations in this research, the input spectrum was assumed to be a 1300K blackbody. Figure 24 shows the spectrum that was used in simulations.

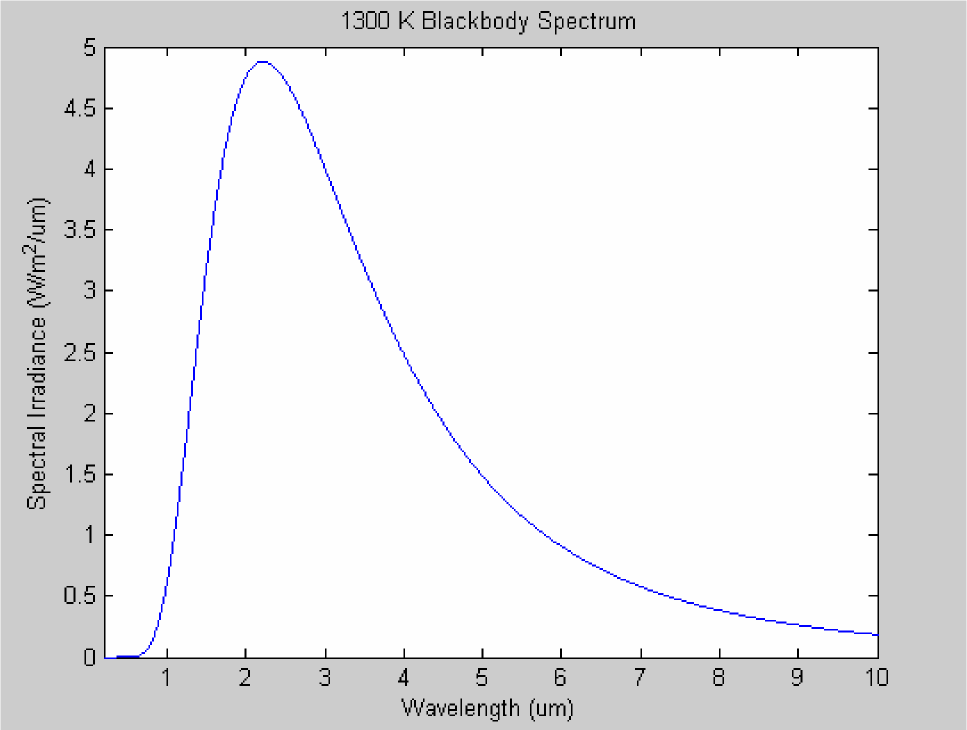

Figure 12. 1300K Blackbody Spectrum

C. THERMOPHOTOVOLTAIC SYSTEM

There are more parts to a thermophotovoltaic system than just the TPV cell. Figure 13 shows the four main components of a typical TPV system.

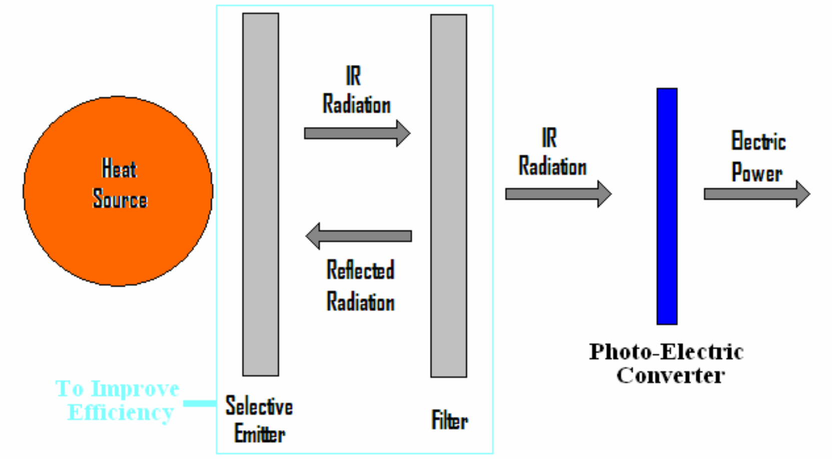

Figure 13. TPV System

1. Heat Source

The first component is a heat source. The temperature of the heat source is a very important factor in the efficiency of the system. This relationship will be discussed in more depth in the next section.

2. Selective Emitter

The second component in the system is a selective emitter. The purpose of this emitter is to help shape the radiation spectrum from the heat source. As with solar cells, radiation absorbed by the cell that does not have enough energy to create an electron-hole pair just adds heat to the cell, thereby lowering the efficiency. Rare earth oxides such as ytterbium oxide (Yb_2O_3) and yttrium aluminum garnet (YAG) have proven to be very effective materials because they emit radiation in a line spectrum instead of a continuous spectrum like a heat source but they are currently in the experimental stages and are not always found in TPV systems [Ref. 10]. A selective emitter was not used in these simulations because the response of the materials used was desired over a wide range of the spectrum. This data is important when designing multijunction cells which will be discussed later.

3. Filter

The filter performs a similar function to the selective emitter. It is designed to reflect incident radiation that does not have enough energy to create an electron-hole pair in the TPV cell. The radiation is reflected back to the emitter. This helps to keep the temperature of emitter as high as possible which improves the efficiency of the system [Ref. 11].

Figure 14 shows an experimental resonant gold film filter [Ref. 11]. Designed by Energetics Development Technology (EDTEK), this filter is etched from a solid gold film in a pattern designed to resonate at a desired frequency [Ref. 11]. The filter can be tuned to resonate at any desired frequency depending on the intended spectrum. Tests have shown that the filter has very good transmission in the desired band and reflects over 98% of out-of-band radiation [Ref. 11]. Filters were not included in the models built here for the same reasons that selective emitters were not used.

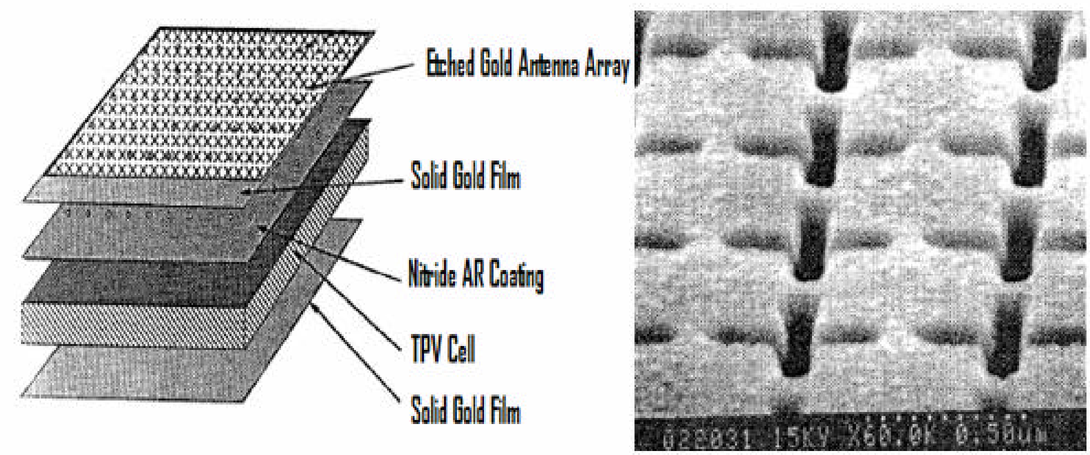

Figure 14. Resonant Filter [After Ref. 11.]

Figure 15 shows the frequency response of a filter built with this technique along with the AM0 spectrum [Ref. 11]. This particular filter was designed to resonate at two distinct frequencies. This capability is useful for multijunction cells which consist of individual cells that are designed to respond to different wavelengths of light.

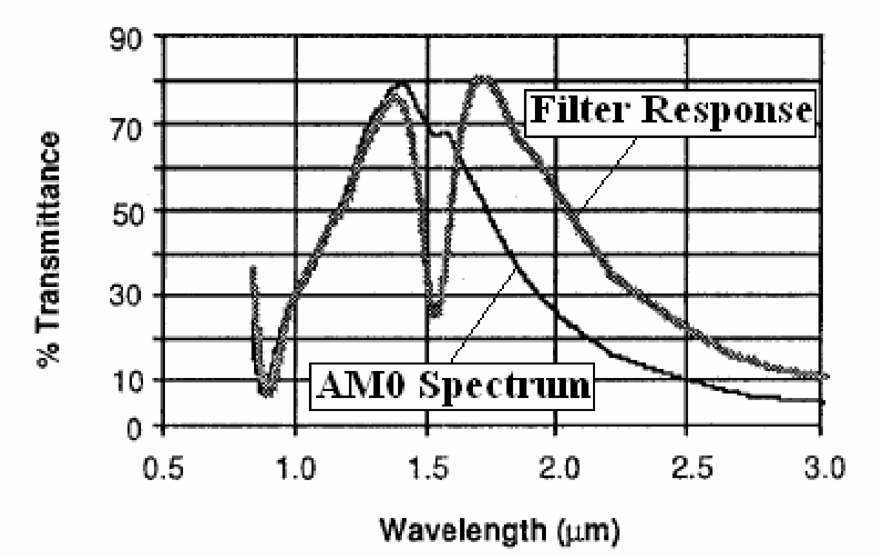

Figure 15. Resonant Filter Frequency Response [From Ref. 11.]

4. Photo-Electric Converter

Conventional RTG's use a thermocouple to convert heat into electricity [Ref. 13]. A thermocouple produces power using what is known as the Seebeck Effect. Seebeck discovered that when two materials from the thermoelectric series were connected, a potential could be measured across them if the two materials were at different temperatures [Ref. 12]. In addition, if the two materials were connected with a wire so as to close the circuit, a small current was forced to flow. In an RTG, a SiGe thermocouple is placed in the vicinity of the heat source with one side exposed to the heat and the other side to a heat sink [Ref. 13]. The electrical power produced is proportional to the difference in temperature between the hot and cold junctions. These devices do a relatively poor job of power conversion, however, only achieving efficiencies of a few percent in optimum working conditions [Ref. 12].

This thesis will explore the thermophotovoltaic cell as a candidate for replacing the thermocouple in RTG's. Such a cell operates in a manner very similar to how a solar cell works. The difference between the two is the band of the electromagnetic spectrum the cell is designed to respond to. Where a solar cell responds to the visible band of the spectrum, thermophotovoltaic cells respond to the infrared region.

In order for the TPV cell to respond to radiant energy from an RTG source, the energy of the radiant photons must be greater than the energy bandgap of the material. As previously mentioned, photon energy is inversely proportional to the temperature of the radiant body. From Table 1 it can be seen that the radiation from a 1300K blackbody source peaks at $2.23\ \mu m$ which is a much longer wavelength than the $0.45\ \mu m$ the sun's spectrum peaks at. This means that materials used for TPV cells must have very low energy bandgaps in order to respond to such long wavelengths of light. Table 2 shows several different semiconductor materials with their respective energy bandgaps and the maximum wavelength of light they can respond to as calculated from Equation 2.2.

	E_g (eV)	$?_{max}$
GaAs	1.42	0.87
Si	1.12	1.11
GaSb	0.72	1.72
Ge	0.66	1.88
InGaSb	0.6	2.07
InGaAsSb	0.55	2.23
InGaAs	0.55	2.23
InAsSbP	0.39	3.18

Table 2. Maximum Frequency Response of Various Materials

In order for the peak of the 1300K blackbody spectrum to occur in the energy band that a TPV cell can respond to, the cell must be made of a material with an energy bandgap lower than $0.55\ \mathrm{eV}$. As can be seen from Table 2 there are materials that have such a low bandgap; however there are tradeoffs to be made. The open-circuit voltage of a cell is closely related to the energy bandgap of the material. As the energy bandgap goes down, so does the open-circuit voltage. A material with a bandgap of $0.39\ \mathrm{eV}$ may only produce an open-circuit voltage of just a few tens of millivolts or less. Such a low voltage drastically reduces the maximum power from the cell in turn reducing the efficiency.

Gallium antimonide (GaSb) is the most commonly published material used for TPV cells. Although it does not have a low enough energy bandgap to respond to most of the radiant energy from an RTG heat source, the cells are relatively easy to fabricate and are capable of producing a significant amount of power per square centimeter. Indium gallium arsenide (InGaAs) is another popular material for TPV cells. As a ternary compound, many of its electrical and optical properties including energy band gap change with varying molar concentrations of indium and gallium. As a $0.55\ \mathrm{eV}$ cell, its low open-circuit voltage is not very suitable for single junction cells, but it is attractive for use in multijunction cells [Ref. 14]. For these reasons, GaSb and InGaAs are the materials that will be studied in this thesis.

This chapter gave an in depth discussion of thermophotovoltaics including the cells themselves and the spectrum they are designed to respond. The next chapter will cover the systems that thermophotovoltaic cells are designed to operate in, radioisotope thermoelectric generators.

THIS PAGE INTENTIONALLY LEFT BLANK

IV. RADIOISIOTOPE THERMOELECTRIC GENERATOR

This chapter presents the radioisotope thermoelectric generator (RTG). As a source of space nuclear power, the use of RTG's, while proven safe, reliable, and necessary for deep space missions, has been greatly debated. The history of RTG's will be discussed including an account of their successes. Environmental issues regarding the use of RTG's will also be mentioned along with the many measures in place to maintain their impeccable safety record. Finally this chapter also includes about possible improvements to RTG's necessary for higher efficiency operation.

A. HISTORY

As space missions have begun to take man-made vehicles and satellites farther and farther from the sun, the need for a better means of power generation has become more important. The intensity of light from the sun reduces with the square of the distance from it meaning that massive solar arrays would be needed in order to produce minimal power on distant missions. NASA has calculated that on missions such as Cassini, the weight of solar arrays needed to provide the desired amount of power would more than double the weight of the entire satellite [Ref. 3].

An alternative to these massive arrays is to bring a fuel supply that will be capable of providing adequate power over the entire lifespan of the vehicle. It is not feasible to use just batteries because the number of batteries required for such a long duration would be far too heavy [Ref. 3]. Conventional fuels are also not viable options due to the poor mass to power ratios [Ref. 3].

Since 1961, the United States Department of Energy (DOE) has supplied NASA with RTG's powered by Pu-238 [Ref. 13]. Table 3 lists some missions that have made use of these RTG's [Ref. 15].

Date	Spacecraft	Power Source	Misson Type	Status
29 JUN 1961	Transit 4A	SNAP-3B7	Navigational	Operated for 15 years. Shut down but still operational.
15 NOV 1961	Transit 4B	SNAP-3B8	Navigational	RTG operated for 9 years
28 SEP 1963	Transit 5-BN-1	SNAP-9A	Navigational	RTG operated as planed. Electrical problems caused failure after 9 months.
05 DEC 1963	Transit 5-BN-2	SNAP-9A	Navigational	RTG operated for 6 years. Navigation failed after 1.5 years.
21 APR 1964	Transit 5-BN-3	SNAP-9A	Navigational	Mission aborted. RTG burned up on reentry as designed.
03 APR 1965	Snapshot	SNAP-10A	Experimental	Successfully achieved orbital operations.
18 MAY 1968	Nimbus-B-1	SNAP-19B2	Meterological	Mission aborted. RTG recovered and recycled.
14 APR 1969	Nimbus III	SNAP-19B3	Meterological	RTG's operated for more than 2.5 years.
14 NOV 1969	Apollo 12	SNAP-27	Lunar Surface	RTG shut down after 8 years of operation.
11 APR 1970	Apollo 13	SNAP-27	Lunar Surface	Mission aborted. Heat Source returned.
31 JAN 1971	Apollo 14	SNAP-27	Lunar Surface	RTG shut down after 6.5 years of operation.
26 JUL 1971	Apollo 15	SNAP-27	Lunar Surface	RTG shut down after 6 years of operation.
02 MAR 1972	Pioneer 10	SNAP-19	Planetary	RTG still operation. Spacecraft now beyond Pluto.

Date	Spacecraft	Power Source	Mission Type	Status
16 APR 1972	Apollo 16	SNAP-27	Lunar Surface	RTG shut down after 5.5 years of operation.
02 APR 1972	Transit	Transit-RTG	Navigational	RTG still operating.
07 DEC 1972	Apollo 17	SNAP-27	Lunar Surface	RTG shut down after 5 years of operation.
05 APR 1973	Pioneer 11	SNAP-19	Planetary	Spacecraft operated to Jupiter and Saturn.
20 AUG 1975	Viking 1	SNAP-19	Mars Surface	RTG shut down after 6 years of operation.
09 SEP 1975	Viking 2	SNAP-19	Mars Surface	RTG operated 4 years until relay link was lost.
14 MAR 1976	LES 8	MHW-RTG	Communication	RTG still operating.
14 MAR 1976	LES 9	MHW-RTG	Communication	RTG still operating.
20 AUG 1977	Voyager 2	MHW-RTG	Planetary	RTG still operating. Operated to Jupiter, Saturn, Uranus, Neptune.
05 SEP 1977	Voyager 1	MHW-RTG	Planetary	RTG still operating. Operated to Jupiter, Saturn, and beyond.
18 OCT 1989	Galileo	GPHS-RTG	Planetary	RTG still operating. Spacecraft orbiting around Jupiter.
06 OCT 1990	Ulysses	GPHS-RTG	Planetary/Solar	RTG still operating. Spacecraft in polar orbit around the sun.
15 OCT 1997	Cassini	3-RTGs	Planetary	RTGs still operatin. Spacecraft en route to Saturn.

Table 3. RTG Missions [After Ref. 15.]

This table shows that RTG’s are capable of providing power over long periods of time. The first RTG sent into space in June of 1961 on the Transit 4A spacecraft is still providing power [Ref. 15]. Figure 16 shows a rendering of a current RTG module [Ref. 16].

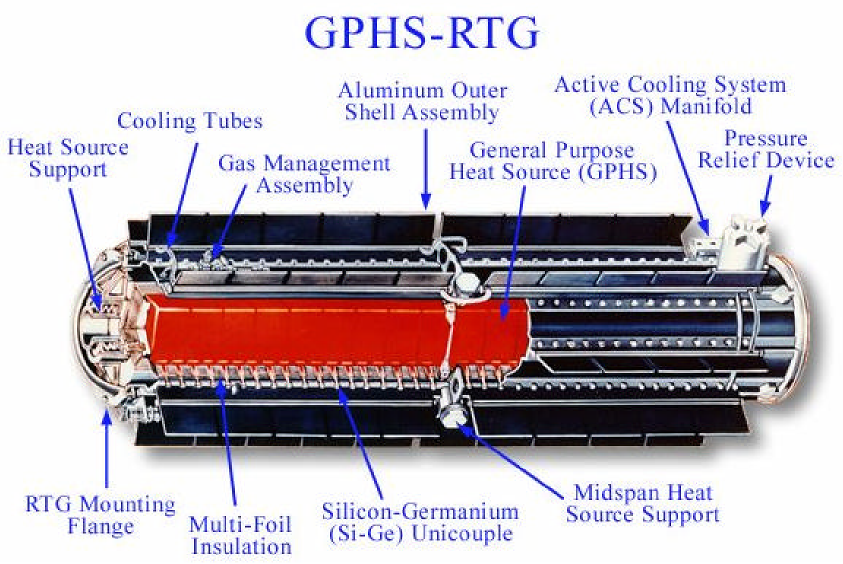
GPHS-RTG
Aluminum Outer Shell Assembly
Active Cooling System (ACS) Manifold
Cooling Tubes
Heat Source Support
Gas Management Assembly
General Purpose Heat Source (GPHS)
Pressure Relief Device
RTG Mounting Flange
Multi-Foil Insulation
Silicon-Germanium (Si-Ge) Unicouple
Midspan Heat Source Support

Figure 16. RTG Module [From Ref. 16.]

B. FUEL SUPPLY

An RTG fuel supply must be able to balance a high power-to-mass ratio with a long lifetime and reasonable safety. As mentioned previously, current RTGs have used Pu-238 as a heat source. Pu-238 has a half-life of 87 years, meaning that after 20 years of operation it will still produce 80% of the power it produced when new [Ref. 17]. Figure 17 shows the power output versus time for a Pu-238 heat source [Ref. 17]. This isotope, when pure, has a relatively large power to mass ratio of 540 W/kg [Ref. 17].

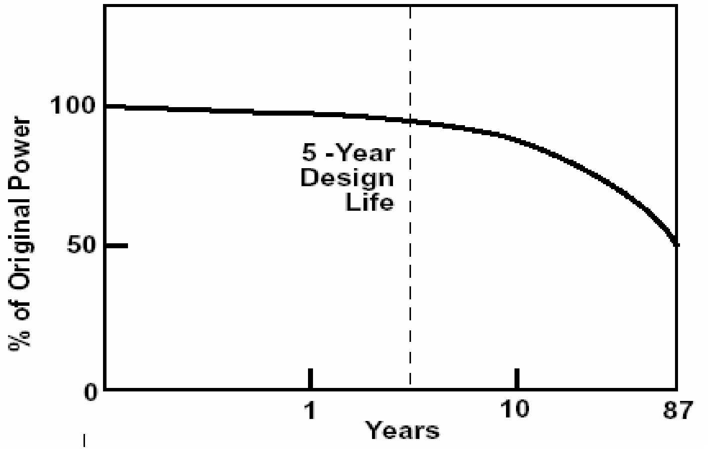

Figure 17. Pu-238 Power Output [From Ref. 17.]

Other fuel supplies have been considered for use with RTG's as well. Strontium 90 (Sr-90) for example was considered as a possible fuel source. With a half life of 28.1 years, Sr-90 decays much faster than Pu-238 [Ref. 18]. After 20 years, it will only produce approximately 60% of the power it originally did [Ref. 18]. In addition, the power to mass ratio when new is only 460 W/kg which is more than 15% lower that that of Pu-238 [Ref. 18].

Although the use of Pu-238 has startled many people, it is actually a rather safe fuel. In order to demonstrate to the public how safe the use of Pu-238 is, President Eisenhower had the picture in Figure 18 published in the newspaper taken in the Oval Office at the White House with senior members United States Atomic Energy Commission (AEC) and an early RTG module [Ref. 17].

Figure 18. “President Shows Atom Generator” [From Ref. 17.]

C. SAFETY

1. Accident History

In total the United States Department of Energy has provided 44 RTG’s and more than 240 general-purpose heat source (GPHS) units since 1961 with only three accidents [Ref. 17]. The first of these accidents occurred on the Transit 5-BN-3 launched in April of 1964. This mission had to be aborted when the launch vehicle failed. The vehicle and RTG burned up in the atmosphere upon reentry where the Pu-238 fuel source was vaporized and dispersed into the upper atmosphere as it was designed to do [Ref. 17]. Shortly after this accident, the RTG module was redesigned to survive atmospheric reentry with the fuel source intact [Ref .17].

The second accident occurred on the Nimbus-B-1 launched in May of 1968 [Ref. 17]. This mission had to be aborted shortly after launch by a range safety destruct [Ref. 17]. The newly designed RTG module held up through reentry and was recovered without any radiation leakage. The fuel source was reused on later missions [Ref. 17].

The third and final accident occurred on Apollo 13 launched in April of 1970. This mission carried an RTG intended to provide power to a lunar seismic station [Ref. 17]. The RTG was located on the lunar module which broke up on reentry into earth’s atmosphere [Ref. 17]. The RTG remained intact and is now located at the bottom of the Tonga Trench in the Pacific Ocean [Ref. 17].

2. Safety Measures

Many features have been added to RTG's to ensure their safe operation under all conditions. Figure 19 shows a diagram of a modern RTG unit [Ref. 19].

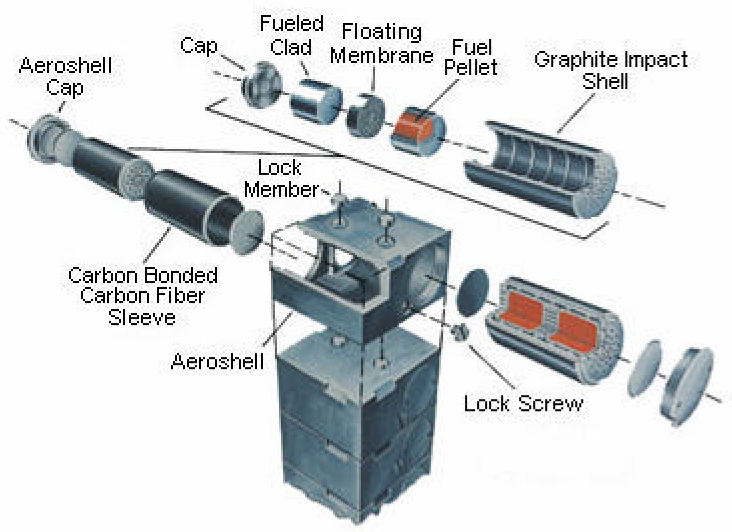

Figure 19. RTG Safety Measures [From Ref. 19.]

It can be seen from the figure that the fuel pellet makes up a very small percentage of the unit while added safety features occupy the majority of the area. The fuel itself has even been modified for safety purposes. The original Pu-238 metal has been replaced with plutonium dioxide [Ref. 17]. This heat resistant ceramic form prevents the fuel from vaporizing under extreme heat conditions such atmospheric reentry [Ref. 17]. The material is also insoluble and has a very low chemical reactivity making it safe even if it ends up in the ocean like the module from Apollo 13 [Ref. 17]. This ceramic form also influences how the material breaks up. Instead of becoming a fine powder that can easily spread, it fractures into large non-respirable chunks [Ref. 17]. As an added safety measure, the fuel is separated into small pellets that are each individually encapsulated in a heat shield and impact shell. The module itself is enclosed in an iridium capsule and surrounded by graphite blocks [Ref. 17]. These are high strength and corrosion and heat resistant materials. The RTG unit is designed to withstand conditions it could never realistically encounter.

The Pu-238 in RTG's is an alpha emitter [Ref. 17]. The majority of alpha particles can be absorbed by a piece of paper or the epidermal layer of human skin [Ref. 17]. RTG's do not utilize either fission of fusion in producing heat [Ref. 17]. Because of this, an RTG could never explode like a nuclear bomb. In addition, no accident involving an RTG could ever create the acute radiation sickness associated with nuclear explosions or meltdowns [Ref. 17].

3. Safety Testing

As previously mentioned, RTG modules are designed to endure conditions they could never realistically face. In order to ensure the safety of the modules, they are tested under extremely harsh conditions [Ref. 17].

a. Fire

Extreme heat upon atmospheric reentry and other unforeseen accidents can cause fires onboard a spacecraft. RTG's have been directly exposed to intense fires with minimal damage [Ref. 17]. Most importantly, no fuel was released during exposure.

b. Blast

A shuttle explosion can cause tremendous shockwaves. The RTG module was tested under blast waves stronger than those expected from such an explosion and once again remained intact without releasing any nuclear fuel or harmful radiation from the unit [Ref. 17].

c. Reentry

In the event that a satellite degrades in orbit enough to reenter the earths atmosphere, it will experience intense amounts of heat. An RTG is designed to survive reentry while preventing the Pu-238 fuel source from vaporizing in the atmosphere. This environment was tested using an arc-jet furnace, and the RTG was able withstand the heat safely [Ref. 17].

d. Earth Impact

Since RTG's were redesigned to survive atmospheric reentry intact, they also had to be strong enough to survive impact with earth's surface. RTG's were tested at the maximum estimated velocity of the module approaching earth's surface of 120 miles per hour. These tests showed that in an impact with water, soil, and sand the module would remain safely intact. An impact with rock or concrete, however, sometimes caused slight leakage resulting in small amounts of low-level radiation in localized areas [Ref. 17].

e. Immersion in Water

Because the vast majority of earth's surface is covered in water, RTG's must be able to survive in an aquatic atmosphere. Long term exposure to sea water proved the protective iridium capsule to be corrosion resistant and the fuel to be highly insoluble [Ref. 17].

f. Shrapnel

In the event of an explosion or impact with space debris, an RTG could be subjected to shrapnel. Aluminum and titanium bullets were used to simulate such shrapnel from a launch explosion. Fragments at speeds much greater than those predicted to be present in such an event were unable to penetrate the module [Ref. 17].

g. Large Fragments

In the event of a solid rocket booster failure, the RTG module could be subject to impact by large fragments of material. To simulate this scenario, large steel plates were fired at an RTG. The studies showed that damage only occurred in the unlikely event that the corner or sharp edge of a large fragment struck the module [Ref. 17].

D. FUTURE IMPROVEMENTS

Current RTG's use silicon/germanium thermocouples discussed in the previous chapter to convert thermal power from the Pu-238 heat source into electrical power [Ref. 13]. These thermocouples operate at very low efficiency levels of only a few percent. The key to improving RTG power production is to find a more efficient way to convert thermal power into electrical power.

1. Dynamic Isotope Power Systems

Dynamic isotope power systems (DIPS) convert thermal energy into electrical energy using moving parts. Created in 1816 by Robert Stirling, the Stirling engine is the most important dynamic isotope power system to space power systems [Ref. 20]. Unlike combustion engines, Stirling engines have a closed gas chamber [Ref. 20]. There are no explosions that take place in a Stirling engine and there is no gas exhausted from the engine. The power to run this engine comes from an external heat source [Ref. 20]. Figure 20 shows a simplified example of a Stirling engine [Ref. 20].

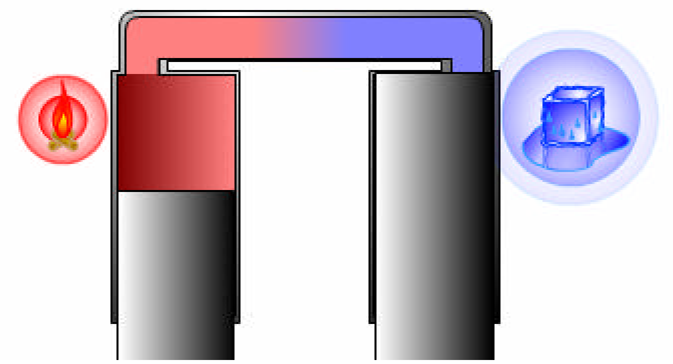

Figure 20. Simplified Stirling Engine [From Ref. 20.]

There are four steps in the Stirling cycle [Ref. 20]:

1. Heat is added to the hot cylinder (left), causing pressure to build. This pushes the left piston down.

2. The left piston moves up and the right piston moves down. This pushes the heated gas from the left cylinder into the cold cylinder on the right where the gas is quickly cooled down. When the gas cools, the pressure goes down making it easier to compress in step 3.

3. The piston in the cold cylinder on the right compresses the gas. Heat generated by this compression is almost instantly removed by the cooled cylinder.

4. The right piston moves up while the left piston moves down forcing the gas into the heated cylinder on the right. This cylinder quickly heats the gas raising the pressure in the cylinder.

The cycle then repeats.

In this four-step cycle, power is only created in the first step. There are two ways to increase the power output of a Stirling engine. The first method is to increase the power output of stage one [Ref. 20]. This is accomplished by raising the pressure of the gas in the hot cylinder which is done by increasing the temperature of the external heat source. The second method for increasing the power output is lowering the gas pressure in the cold cylinder [Ref. 20]. This is accomplished by lowering the temperature of the cylinder. The Stirling engine, like a thermocouple, produces a power output related to the difference in temperature of the hot and cold cylinders.

The Stirling engine is not suitable for widespread use for two main reasons. Because the heat source is external to the engine, it takes some time for the engine to warm up before it can produce useful power [Ref. 20]. Secondly, the engine is slow to respond to changes in the power supply [Ref. 20].

Stirling engines do however, show promise as a means of power generation for space based systems. NASA Glenn has been developing Stirling engine technology since the 1970’s and has been developing radioisotope power systems for deep space missions since 1990 [Ref. 21]. Figure 21 shows a Stirling generator developed by NASA Glenn [Ref. 21].

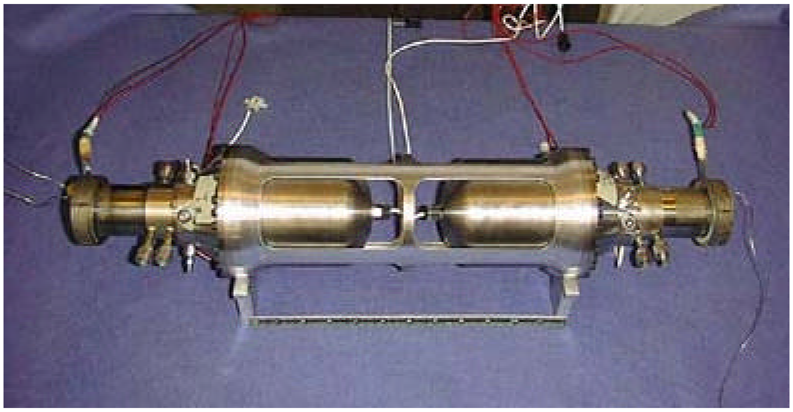

Figure 21. 110 Watt Electric Stirling Generator [From Ref. 21.]

This figure shows two synchronized 55 watt electric generators. This configuration reduces vibrations in the system. The addition of internal precision springs and dampers causes this engine to operate at a resonant frequency that increases the efficiency of the system. This model has been tested to work at an efficiency level of over 20% [Ref. 21].

2. Alkaline Metal Thermal-to-Electric Conversion

Figure 22 shows the schematic diagram of a simple alkaline metal thermal-to-electric conversion (AMTEC) system [Ref. 22].

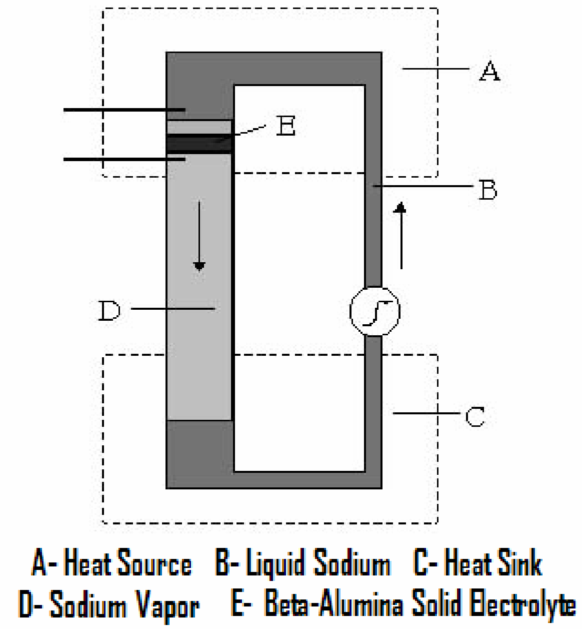
A
E
B
D
C
A- Heat Source B- Liquid Sodium C- Heat Sink
D- Sodium Vapor E- Beta-Alumina Solid Electrolyte

Figure 22. AMTEC Schematic [From Ref. 22.]

The key to this converter is the beta-alumina solid electrolyte (BASE). This conducts positive sodium ions much better than it conducts sodium atoms or electrons [Ref. 22]. When heat is applied to one side, a sodium pressure difference occurs across the base and the positive ions move through the base and collect on the low pressure side leaving electrons to collect on the high pressure side [Ref. 22]. This creates a potential across the base that can force a current to flow through a load [Ref. 22]. Similar to the previously discussed thermoelectric converters, the power produced by an AMTEC system is dependent on a large temperature difference between the hot and cold ends, but currently the efficiency of such systems is very low [Ref. 22].

3. Thermophotovoltaic Cells

Thermophotovoltaic (TPV) cells are currently the most promising thermoelectric converters for replacing the thermocouple in RTG's. Although they are currently not capable of the operating efficiencies of Stirling engines, TPV cells have the advantage of no moving parts [Ref. 3]. These cells are discussed in more depth in the previous chapter.

The radioisotope thermoelectric generator was introduced in this chapter. The current system as well as possible future improvements were covered. The next chapter will begin the discussion on the simulation software used in this thesis.

THIS PAGE INTENTIONALLY LEFT BLANK

V. SIMULATION SOFTWARE

There is currently a great deal of research being done on building accurate models of solar and thermophotovoltaic cells. While some models can provide relatively accurate results in limited cases, there is no widely available software package that is capable of modeling all of the necessary parameters needed to provide models of cells of various materials under many different spectra. This thesis explores the use of Silvaco Virtual Wafer Fabrication software to accomplish this task.

A. SILVACO

Silvaco International is a software company that provides programs for modeling all areas of electronics including digital and analog circuits [Ref. 23]. The company has software ranging from simple Spice modeling to advanced integrated circuit layout and extraction tools. The Virtual Wafer Fabrication package is part of Silvaco's TCAD suite. It was designed to accurately emulate physical wafer manufacturing [Ref. 23]. The package allows users to easily optimize all aspects of IC design before actually fabricating them. ATLAS is the main program in this Virtual Wafer Fabrication package that will be used in this research. This program can handle one-, two-, and three-dimensional designs and contains the following comprehensive models [Ref. 23]:

- DC, AC small-signal, and full time-dependency
- Drift-diffusion transport models
- Energy balance and hydrodynamic transport models
- Lattice heating and heatsinks
- Graded and abrupt heterojunctions
- Optoelectronic interactions with general ray tracing
- Amorphous and polycrystalline materials
- General circuit environments

- Stimulated emission and radiation
- Fermi-Dirac and Boltzmann statistics
- Advanced mobility models
- Heavy doping effects
- Full acceptor and donor trap dynamics
- Ohmic, Schottky, and insulating contacts
- SRH, radiative, Auger, and surface recombination
- Impact ionization (local and non-local)
- Floating gates
- Band-to-band and Fowler-Nordheim tunneling
- Hot carrier injection
- Thermionic emission currents

ATLAS is a powerful program, but it relies on the aid of several other Silvaco programs to build an accurate model of a circuit. The program Deckbuild is the run time environment for this software package. A TPV cell can be defined graphically from the command line in this program in a method that will be discussed later. ATHENA, the process simulator, actually builds the devices defined by the commands entered in the Deckbuild interface [Ref. 23]. DevEdit is another program that allows a user to define cell graphically by defining mesh lines and nodes on a plane [Ref. 23]. This can also be done directly through Deckbuild as will be discussed later. In addition to run time output, ATLAS also writes *.log files which contain the output data solved for during simulations. The output gathered from these simulations was voltage and current levels and photogeneration rates. The included program TonyPlot can input these *.log files and present the information in a graphical form. Figure 23 shows a block diagram of how these programs interact to solve a particular TPV cell [Ref. 23].

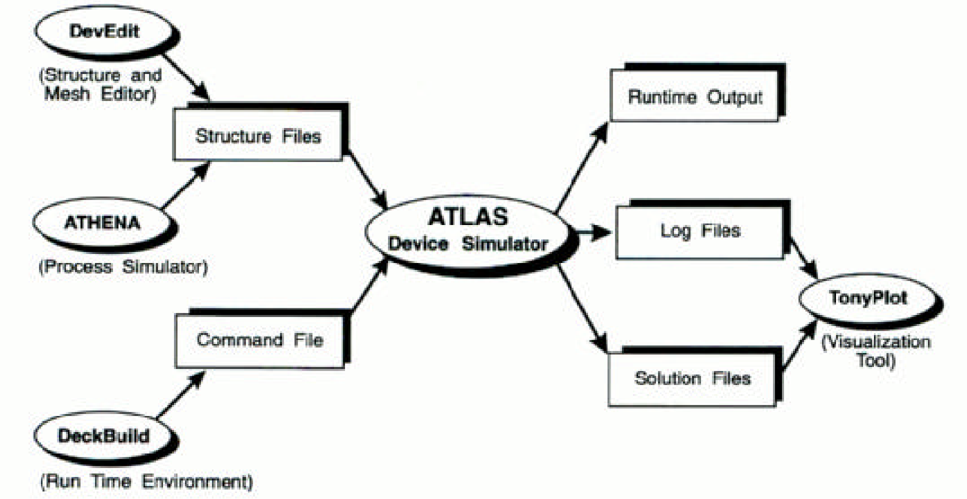

Figure 23. Simulator Block Diagram [From Ref. 23.]

B. DEFINING A CELL

In this thesis, solar and TPV cells were defined graphically in ATLAS through the Deckbuild interface. In order to fully define a cell, it was necessary to enter not just dimensions, but also material properties. The following format was used in building each model.

- Defining constants (cell dimensions, doping levels, shading, etc.)
- Defining mesh boundaries using the previously defined constants
- Building the X- mesh
- Building the Y-mesh
- Defining regions (anode, cathode, contacts, etc.)
- Placing electrodes
- Defining doping levels in each region
- Defining material properties (electrical, optical, band, etc.)
- Adding incident spectrum
- Solving

1. Defining Constants

ATLAS allows a user the option of building a model directly by inputting dimensions in numbers or indirectly by entering dimensions as variables names that have been previously defined. In this thesis, it was necessary to be able to change various dimensions quickly and easily so the second method of defining a cell was utilized.

The first portion of the code was dedicated to defining constants that would later be used in calculations. For example

```
set cathodethickness=10
set cathodedoping=1.000000e+020
set anodethickness=.37
set anodedoping=9.8e19
set bsfthickness=15.000000
set bsfdoping=1.000000e+020
```

defines constants that represent the thickness and doping level for the cathode, anode, and BSF layers of a cell. These variables can now be used later in the program. The benefit to defining dimensions in this manner is that by simply changing the variable definition, the whole model is altered to reflect this change making iterations quick and easy to execute.

2. Defining Mesh Boundaries

ATLAS solves equations at many different nodes in a defined area. These nodes are defined by meshes. The constants defined in the first part of the ATLAS code are used in defining mesh boundaries. The following commands are an example of how mesh boundaries are defined in a cell.

```
set bsfL=0
set bsfH=$bsfL-$bsfthickness
set bsfdivs=$bsfthickness/$divs
set catL=$bsfH

set catH=$catL-$cathodethickness

set catdivs=$cathodethickness/$divs

set anoL=$catH

set anoH=$anoL-$anodethickness

set anodivs=$anodethickness/$divs
```

The dollar sign is an indication to ATLAS that the following string is a user defined constant. In ATLAS, moving up on the Y-axis is in the negative direction so these commands define a cell by starting at $Y = 0$ and building upwards including divisions in each region.

3. Building the X- and Y- Meshes

ATLAS requires that each region boundary fall on a mesh. In order to ensure that this is the case, mesh lines are manually drawn at each of these boundaries using the following commands.

```
x.mesh loc=0 spac=$cellwdiv

x.mesh loc=$contLL spac=$capwdiv

x.mesh loc=$contRR spac=$capwdiv

x.mesh loc=$cellwidth spac=$cellwdiv

y.mesh loc=$contH spac=$contdivs

y.mesh loc=$capH spac=$capdivs

y.mesh loc=$catH spac=$catdivs

y.mesh loc=$anoH spac=$anodivs

y.mesh loc=$bsfH spac=$bsfdivs

y.mesh loc=$bsfL spac=$bsfdivs
```

Each of these command lines defines both a location and a spacing interval. ATLAS will draw mesh lines at each defined location as well as lines at the defined spacing interval. When two defined mesh lines with different spacing intervals are next to each other, ATLAS will automatically grade the mesh spacing between the two lines. Figure 24 shows an example of a typical mesh.

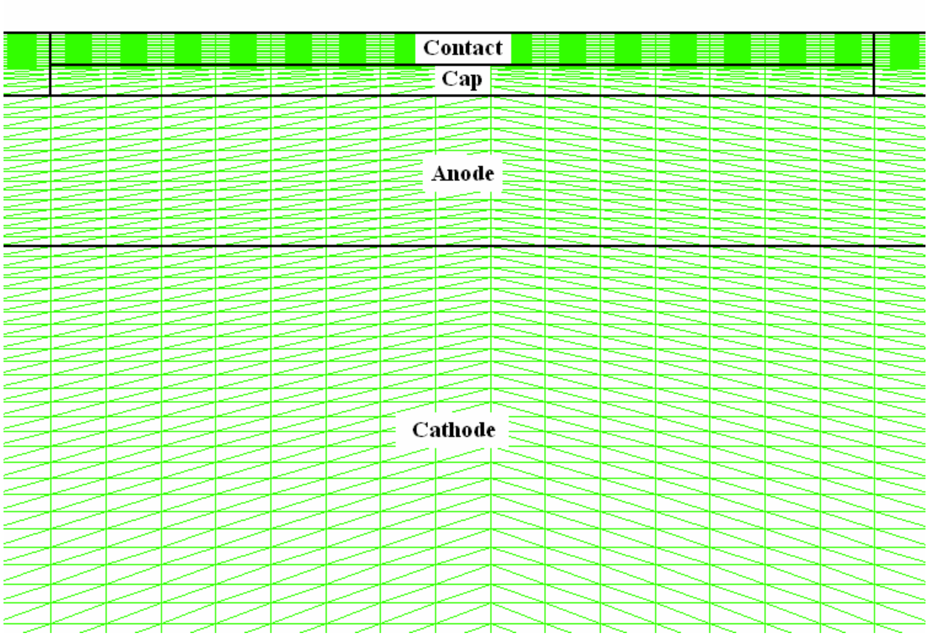

Figure 24. Typical Mesh

When defining a mesh, it is important to take careful note of the spacing. In order to get an accurate solution, the mesh must be fine enough to get an accurate representation of the cell. If the mesh is too fine, however, it will take an unnecessarily long time to solve all of the nodes.

4. Defining Regions

Each layer of a cell must be defined by a material and region boundaries. As previously mentioned, these boundaries must fall on already defined mesh lines. The following commands are used to define regions in the GaSb cell shown in Figure 25. The bracketed numbers represent the value of each variable used in micrometers and are not included in the actual code. This cell has a 0.1 *m*m thick cap, 0.37 *m*m anode, and a 10 *m*m thick cathode. The BSF layer defined in these commands cannot be seen in Figure 25.

```
#Anode
region num=5 material=GaSb x.min=0 x.max=$cellwidth[500]
        y.min=$anoH[-350.37] y.max=$anoL[-350]
#Cathode
region num=6 material=GaSb x.min=0 x.max=$cellwidth[500]
        y.min=$catH[-350] y.max=$catL[-340]
#BSF
region num=7 material=GaSb x.min=0 x.max=$cellwidth[500]
        y.min=$bsfH[-340] y.max=$bsfL[0]
```

Figure 25 shows a plot of cell regions generated by TonyPlot.

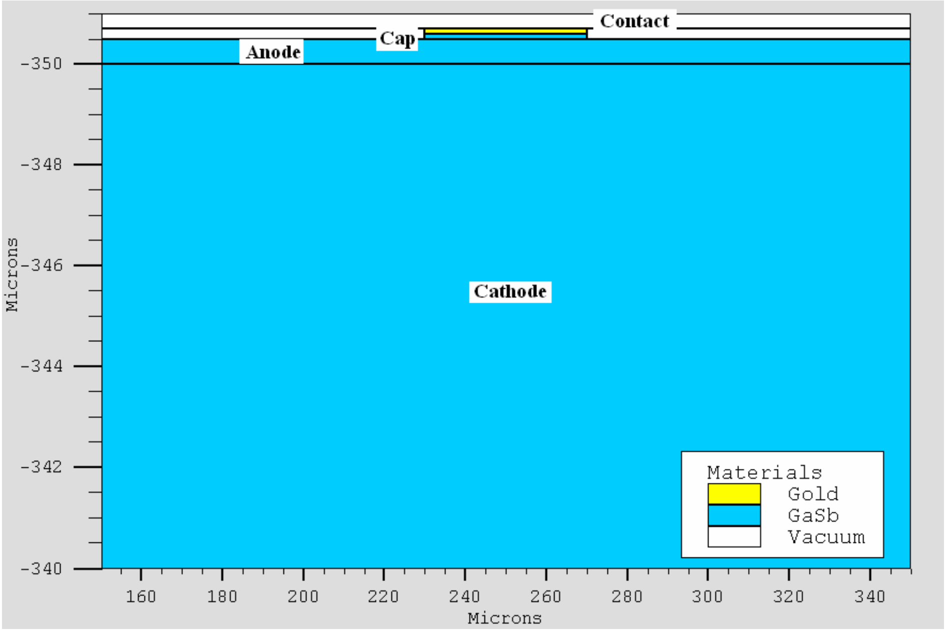

Figure 25.   Cell Regions

5. Placing Electrodes

Once the cell regions are fully defined, electrodes must be defined to electrically connect to the cell. ATLAS allows a user to define an ideal contact or specify a particular material with non-ideal properties. It is even possible to add external discrete components to the cell such as resistors, inductors, and capacitors. Electrodes are defined using the following commands.

```
electrode name=anode material=Gold x.min=$contLL x.max=$contRR
    y.min=$contH y.max=$contL

electrode name=cathode material=Gold x.min=0 x.max=$cellwidth
    y.min=$bsfL y.max=$bsfL
```

6. Defining Doping Levels

The doping level in each region can be defined independently using the following commands.

```
# Anode

doping uniform region=5 p.type conc=$anodedoping

# Cathode

doping uniform region=6 n.type conc=$cathodedoping
```

This defines a constant doping level in a region. The boundaries between two regions will have abrupt junctions. For more realistic and more complex doping schemes, Silvaco provides a C-Interpreter, which allows a user to define any conceivable doping.

7. Defining Material Properties

Using the following commands, the user can define as many material properties as are available.

```
material material=GaSb COPT=5e-10

material material=GaSb EG300=.726 PERMITTIVITY=14.4
    AFFINITY=4.06
```

```
material material=GaSb NC300=2.1e17 NV300=1.8e19

material material=GaSb index.file=GaSb.opt
```

These commands define optical recombination, energy band gap, permittivity, electron affinity, available conduction and valence band states, and optical parameters for the material gallium antimonide (GaSb). The index file ‘GaSb.opt’ contains refractive index and extinction parameters for a span of wavelengths in the area of interest. This is one of the most important material properties to accurately define and subsequently one of the most difficult to find. Figure 26 shows a plot of the data from ‘GaSb.opt’.

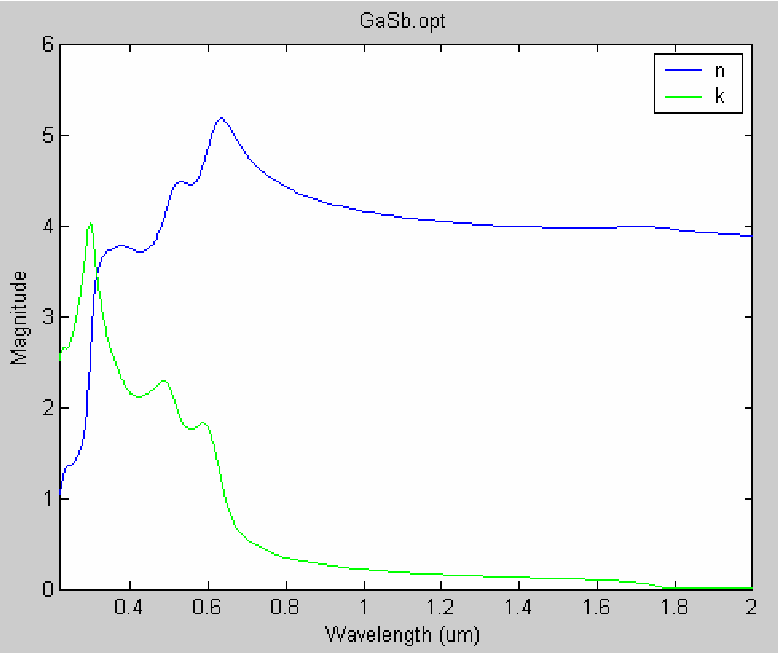

Figure 26. ‘GaSb.opt’ [Data for Plot is From Ref. 21]

8. Incident Spectrum

ATLAS allows a user to define a spectrum with a *.spec file as follows.

```
beam num=1 x.origin=0 y.origin=$lightY angle=90 back.refl
        power.file=1300BB.spec wavel.start=0.207 wavel.end=5
        wavel.num=1000
```

The *.spec file gives the spectral radiance at various wavelengths in the region of interest. This command tells ATLAS to read in the data from the file '1300BB.spec' and to solve a cell using 1000 evenly spaced rays in the interval from $0.207\ \mu\text{m} - 5\ \mu\text{m}$. The command also defines the origin of the beams and the incident angle.

9. Solving

The cell and its environment are now completely defined in ATLAS and the program can now use this model to solve. The equations that are to be solved depend on what type of output is desired. This thesis concentrates on current-voltage relationships and photogeneration rates. By providing ATLAS with a number of current levels, it can solve for the associated voltage levels in order to produce an *I-V* curve as follows.

```
solve ianode=0 b1=$I

solve ianode=-$i1 b1=$I

solve ianode=-$i2 b1=$I

solve ianode=-$i3 b1=$I

solve ianode=-$i4 b1=$I

…
```

If photogeneration rates are desired, the user can tell ATLAS to solve for the photogeneration with discrete wavelengths of light incident on the cell as follows.

```
solve b1=0.1 lambda=0.3

solve b1=0.1 lambda=0.4

solve b1=0.1 lambda=0.5

solve b1=0.1 lambda=0.6

…
```

The output of the data generated from solving these equation is stored in a *.log file which can be viewed graphically using TonyPlot.

10. Source Code

The sample code given in this section was taken from a model for a GaSb cell. The full source code for both this cell and an InGaAs cell can be found in Appendix A.

C. MATLAB

The Silvaco software package is capable of performing all of the actions necessary to model a cell and graph the output, but it was often useful to use Matlab programs to supplement Silvaco for some operations.

1. Iterations

While ATLAS is capable of solving many very complex equations, it does lack some very basic programming capabilities such as conditional statements and loops that are necessary for performing iterations. Several programs (found in Appendix B) were written in Matlab to execute these functions. The program ‘atlasrun.m’ was used to run the iterations. In each iteration, ‘atlasrun.m’ would run an input deck with ATLAS, read and analyze the output data, iterate a parameter in the input deck, and rerun ATLAS. The program ‘ivmaxp.m’ solved for open-circuit voltage, short circuit current, maximum power, fill factor, and efficiency for each iteration and recorded this data in an output file. ‘filerw.m’ was used to iterate a specified parameter in the input deck after each run.

2. Plotting

The TonyPlot program provided by Silvaco is capable of producing plots of all data that is generated by ATLAS, but it often more convenient to use Matlab to plot the data. In addition to running the iteration scheme, ‘atlasrun.m’ would also update an efficiency plot after each run of ATLAS. Since most optimization schemes took several hours to run, this feature provided up to date visual feedback on the progress of the routine. The program ‘filerw.m’ was also used to plot *I-V* curves with a marked maximum power point on each curve.

All of these programs can be found in full in Appendix B.

This chapter covered the simulation software used in this thesis. Silvaco and Matlab were both utilized extensively for building and analyzing TPV cell models. The next chapter will cover the actual models built along with their resulting outputs.

VI. MODELS AND RESULTS

This chapter discusses the models that were built in ATLAS. In each case, a sample model was built and the output of this model was compared to accepted values. Once the model was verified, it was optimized for both AM0 and the spectrum from a 1300K blackbody using an iteration routine written in Matlab.

A. MODEL CONFIRMATION

Before a TPV cell could be optimized for a blackbody spectrum, it was first necessary to confirm that the model being used was accurate. Although there was no data available on cells under a 1300K blackbody spectrum, there was available data on many different cells under the AM0 spectrum. In addition, using Equation 2.2 the frequency response of a cell could be estimated. The assumption is that if the model can accurately predict the output of a cell under AM0 and has the proper frequency response, it should also accurately predict the output under a different spectrum.

1. Gallium Arsenide

Gallium Arsenide (GaAs), while not suitable for TPV applications, is one of the most widely used materials for solar cells and therefore the maximum current-voltage relationship for this cell is very well documented. A 1 cm^2 GaAs cell should provide approximately $I_{sc} = 31\text{ mA}$ and $V_{oc} = 1\text{ V}$ [Ref. 3]. The cell in Figure 27 was built and tested in ATLAS. ATLAS was found to do a poor job of modeling antireflective coatings, so a 5% loss was assumed in all models. With present AR coating technology this is a very reasonable assumption.

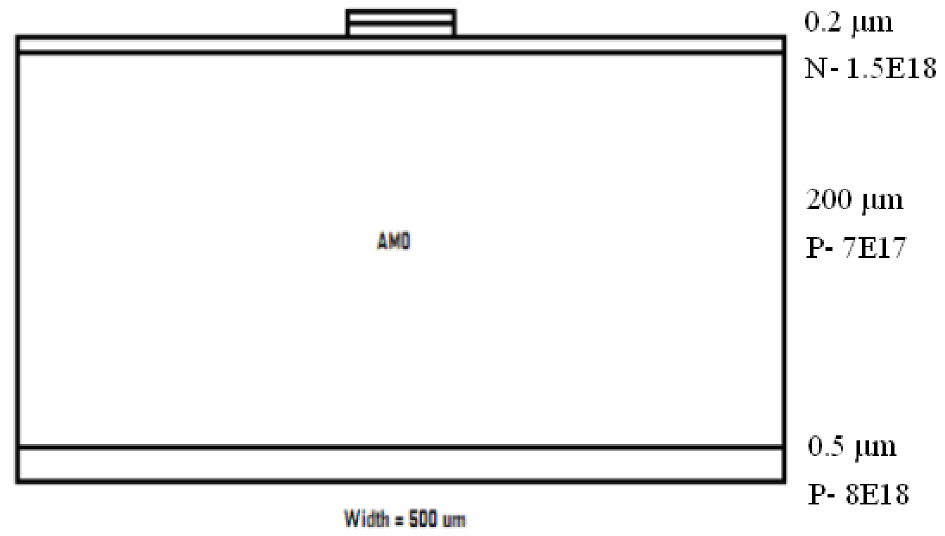

Figure 27. GaAs Solar Cell

Figure 28 shows the IV curve from this cell.

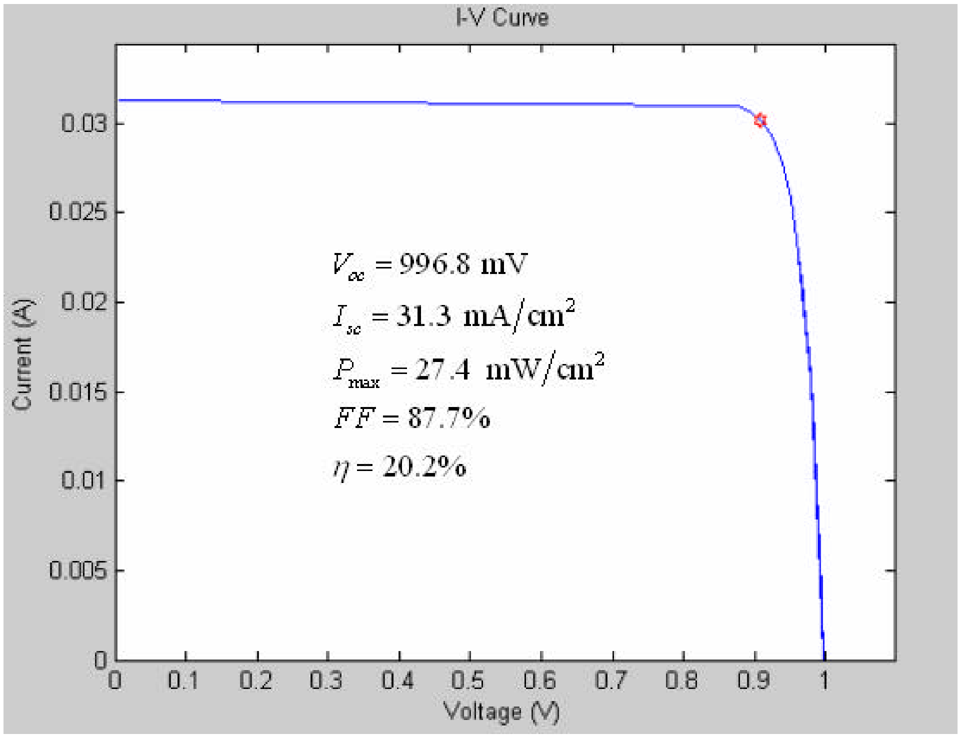

Figure 28. GaAs Cell Results

From Equation 2.2, the spectral response of a GaAs cell should approach zero at a wavelength of approximately 0.89 µm . Figure 29 shows the calculated spectral response with a peak at 0.87 µm compared to the normalized AM0 spectrum. As expected, this graph does approach zero at 0.89 µm . It is also important to note that the spectral response is closely correlated to the spectrum, thus the large power output.

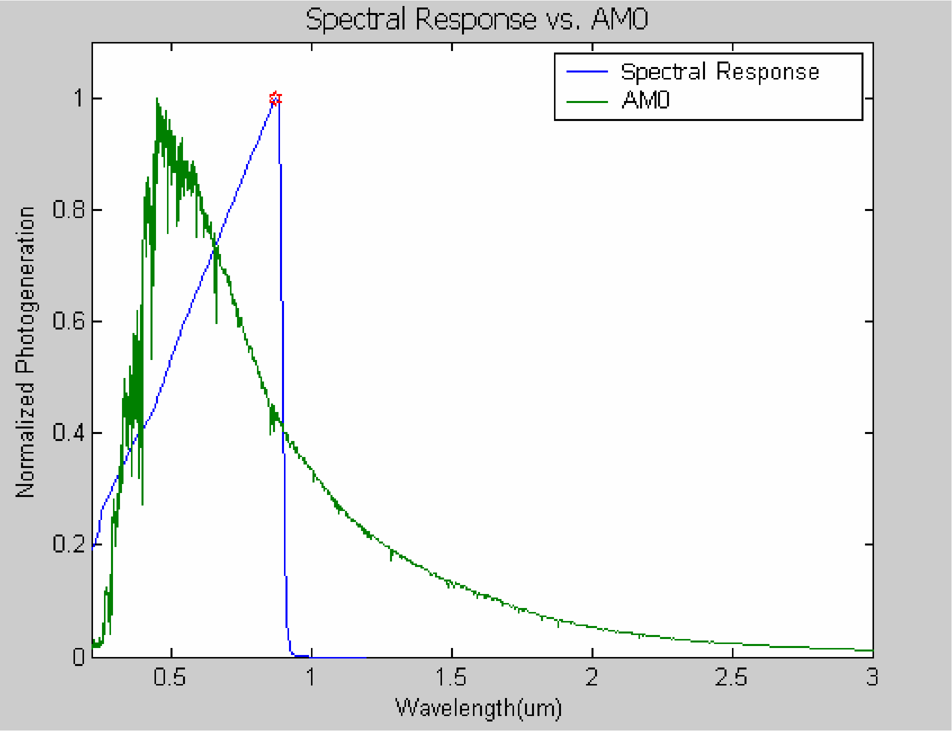

Figure 29. Spectral Response of GaAs

It is important that this graph go to zero in the correct place. This may not affect some cells under AM0 because only a relatively small amount of energy is in the spectrum above where the response goes to zero, but the spectrum from a 1300K blackbody, however, contains most of its energy at wavelengths longer than the cell should be able to respond to. If the spectral response does not go to zero, the model will allow the cell to respond to these higher wavelengths and give incorrect results.

This GaAs cell model demonstrates that ATLAS is capable of providing a very accurate model of a solar cell.

2. Gallium Antimonide

The next cell built was a gallium antimonide (GaSb) cell. This material is currently one of the best candidates for replacing the thermocouples currently used in RTG's. It was difficult to find data to compare with the results of this model. Most publications in this area measure these cells under concentrators and skew the efficiency calculations to appear more favorable. One documented cell claimed to achieve approximately $V_{oc} = 33 \text{ mV}$ and $I_{sc} = 34.7 \text{ mA}$ under AM1.5 from a 1 cm^2 cell [Ref. 24]. This cell model seen in Figure 30, measured under AM0 produced the output shown in Figure 31.

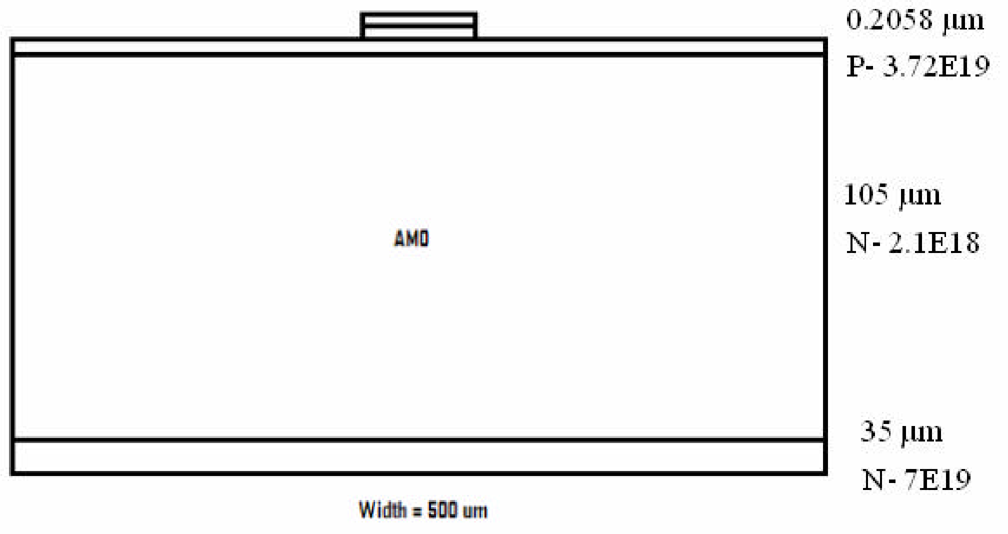

Figure 30. GaSb Solar Cell

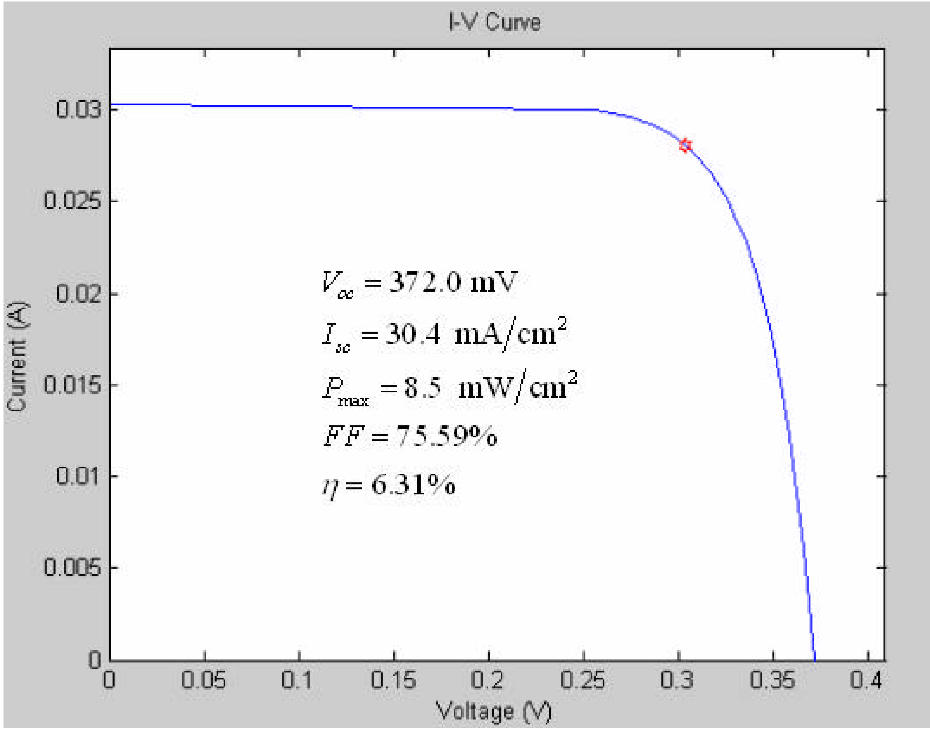

Figure 31. GaSb Solar Cell *I-V* Characteristics

In addition to testing this cell under AM0, the incident spectrum was altered to model the spectrum from a concentrator at 68 and 70 suns concentration [Ref. 25]. The results from these runs very closely correlated with published data on this cell.

From Equation 2.2 the spectral response of a GaSb cell should approach zero at a wavelength of 1.7 µm. Figure 32 shows the spectral response of a GaSb cell compared to the normalized AM0 spectrum. It can be seen from the figure that this response peaks at $l = 1.65$ µm, and, as expected, it approaches zero at the correct wavelength.

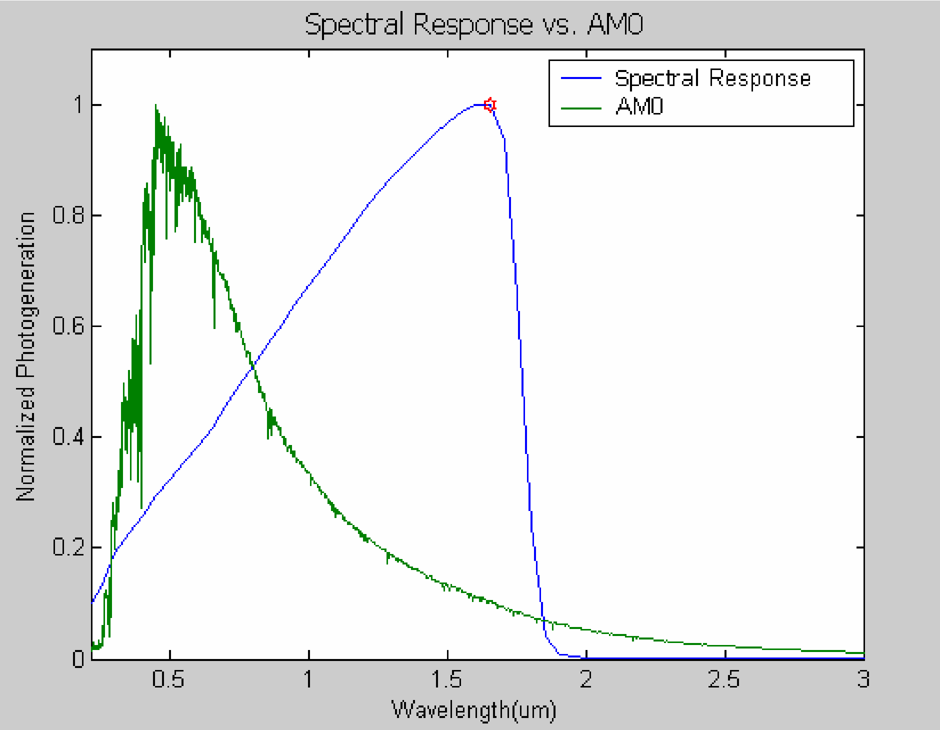

Figure 32. Spectral Response of GaSb

3. Indium Gallium Arsenide

The final cell built was an indium gallium arsenide. The bandgap of this material is related to the molar concentration of gallium in the compound. By varying this concentration, the bandgap can be varied from 0.35 eV to 1.42 eV [Ref. 26]. At an In/Ga concentration of 0.72/0.28 InGaAs has an energy bandgap of 0.55 eV [Ref. 14]. It is this cell that was modeled here.

Unlike GaSb, there was a great deal of published data on InGaAs cells under AM0 and other spectra as well. Unfortunately, because research on this material is in the early stages, there is still a great deal of inconsistency in published results. The recorded short circuit current data varied greatly from $30\text{mA}/\text{cm}^2$ to $60\text{mA}/\text{cm}^2$ and recorded open-circuit voltage data varied from 0.2 V to 0.4 V, so it was difficult to determine the accuracy of this model [Ref. 26]. The cell in Figure 33 was built and found to give results that fell within this range. The actual output of this model can be seen in Figure 34.

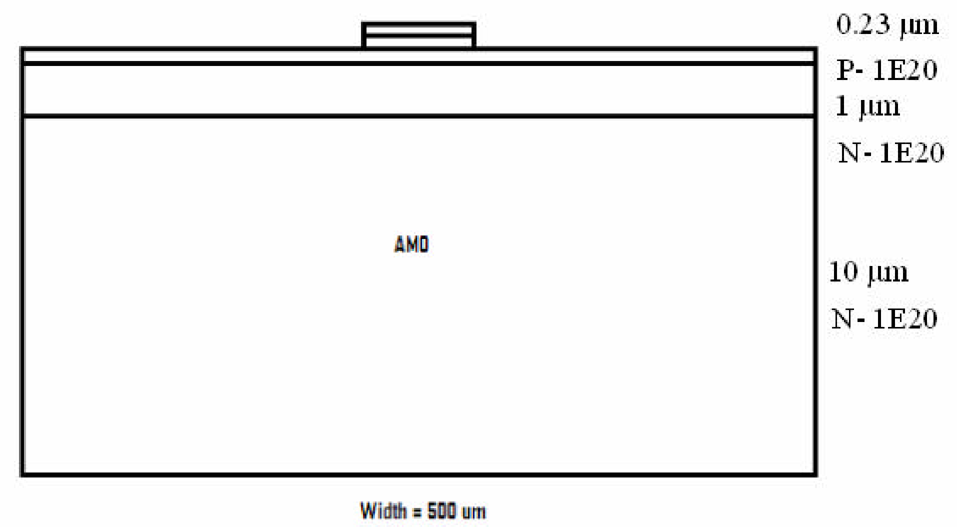

Figure 33. InGaAs Solar Cell

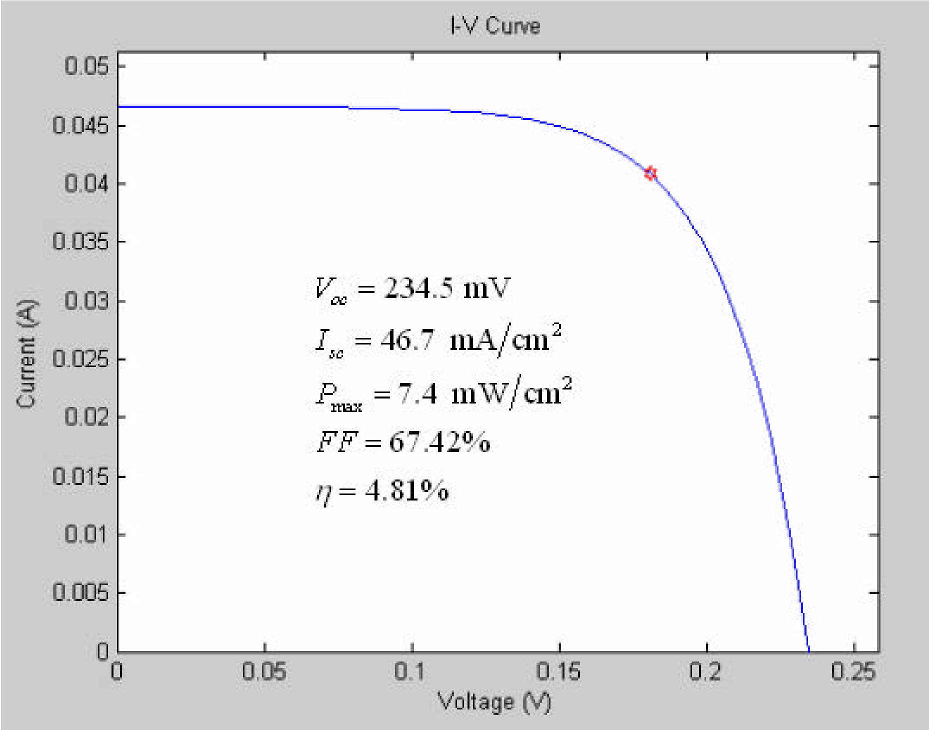

Figure 34. InGaAs Solar Cell *I-V* Characteristics

The spectral response of this InGaAs cell should approach zero at a wavelength of 2.25 µm according to Equation 2.2. Figure 35 shows the computed spectral response of this cell. The spectral response peaks at $l = 1.55$ µm and approaches zero at the correct wavelength.

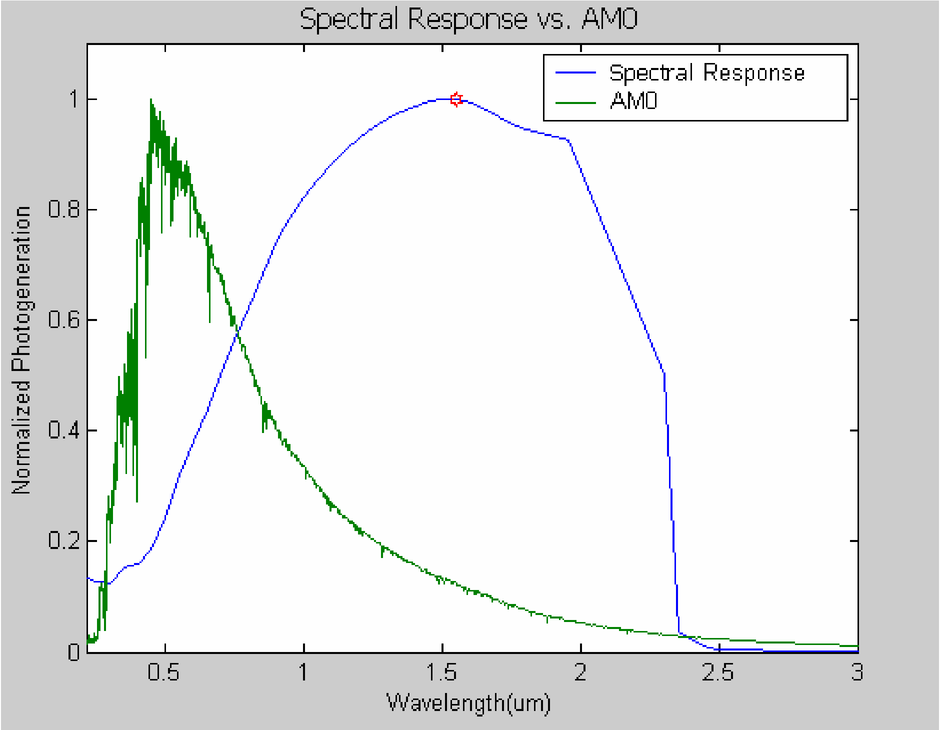

Figure 35. Spectral Response of InGaAs

All of the cells tested provided an accurate model under the AM0 spectrum and produced the expected spectral responses.

B. THERMOPHOTOVOLTAIC CELLS

The previous chapter established the validity of the cell models. The next step was to take these models and optimize them for the spectrum of a 1300K blackbody. In order to do this, the Matlab programs previously discussed were used to run iteration routines to find the optimum thicknesses and doping levels for each layer of a cell.

1. Gallium Antimonide

Figure 36 below shows the optimum GaSb cell found.

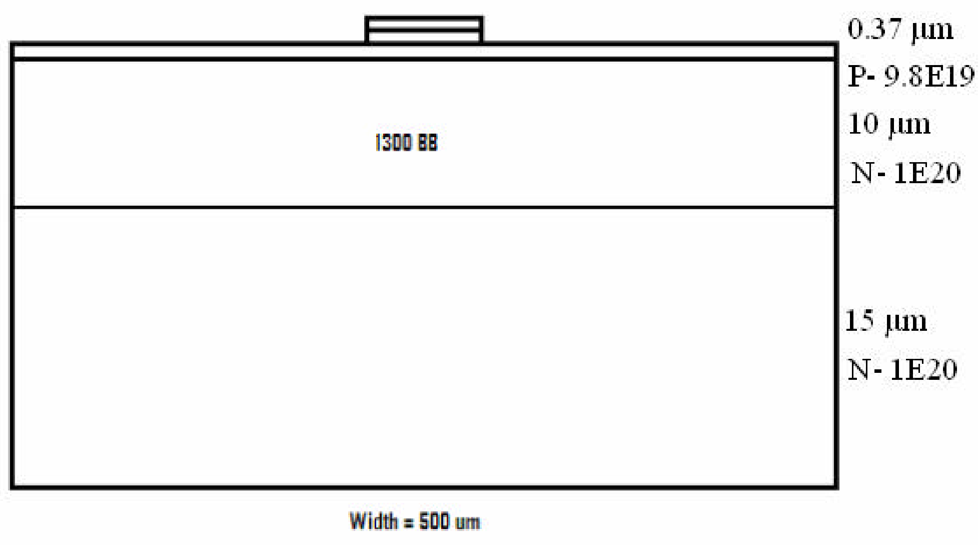

Figure 36. GaSb TPV Cell

Figure 37 shows the output from this cell.

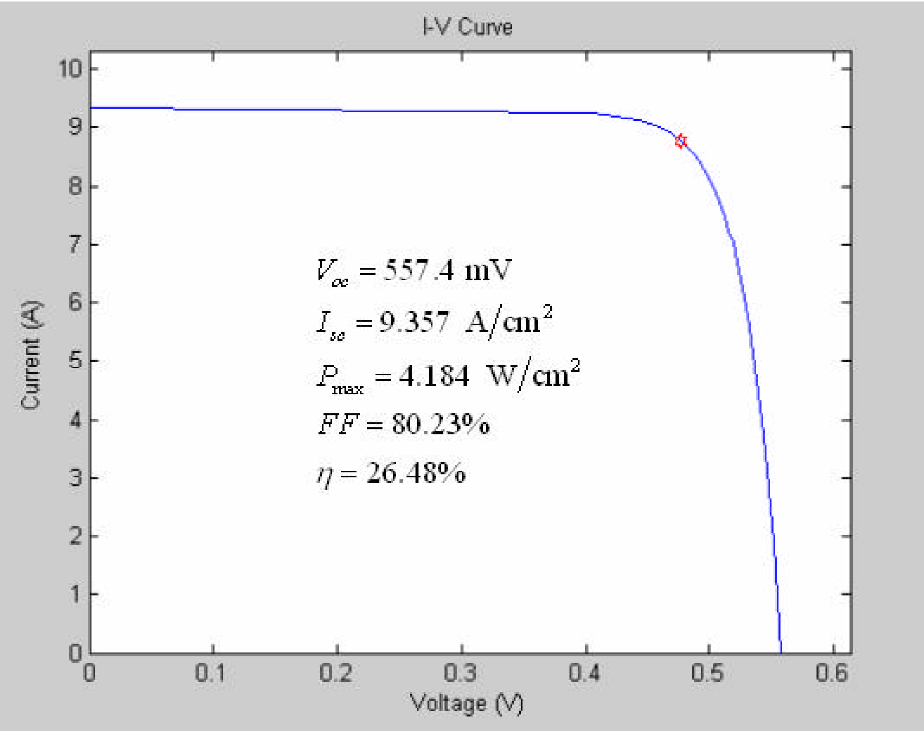

Figure 37. GaSb TPV Cell *I-V* Characteristics

The photogeneration rate was also measured from this cell. Figure 38 shows the photogeneration rate at incrementally increasing wavelengths from $l = 0.2\ \mu\text{m} - 2.0\ \mu\text{m}$.

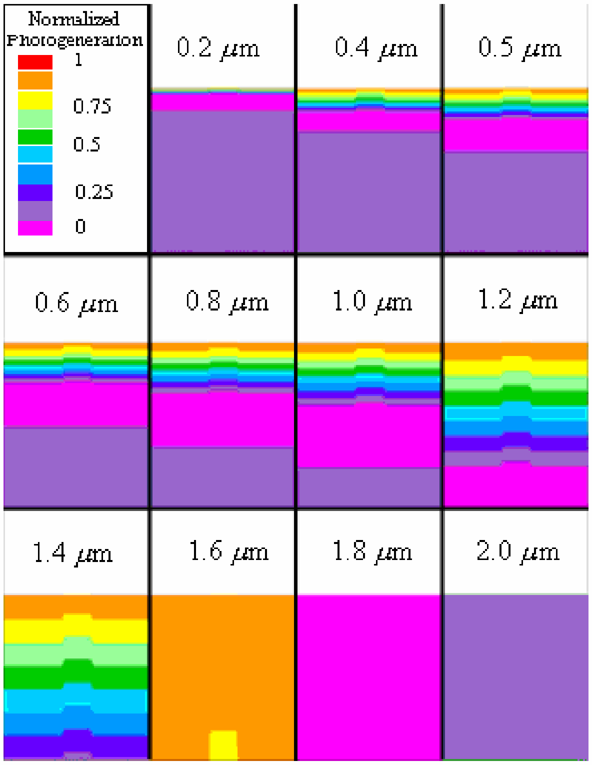

Figure 38. GaSb Photogeneration Rate

In this picture, brighter colors represent higher photogeneration rates. It can be seen that longer wavelengths of light are absorbed deeper in the cell and cause more photogeneration to occur. At very short and very long wavelengths of light, however, there is almost no photogeneration.

2. Indium Gallium Arsenide

Figure 39 shows the optimum InGaAs cell found.

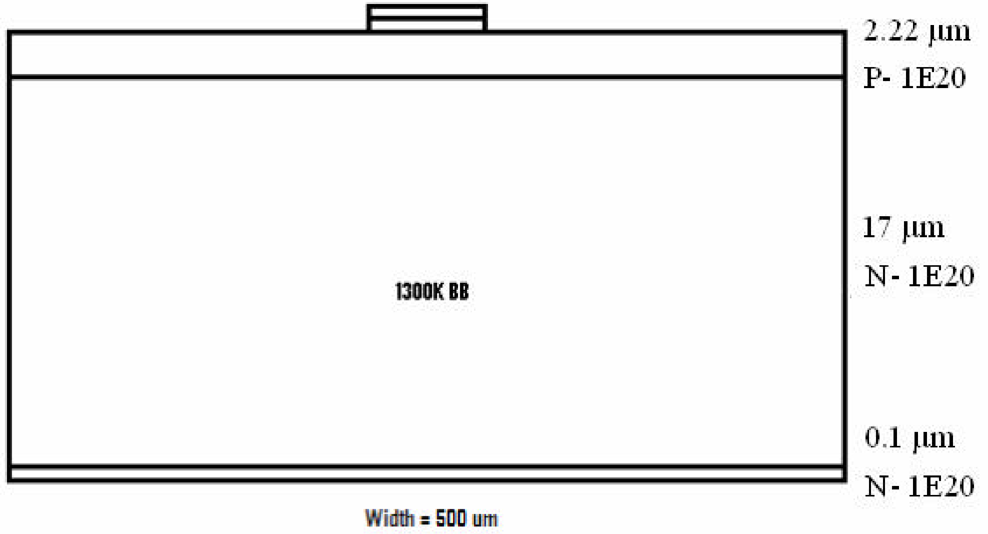

Figure 39. InGaAs TPV Cell

Figure 40 shows the output of this cell when the spectrum of 1300K blackbody was applied to it.

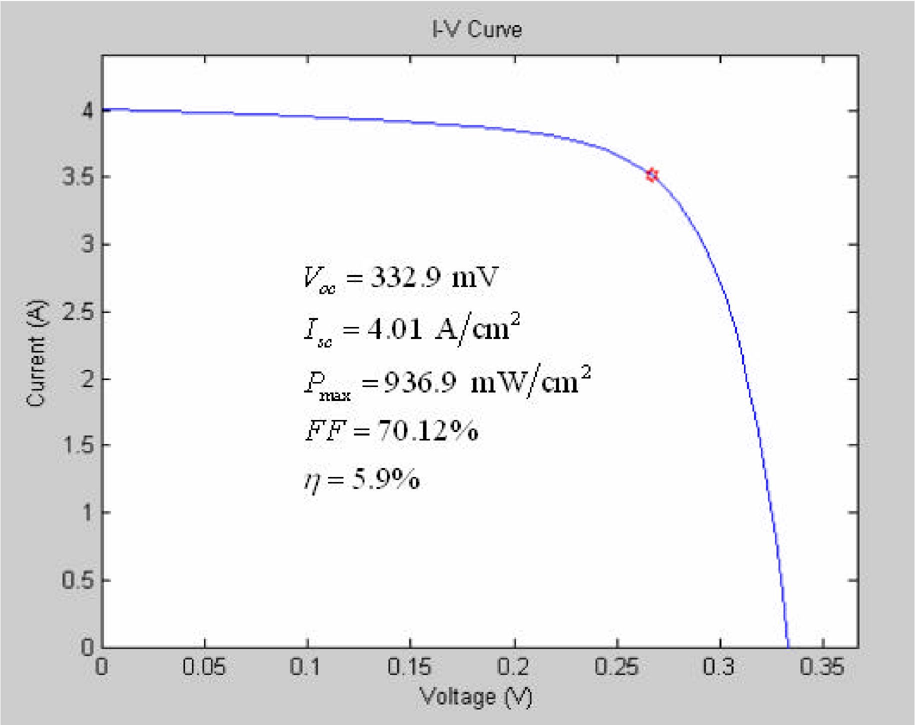

Figure 40. InGaAs TPV Cell *I-V* Characteristics

The results from this cell were compared to published data on a similar InGaAs cell under a 1225K blackbody spectrum.

The photogeneration rate in this cell was measured in the same manner as the GaSb cell. Figure 41 shows the photogeneration for this cell with incrementally increasing wavelengths of light from $l = 0.2\ \mu\text{m} - 2.3\ \mu\text{m}$.

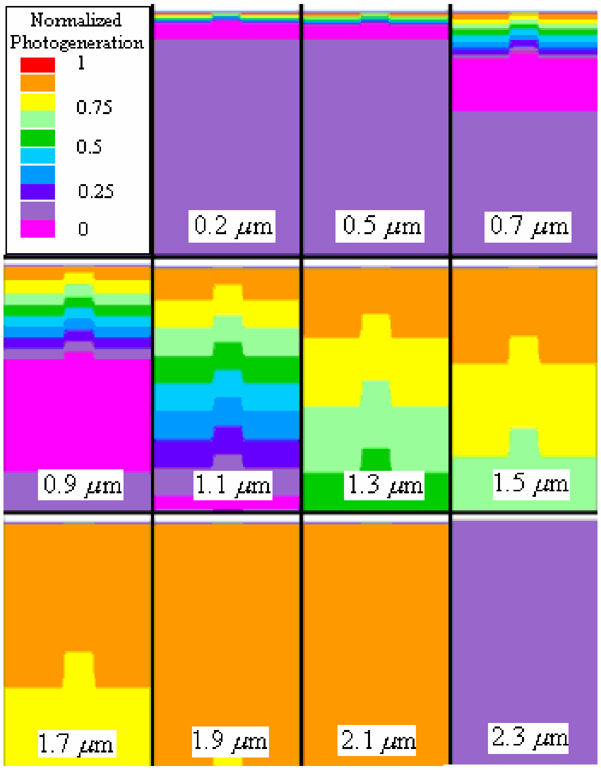

Figure 41. InGaAs Photogeneration Rate

Again it can be seen that longer wavelengths of light are absorbed deeper in the cell and produce more photogeneration until the incident light no longer has enough energy to induce photogeneration. From these photogeneration figures and the previous spectral response graphs, it can be deduced that cells generally absorb light most efficiently that has energy only slightly higher than the energy bandgap of the material.

This chapter compared simulated cell results under the AM0 spectrum to measured data in order to verify the models. The cells were then optimized for the spectrum from a 1300K blackbody and the results of these cells were presented. The next chapter discusses conclusions reached from this thesis and recommendations for future work in this area.

THIS PAGE INTENTIONALLY LEFT BLANK

VII. CONCLUSIONS AND RECOMMENDATIONS

This thesis developed and demonstrated reliable models of GaSb and InGaAs thermophotovoltaic cells for both the AM0 spectrum and the spectrum of 1300K blackbody. In addition to the Silvaco models, several programs were written to enable Matlab to communicate with Silvaco for running simulations and analyzing data. With the development of models for other cell materials and possible multijunction configurations, Silvaco's ATLAS software could prove to be an invaluable tool for TPV industry and for the cell designers.

This thesis assumed the heat source to be a 1300K blackbody, but with very little effort any other spectrum could be applied to these cells. The Matlab program developed here can produce the spectrum from any temperature blackbody over any range of wavelengths, calculating the radiance at each wavelength along with the total power under the curve. The optimization routines would run exactly the same way.

The models built here could easily be configured to model other cell materials as well. The most difficult part of building an accurate cell model is providing accurate material properties. These properties are difficult to find for some of the newer, more exotic ternary and quaternary materials. Optical parameters, one of the most important material properties for building an accurate model, can often only be found for wavelengths of light up to 1 or 2 µm but, for TPV applications, this data is necessary for much longer wavelengths of light. Silvaco, while a powerful simulation tool, cannot accurately solve all the equations to model a cell without the proper variables.

Once initial cell models are built, however, they can provide a cell designer instant feedback on the impact of changes made in any given design. With the lack of accurate TPV cell models, the current design process consists of building and testing many different cells in order to find the most efficient design. The method presented in this thesis allows a cell designer the option of using any configuration of any definable materials with any conceivable doping schemes. Other ongoing research is even adding the capability of predicting the impact of radiation on a cell. No other model has shown the versatility and ease of design for TPV cells as the Silvaco software used here.

The next step in this research is to model a multijunction TPV cell. Recent research by Green [Ref. 27] and Michalopoulos [Ref. 28] has proven that Atlas is capable of modeling and optimizing multijunction solar cells. A multijunction configuration would have the potential to greatly improve the heat to electrical conversion efficiency of the TPV cell as well.

APPENDIX A: ATLAS CODE

This appendix contains the Silvaco input decks that were used to build the models in this thesis for GaAs, GaSb, and InGaAs.

A. GALLIUM ARSENIDE

1. *I-V* Curve

```
go atlas

#############################################
## Parameters
##
## Cell Width (um)
set cellwidth=500
##
## Cap/Contact (%)
set contactpercent=8
##
## Standard # of Divisions
set divs=10
##
## Contact
set contactthickness=.1
##
## Cap
set capthickness=.3
set capdoping=3e18
##
## Cathode
set cathodethickness=.2
set cathodedoping=1.5e18
##
## Anode
set anodethickness=200
set anodedoping=7e17
##
## Back Surface Field (BSF)
set bsfthickness=.5
set bsfdoping=8e18
##
#############################################

set cellwdiv=$cellwidth/$divs
set 3D=100e6 /$cellwidth
set capwidth=.01*$contactpercent*$cellwidth
set capwdiv=$capwidth/$divs

set bsfL=0
set bsfH=$bsfL-$bsfthickness
set bsfdivs=$bsfthickness/$divs

set anoL=$bsfH
set anoH=$anoL-$anodethickness
set anodivs=$anodethickness/$divs

set catL=$anoH
set catH=$catL-$cathodethickness
set catdivs=$cathodethickness/$divs

set capL=$catH
set capH=$capL-$capthickness
set capdivs=$capthickness/$divs

set contL=$capH
set contH=$contL-$contactthickness
set contdivs=$contactthickness/$divs
set contcenter=$cellwidth/2
set contRR=$contcenter+$capwidth/2
set contLL=$contcenter-$capwidth/2

set lightY=$contH-5


mesh width=$3D
#X-Mesh
x.mesh loc=0 spac=$cellwdiv
x.mesh loc=$contLL spac=$capwdiv
x.mesh loc=$contRR spac=$capwdiv
x.mesh loc=$cellwidth spac=$cellwdiv


#Y-Mesh
y.mesh loc=$contH spac=$contdivs
y.mesh loc=$capH spac=$capdivs
y.mesh loc=$catH spac=$catdivs
y.mesh loc=$anoH spac=$anodivs
y.mesh loc=$bsfH spac=$bsfdivs
y.mesh loc=$bsfL spac=$bsfdivs


#Regions
##Contacts
region num=1 material=Gold x.min=$contLL x.max=$contRR y.min=$contH
y.max=$contL
##Caps
region num=2 material=GaAs x.min=$contLL x.max=$contRR y.min=$capH y.max=$capL
##Vacuums
region num=3 material=Vacuum x.min=0 x.max=$contLL y.min=$contH y.max=$capL
region num=4 material=vacuum x.min=$contRR x.max=$cellwidth y.min=$contH
y.max=$capL
#Cathode
region num=5 material=GaAs x.min=0 x.max=$cellwidth y.min=$catH y.max=$catL
#Anode
region num=6 material=GaAs x.min=0 x.max=$cellwidth y.min=$anoH y.max=$anoL
#BSF
region num=7 material=GaAs x.min=0 x.max=$cellwidth y.min=$bsfH y.max=$bsfL


##Electrodes
electrode name=cathode material=Gold x.min=$contLL x.max=$contRR y.min=$contH
y.max=$contL
electrode name=anode material=Gold x.min=0 x.max=$cellwidth y.min=$bsfL
y.max=$bsfL
```

```
#Doping
# Cap
doping uniform region=2 n.type conc=$capdoping
# Cathode
doping uniform region=5 n.type conc=$cathodedoping
# Anode
doping uniform region=6 p.type conc=$anodedoping
# BSF
doping uniform region=7 p.type conc=$bsfdoping


#Material properties
material COPT=7e-10
# Vacuum
material material=Vacuum real.index=3.3 imag.index=0
# GaAs
material material=GaAs EG300=1.42 PERMITTIVITY=13.1 AFFINITY=4.07
material material=GaAs NC300=4.7e17 NV300=7e18
material material=GaAs index.file=GaAs.opt
# Gold
material material=Gold real.index=1.2 imag.index=1.8
# Models
models region=3 CONMOB
models region=4 CONMOB
models region=8 CONMOB
models region=9 CONMOB
models region=10 CONMOB
models OPTR print

#Light beams
beam num=1 x.origin=0 y.origin=$lightY angle=90 back.refl
power.file=AM0silv.spec wavel.start=0.21 wavel.end=4 wavel.num=50


### SOLVING I-V CURVE

set suns=1
set I=$suns*.95
set a=$I*.9

solve init
method gummel newton maxtraps=10 itlimit=25
solve b1=$a

method newton maxtraps=10 itlimit=100
solve b1=$I

extract name="isc" max(curve(v."anode", i."cathode"))

set isc=$isc*$3D
set i1=$isc/10
set i2=$i1+$isc/10
set i3=$i2+$isc/10
set i4=$i3+$isc/10
set i5=$i4+$isc/10
set i6=$i5+$isc/20
set i7=$i6+$isc/20
set i8=$i7+$isc/20
set i9=$i8+$isc/20
set i10=$i9+$isc/20
set i11=$i10+$isc/40
set i12=$i11+$isc/40
set i13=$i12+$isc/40
set i14=$i13+$isc/40
set i15=$i14+$isc/40
set i16=$i15+$isc/80
set i17=$i16+$isc/80
set i18=$i17+$isc/80
set i19=$i18+$isc/80
set i20=$i19+$isc/80
set i21=$i20+$isc/80
set i22=$i21+$isc/80
set i23=$i22+$isc/80
set i24=$i23+$isc/80
set i25=$i24+$isc/80

contact name=anode current

method newton maxtraps=4 itlimit=100

log outfile=gaas.log
struct outfile=gaas.str

solve ianode=0 b1=$I
solve ianode=-$i1 b1=$I
solve ianode=-$i2 b1=$I
solve ianode=-$i3 b1=$I
solve ianode=-$i4 b1=$I
solve ianode=-$i5 b1=$I
solve ianode=-$i6 b1=$I
solve ianode=-$i7 b1=$I
solve ianode=-$i8 b1=$I
solve ianode=-$i9 b1=$I
solve ianode=-$i10 b1=$I
solve ianode=-$i11 b1=$I
solve ianode=-$i12 b1=$I
solve ianode=-$i13 b1=$I
solve ianode=-$i14 b1=$I
solve ianode=-$i15 b1=$I
solve ianode=-$i16 b1=$I
solve ianode=-$i17 b1=$I
solve ianode=-$i18 b1=$I
solve ianode=-$i19 b1=$I
solve ianode=-$i20 b1=$I
solve ianode=-$i21 b1=$I
solve ianode=-$i22 b1=$I
solve ianode=-$i23 b1=$I
solve ianode=-$i24 b1=$I
solve ianode=-$i25 b1=$I

log off



tonyplot gaas.log -set onecon.set
tonyplot gaas.str
```

2. Frequency Response

```
go atlas

#############################################
## Parameters
##
## Cell Width (um)
```

```
set cellwidth=500
##
## Cap/Contact (%)
set contactpercent=8
##
## Standard # of Divisions
set divs=10
##
## Contact
set contactthickness=.1
##
## Cap
set capthickness=.3
set capdoping=3e18
##
## Cathode
set cathodethickness=.2
set cathodedoping=1.5e18
##
## Anode
set anodethickness=200
set anodedoping=7e17
##
## Back Surface Field (BSF)
set bsfthickness=.5
set bsfdoping=8e18
##
##############################################

set cellwdiv=$cellwidth/$divs
set 3D=100e6 /$cellwidth
set capwidth=.01*$contactpercent*$cellwidth
set capwdiv=$capwidth/$divs

set bsfL=0
set bsfH=$bsfL-$bsfthickness
set bsfdivs=$bsfthickness/$divs

set anoL=$bsfH
set anoH=$anoL-$anodethickness
set anodivs=$anodethickness/$divs

set catL=$anoH
set catH=$catL-$cathodethickness
set catdivs=$cathodethickness/$divs

set capL=$catH
set capH=$capL-$capthickness
set capdivs=$capthickness/$divs

set contL=$capH
set contH=$contL-$contactthickness
set contdivs=$contactthickness/$divs
set contcenter=$cellwidth/2
set contRR=$contcenter+$capwidth/2
set contLL=$contcenter-$capwidth/2

set lightY=$contH-5


mesh width=$3D
#X-Mesh
x.mesh loc=0 spac=$cellwdiv
```

```
x.mesh loc=$contLL spac=$capwdiv
x.mesh loc=$contRR spac=$capwdiv
x.mesh loc=$cellwidth spac=$cellwdiv


#Y-Mesh
y.mesh loc=$contH spac=$contdivs
y.mesh loc=$capH spac=$capdivs
y.mesh loc=$catH spac=$catdivs
y.mesh loc=$anoH spac=$anodivs
y.mesh loc=$bsfH spac=$bsfdivs
y.mesh loc=$bsfL spac=$bsfdivs


#Regions
##Contacts
region num=1 material=Gold x.min=$contLL x.max=$contRR y.min=$contH
y.max=$contL
##Caps
region num=2 material=GaAs x.min=$contLL x.max=$contRR y.min=$capH y.max=$capL
##Vacuums
region num=3 material=Vacuum x.min=0 x.max=$contLL y.min=$contH y.max=$capL
region num=4 material=vacuum x.min=$contRR x.max=$cellwidth y.min=$contH
y.max=$capL
#Cathode
region num=5 material=GaAs x.min=0 x.max=$cellwidth y.min=$catH y.max=$catL
#Anode
region num=6 material=GaAs x.min=0 x.max=$cellwidth y.min=$anoH y.max=$anoL
#BSF
region num=7 material=GaAs x.min=0 x.max=$cellwidth y.min=$bsfH y.max=$bsfL


##Electrodes
electrode name=cathode material=Gold x.min=$contLL x.max=$contRR y.min=$contH
y.max=$contL
electrode name=anode material=Gold x.min=0 x.max=$cellwidth y.min=$bsfL
y.max=$bsfL



#Doping
# Cap
doping uniform region=2 n.type conc=$capdoping
# Cathode
doping uniform region=5 n.type conc=$cathodedoping
# Anode
doping uniform region=6 p.type conc=$anodedoping
# BSF
doping uniform region=7 p.type conc=$bsfdoping


#Material properties
material COPT=7e-10
# Vacuum
material material=Vacuum real.index=3.3 imag.index=0
# GaAs
material material=GaAs EG300=1.42 PERMITTIVITY=13.1 AFFINITY=4.07
material material=GaAs NC300=4.7e17 NV300=7e18
material material=GaAs index.file=GaAs.opt
# Gold
material material=Gold real.index=1.2 imag.index=1.8
# Models
models region=3 CONMOB
models region=4 CONMOB
models region=8 CONMOB
models region=9 CONMOB
models region=10 CONMOB
models OPTR print

#Light beams
beam num=1 x.origin=0 y.origin=$lightY angle=90 back.refl
power.file=AM0silv.spec wavel.start=0.21 wavel.end=4 wavel.num=50

### SOLVING I-V CURVE

set suns=1
set I=$suns*.95
set a=$I*.9

solve init
method gummel newton maxtraps=10 itlimit=25
solve b1=$a

method newton maxtraps=10 itlimit=100
solve b1=$I




extract name="isc" max(curve(v."anode", i."cathode"))


output con.band val.band
solve init
log outfile=freq.log

solve b1=0.1 lambda=0.22
solve b1=0.1 lambda=0.225
solve b1=0.1 lambda=0.23
solve b1=0.1 lambda=0.235
solve b1=0.1 lambda=0.24
solve b1=0.1 lambda=0.245
solve b1=0.1 lambda=0.25
solve b1=0.1 lambda=0.255
solve b1=0.1 lambda=0.26
solve b1=0.1 lambda=0.265
solve b1=0.1 lambda=0.27
solve b1=0.1 lambda=0.275
solve b1=0.1 lambda=0.28
solve b1=0.1 lambda=0.285
solve b1=0.1 lambda=0.29
solve b1=0.1 lambda=0.295
solve b1=0.1 lambda=0.30
solve b1=0.1 lambda=0.305
solve b1=0.1 lambda=0.31
solve b1=0.1 lambda=0.315
solve b1=0.1 lambda=0.32
solve b1=0.1 lambda=0.325
solve b1=0.1 lambda=0.33
solve b1=0.1 lambda=0.335
solve b1=0.1 lambda=0.34
solve b1=0.1 lambda=0.345
solve b1=0.1 lambda=0.35
solve b1=0.1 lambda=0.355
solve b1=0.1 lambda=0.36
solve b1=0.1 lambda=0.365
solve b1=0.1 lambda=0.37
solve b1=0.1 lambda=0.375
solve b1=0.1 lambda=0.38
solve b1=0.1 lambda=0.385
solve b1=0.1 lambda=0.39
solve b1=0.1 lambda=0.395
solve b1=0.1 lambda=0.40
solve b1=0.1 lambda=0.405
solve b1=0.1 lambda=0.41
solve b1=0.1 lambda=0.415
solve b1=0.1 lambda=0.42
solve b1=0.1 lambda=0.425
solve b1=0.1 lambda=0.43
solve b1=0.1 lambda=0.435
solve b1=0.1 lambda=0.44
solve b1=0.1 lambda=0.445
solve b1=0.1 lambda=0.45
solve b1=0.1 lambda=0.455
solve b1=0.1 lambda=0.46
solve b1=0.1 lambda=0.465
solve b1=0.1 lambda=0.47
solve b1=0.1 lambda=0.475
solve b1=0.1 lambda=0.48
solve b1=0.1 lambda=0.485
solve b1=0.1 lambda=0.49
solve b1=0.1 lambda=0.495
solve b1=0.1 lambda=0.50
solve b1=0.1 lambda=0.505
solve b1=0.1 lambda=0.51
solve b1=0.1 lambda=0.515
solve b1=0.1 lambda=0.52
solve b1=0.1 lambda=0.525
solve b1=0.1 lambda=0.53
solve b1=0.1 lambda=0.535
solve b1=0.1 lambda=0.54
solve b1=0.1 lambda=0.545
solve b1=0.1 lambda=0.55
solve b1=0.1 lambda=0.555
solve b1=0.1 lambda=0.56
solve b1=0.1 lambda=0.565
solve b1=0.1 lambda=0.57
solve b1=0.1 lambda=0.575
solve b1=0.1 lambda=0.58
solve b1=0.1 lambda=0.585
solve b1=0.1 lambda=0.59
solve b1=0.1 lambda=0.595
solve b1=0.1 lambda=0.60
solve b1=0.1 lambda=0.605
solve b1=0.1 lambda=0.61
solve b1=0.1 lambda=0.615
solve b1=0.1 lambda=0.62
solve b1=0.1 lambda=0.625
solve b1=0.1 lambda=0.63
solve b1=0.1 lambda=0.635
solve b1=0.1 lambda=0.64
solve b1=0.1 lambda=0.645
solve b1=0.1 lambda=0.65
solve b1=0.1 lambda=0.655
solve b1=0.1 lambda=0.66
solve b1=0.1 lambda=0.665
solve b1=0.1 lambda=0.67
solve b1=0.1 lambda=0.675
solve b1=0.1 lambda=0.68
solve b1=0.1 lambda=0.685
solve b1=0.1 lambda=0.69
solve b1=0.1 lambda=0.695
solve b1=0.1 lambda=0.70
solve b1=0.1 lambda=0.705
solve b1=0.1 lambda=0.71
solve b1=0.1 lambda=0.715
solve b1=0.1 lambda=0.72
solve b1=0.1 lambda=0.725
solve b1=0.1 lambda=0.73
solve b1=0.1 lambda=0.735
solve b1=0.1 lambda=0.74
solve b1=0.1 lambda=0.745
solve b1=0.1 lambda=0.75
solve b1=0.1 lambda=0.755
solve b1=0.1 lambda=0.76
solve b1=0.1 lambda=0.765
solve b1=0.1 lambda=0.77
solve b1=0.1 lambda=0.775
solve b1=0.1 lambda=0.78
solve b1=0.1 lambda=0.785
solve b1=0.1 lambda=0.79
solve b1=0.1 lambda=0.795
solve b1=0.1 lambda=0.80
solve b1=0.1 lambda=0.805
solve b1=0.1 lambda=0.81
solve b1=0.1 lambda=0.815
solve b1=0.1 lambda=0.82
solve b1=0.1 lambda=0.825
solve b1=0.1 lambda=0.83
solve b1=0.1 lambda=0.835
solve b1=0.1 lambda=0.84
solve b1=0.1 lambda=0.845
solve b1=0.1 lambda=0.85
solve b1=0.1 lambda=0.855
solve b1=0.1 lambda=0.86
solve b1=0.1 lambda=0.865
solve b1=0.1 lambda=0.87
solve b1=0.1 lambda=0.875
solve b1=0.1 lambda=0.88
solve b1=0.1 lambda=0.885
solve b1=0.1 lambda=0.89
solve b1=0.1 lambda=0.895
solve b1=0.1 lambda=0.90
solve b1=0.1 lambda=0.905
solve b1=0.1 lambda=0.91
solve b1=0.1 lambda=0.915
solve b1=0.1 lambda=0.92
solve b1=0.1 lambda=0.925
solve b1=0.1 lambda=0.93
solve b1=0.1 lambda=0.935
solve b1=0.1 lambda=0.94
solve b1=0.1 lambda=0.945
solve b1=0.1 lambda=0.95
solve b1=0.1 lambda=0.955
solve b1=0.1 lambda=0.96
solve b1=0.1 lambda=0.965
solve b1=0.1 lambda=0.97
solve b1=0.1 lambda=0.975
solve b1=0.1 lambda=0.98
solve b1=0.1 lambda=0.985
solve b1=0.1 lambda=0.99
solve b1=0.1 lambda=0.995
solve b1=0.1 lambda=1.00
log off
```

B. GALLIUM ANTIMONIDE

1. *I-V* Curve

```
go atlas

#############################################
## Parameters
##
## Cell Width (um)
set cellwidth=500
##
## Cap/Contact (%)
set contactpercent=8
##
## Standard # of Divisions
set divs=20
##
## Contact
set contactthickness=.1
##
## Cap  (there is no cap in this model)
set capthickness=.1
set capdoping=3e18
##
## Cathode(N-type)
set cathodethickness=10
set cathodedoping=1.000000e+020
##
## Anode(P-type)  (.2-.5um)
set anodethickness=.37
set anodedoping=9.8e19
##
## Back Surface Field (BSF)
set bsfthickness=15.000000
set bsfdoping=1.000000e+020
##
#############################################

set cellwdiv=$cellwidth/$divs
set 3D=100e6 /$cellwidth
set capwidth=.01*$contactpercent*$cellwidth
set capwdiv=$capwidth/$divs

set bsfL=0
set bsfH=$bsfL-$bsfthickness
set bsfdivs=$bsfthickness/$divs

set catL=$bsfH
set catH=$catL-$cathodethickness
set catdivs=$cathodethickness/$divs

set anoL=$catH
set anoH=$anoL-$anodethickness
set anodivs=$anodethickness/$divs

set capL=$anoH
set capH=$capL-$capthickness
set capdivs=$capthickness/$divs

set contL=$capH
set contH=$contL-$contactthickness
set contdivs=$contactthickness/$divs
set contcenter=$cellwidth/2
set contRR=$contcenter+$capwidth/2
set contLL=$contcenter-$capwidth/2

#Sets light source 200um above surface (try different heights)
set lightY=$contH-200


mesh width=$3D
#X-Mesh
x.mesh loc=0 spac=$cellwdiv
x.mesh loc=$contLL spac=$capwdiv
x.mesh loc=$contRR spac=$capwdiv
x.mesh loc=$cellwidth spac=$cellwdiv


#Y–Mesh
y.mesh loc=$contH spac=$contdivs
y.mesh loc=$capH spac=$capdivs
y.mesh loc=$catH spac=$catdivs
y.mesh loc=$anoH spac=$anodivs
y.mesh loc=$bsfH spac=$bsfdivs
y.mesh loc=$bsfL spac=$bsfdivs


#Regions
##Contacts
region num=1 material=Gold x.min=$contLL x.max=$contRR y.min=$contH
y.max=$contL
##Cap
region num=2 material=GaSb x.min=$contLL x.max=$contRR y.min=$capH
y.max=$capL
##Vacuums
region num=3 material=Vacuum x.min=0 x.max=$contLL y.min=$contH
y.max=$capL
region num=4 material=vacuum x.min=$contRR x.max=$cellwidth
y.min=$contH y.max=$capL
#Anode
region num=5 material=GaSb x.min=0 x.max=$cellwidth y.min=$anoH
y.max=$anoL
#Cathode
region num=6 material=GaSb x.min=0 x.max=$cellwidth y.min=$catH
y.max=$catL
#BSF
```

```
region num=7 material=GaSb x.min=0 x.max=$cellwidth y.min=$bsfH
y.max=$bsfL

##Electrodes
electrode name=anode material=Gold x.min=$contLL x.max=$contRR
y.min=$contH y.max=$contL
electrode name=cathode material=Gold x.min=0 x.max=$cellwidth
y.min=$bsfL y.max=$bsfL



#Doping  (In this model there are no specified doping levels, try sev-
eral)
# Cap
doping uniform region=2 p.type conc=$capdoping
# Anode
doping uniform region=5 p.type conc=$anodedoping
# Cathode
doping uniform region=6 n.type conc=$cathodedoping
# BSF
doping uniform region=7 n.type conc=$bsfdoping


#Material properties
# Vacuum
material material=Vacuum real.index=3.8 imag.index=0
# GaSb
material material=GaSb COPT=5e-10
material material=GaSb EG300=.726 PERMITTIVITY=14.4 AFFINITY=4.06
material material=GaSb NC300=2.1e17 NV300=1.8e19
material material=GaSb index.file=GaSb.opt
# Gold
material material=Gold real.index=1.2 imag.index=1.8
# Models
models OPTR print

#Light beams
beam num=1 x.origin=0 y.origin=$lightY angle=90 back.refl
power.file=1300BB.spec wavel.start=0.207 wavel.end=5 wavel.num=1000


### SOLVING I-V CURVE

set suns=1
set I=$suns*.95
set a=$I*.9

solve init
method gummel newton maxtraps=10 itlimit=25
solve b1=$a

method newton maxtraps=10 itlimit=100
solve b1=$I

extract name="isc" max(curve(v."anode", i."cathode"))

set isc=$isc*$3D
set i1=$isc/10
set i2=$i1+$isc/10
set i3=$i2+$isc/10
set i4=$i3+$isc/10
set i5=$i4+$isc/10
set i6=$i5+$isc/20
set i7=$i6+$isc/20
set i8=$i7+$isc/20
set i9=$i8+$isc/20
set i10=$i9+$isc/20
set i11=$i10+$isc/40
set i12=$i11+$isc/40
set i13=$i12+$isc/40
set i14=$i13+$isc/40
set i15=$i14+$isc/40
set i16=$i15+$isc/80
set i17=$i16+$isc/80
set i18=$i17+$isc/80
set i19=$i18+$isc/80
set i20=$i19+$isc/80
set i21=$i20+$isc/80
set i22=$i21+$isc/80
set i23=$i22+$isc/80
set i24=$i23+$isc/80
set i25=$i24+$isc/80

contact name=anode current

method newton maxtraps=4 itlimit=100

log outfile=gasb.log
struct outfile=gasb.str

solve ianode=0 b1=$I
solve ianode=-$i1 b1=$I
solve ianode=-$i2 b1=$I
solve ianode=-$i3 b1=$I
solve ianode=-$i4 b1=$I
solve ianode=-$i5 b1=$I
solve ianode=-$i6 b1=$I
solve ianode=-$i7 b1=$I
solve ianode=-$i8 b1=$I
solve ianode=-$i9 b1=$I
solve ianode=-$i10 b1=$I
solve ianode=-$i11 b1=$I
solve ianode=-$i12 b1=$I
solve ianode=-$i13 b1=$I
solve ianode=-$i14 b1=$I
solve ianode=-$i15 b1=$I
solve ianode=-$i16 b1=$I
solve ianode=-$i17 b1=$I
solve ianode=-$i18 b1=$I
solve ianode=-$i19 b1=$I
solve ianode=-$i20 b1=$I
solve ianode=-$i21 b1=$I
solve ianode=-$i22 b1=$I
solve ianode=-$i23 b1=$I
solve ianode=-$i24 b1=$I
solve ianode=-$i25 b1=$I

log off

tonyplot gasb.log -set onecon.set
tonyplot gasb.str
```

2. Frequency Response

```
go atlas

############################################
## Parameters
##
## Cell Width (um)
set cellwidth=500
##
## Cap/Contact (%)
set contactpercent=8
##
## Standard # of Divisions
set divs=20
##
## Contact
set contactthickness=.1
##
## Cap  (there is no cap in this model)
set capthickness=.1
set capdoping=3e18
##
## Cathode(N-type)
set cathodethickness=10
set cathodedoping=1.000000e+020
##
## Anode(P-type)  (.2-.5um)
set anodethickness=.37
set anodedoping=9.8e19
##
## Back Surface Field (BSF)
set bsfthickness=15.000000
set bsfdoping=1.000000e+020
##
############################################

set cellwdiv=$cellwidth/$divs
set 3D=50e6 /$cellwidth
set capwidth=.01*$contactpercent*$cellwidth
set capwdiv=$capwidth/$divs

set bsfL=0
set bsfH=$bsfL-$bsfthickness
set bsfdivs=$bsfthickness/$divs

set catL=$bsfH
set catH=$catL-$cathodethickness
set catdivs=$cathodethickness/$divs

set anoL=$catH
set anoH=$anoL-$anodethickness
set anodivs=$anodethickness/$divs
set capL=$anoH
set capH=$capL-$capthickness
set capdivs=$capthickness/$divs

set contL=$capH
set contH=$contL-$contactthickness
set contdivs=$contactthickness/$divs
set contcenter=$cellwidth/2
set contRR=$contcenter+$capwidth/2
set contLL=$contcenter-$capwidth/2

#Sets light source 200um above surface (try different heights)
set lightY=$contH-200


mesh width=$3D
#X-Mesh
x.mesh loc=0 spac=$cellwdiv
x.mesh loc=$contLL spac=$capwdiv
x.mesh loc=$contRR spac=$capwdiv
x.mesh loc=$cellwidth spac=$cellwdiv


#Y-Mesh
y.mesh loc=$contH spac=$contdivs
y.mesh loc=$capH spac=$capdivs
y.mesh loc=$catH spac=$catdivs
y.mesh loc=$anoH spac=$anodivs
y.mesh loc=$bsfH spac=$bsfdivs
y.mesh loc=$bsfL spac=$bsfdivs


#Regions
##Contacts
region num=1 material=Gold x.min=$contLL x.max=$contRR y.min=$contH
y.max=$contL
##Cap
region num=2 material=GaSb x.min=$contLL x.max=$contRR y.min=$capH y.max=$capL
##Vacuums
region num=3 material=Vacuum x.min=0 x.max=$contLL y.min=$contH y.max=$capL
region num=4 material=vacuum x.min=$contRR x.max=$cellwidth y.min=$contH
y.max=$capL
#Anode
region num=5 material=GaSb x.min=0 x.max=$cellwidth y.min=$anoH y.max=$anoL
#Cathode
region num=6 material=GaSb x.min=0 x.max=$cellwidth y.min=$catH y.max=$catL
#BSF
region num=7 material=GaSb x.min=0 x.max=$cellwidth y.min=$bsfH y.max=$bsfL

##Electrodes
electrode name=anode material=Gold x.min=$contLL x.max=$contRR y.min=$contH
y.max=$contL
electrode name=cathode material=Gold x.min=0 x.max=$cellwidth y.min=$bsfL
y.max=$bsfL

#Doping  (In this model there are no specified doping levels, try several)
# Cap
doping uniform region=2 p.type conc=$capdoping
# Anode
doping uniform region=5 p.type conc=$anodedoping
# Cathode
doping uniform region=6 n.type conc=$cathodedoping
```

```
# BSF
doping uniform region=7 n.type conc=$bsfdoping

material COPT=7e-10
# Vacuum
material material=Vacuum real.index=3.3 imag.index=0
# GaSb
material material=GaSb EG300=.72 PERMITTIVITY=15.7 AFFINITY=4.06
material material=GaSb NC300=2.07846e17 NV300=1.81865e17
material material=GaSb index.file=GaAs.opt
# Gold
material material=Gold real.index=1.2 imag.index=1.8
# Models
models OPTR print

#Light beams
beam num=1 x.origin=0 y.origin=$lightY angle=90 back.refl
power.file=1300BB.spec wavel.start=0.1 wavel.end=7 wavel.num=100

set I=.1

solve init
solve b1=$I

extract name="isc" max(curve(v."anode", i."cathode"))

output con.band val.band
solve init
log outfile=freq.log
solve b1=0.1 lambda=0.22

solve b1=0.1 lambda=0.3
solve b1=0.1 lambda=0.4
solve b1=0.1 lambda=0.5
solve b1=0.1 lambda=0.6
solve b1=0.1 lambda=0.7
solve b1=0.1 lambda=0.8
solve b1=0.1 lambda=.82
solve b1=0.1 lambda=.84
solve b1=0.1 lambda=.86
solve b1=0.1 lambda=.88
solve b1=0.1 lambda=0.9
solve b1=0.1 lambda=1.0
solve b1=0.1 lambda=1.1
solve b1=0.1 lambda=1.2
solve b1=0.1 lambda=1.3
solve b1=0.1 lambda=1.4
solve b1=0.1 lambda=1.5
solve b1=0.1 lambda=1.6
solve b1=0.1 lambda=1.7
solve b1=0.1 lambda=1.8
solve b1=0.1 lambda=1.9
solve b1=0.1 lambda=2.0
solve b1=0.1 lambda=2.1
solve b1=0.1 lambda=2.2
solve b1=0.1 lambda=2.3
solve b1=0.1 lambda=2.4
solve b1=0.1 lambda=2.5
solve b1=0.1 lambda=2.6
solve b1=0.1 lambda=2.7
solve b1=0.1 lambda=2.8
solve b1=0.1 lambda=2.9
solve b1=0.1 lambda=3.0
solve b1=0.1 lambda=3.1
solve b1=0.1 lambda=3.2
solve b1=0.1 lambda=3.3
solve b1=0.1 lambda=3.4
solve b1=0.1 lambda=3.5
solve b1=0.1 lambda=3.6
solve b1=0.1 lambda=3.7
solve b1=0.1 lambda=3.8
solve b1=0.1 lambda=3.9
solve b1=0.1 lambda=4.0
solve b1=0.1 lambda=4.1
solve b1=0.1 lambda=4.2
solve b1=0.1 lambda=4.3
solve b1=0.1 lambda=4.4
solve b1=0.1 lambda=4.5
solve b1=0.1 lambda=4.6
solve b1=0.1 lambda=4.7
solve b1=0.1 lambda=4.8
solve b1=0.1 lambda=4.9
solve b1=0.1 lambda=5.0
solve b1=0.1 lambda=5.1
solve b1=0.1 lambda=5.2
solve b1=0.1 lambda=5.3
solve b1=0.1 lambda=5.4
solve b1=0.1 lambda=5.5
solve b1=0.1 lambda=5.6
solve b1=0.1 lambda=5.7
solve b1=0.1 lambda=5.8
solve b1=0.1 lambda=5.9
solve b1=0.1 lambda=5.0
solve b1=0.1 lambda=6.1
solve b1=0.1 lambda=6.2
solve b1=0.1 lambda=6.3
solve b1=0.1 lambda=6.4
solve b1=0.1 lambda=6.5
solve b1=0.1 lambda=6.6
solve b1=0.1 lambda=6.7
solve b1=0.1 lambda=6.8
solve b1=0.1 lambda=6.9
solve b1=0.1 lambda=7.0
log off
```

C. INDIUM GALLIUM ARSENIDE

1. *I-V* Curve

```
go atlas

#############################################
## Parameters
##
## Cell Width (um)
set cellwidth=500
##
## Cap/Contact (%)
```

```
set contactpercent=8
##
## Standard # of Divisions
set divs=20
##
## Contact
set contactthickness=.1
##
##
##Molar Concentration of In(1-x)Ga(x)As(x)
set x=.28
set perm=15.1-2.87*$x+.67*$x^2
set affin=4.9-.83*$x
set n=3.51-.21*$x
##
## Cap  (there is no cap in this model)
set capthickness=.1
set capdoping=3e18
##
## Cathode(N-type)
set cathodethickness=17
set cathodedoping=1e20
##
## Anode(P-type)  (.2-.5um)
set anodethickness=2.22
set anodedoping=1e20
##
## Back Surface Field (BSF)
set bsfthickness=.1
set bsfdoping=1e20
##
#############################################

set cellwdiv=$cellwidth/$divs
set 3D=100e6 /$cellwidth
set capwidth=.01*$contactpercent*$cellwidth
set capwdiv=$capwidth/$divs

set bsfL=0
set bsfH=$bsfL-$bsfthickness
set bsfdivs=$bsfthickness/$divs

set catL=$bsfH
set catH=$catL-$cathodethickness
set catdivs=$cathodethickness/$divs

set anoL=$catH
set anoH=$anoL-$anodethickness
set anodivs=$anodethickness/$divs

set capL=$anoH
set capH=$capL-$capthickness
set capdivs=$capthickness/$divs

set contL=$capH
set contH=$contL-$contactthickness
set contdivs=$contactthickness/$divs
set contcenter=$cellwidth/2
set contRR=$contcenter+$capwidth/2
set contLL=$contcenter-$capwidth/2

#Sets light source 200um above surface (try different heights)
set lightY=$contH-200


mesh width=$3D
#X-Mesh
x.mesh loc=0 spac=$cellwdiv
x.mesh loc=$contLL spac=$capwdiv
x.mesh loc=$contRR spac=$capwdiv
x.mesh loc=$cellwidth spac=$cellwdiv


#Y–Mesh
y.mesh loc=$contH spac=$contdivs
y.mesh loc=$capH spac=$capdivs
y.mesh loc=$catH spac=$catdivs
y.mesh loc=$anoH spac=$anodivs
y.mesh loc=$bsfH spac=$bsfdivs
y.mesh loc=$bsfL spac=$bsfdivs


#Regions
##Contacts
region num=1 material=Gold x.min=$contLL x.max=$contRR y.min=$contH
y.max=$contL
##Cap
region num=2 material=InGaAs x.min=$contLL x.max=$contRR y.min=$capH
y.max=$capL
##Vacuums
region num=3 material=Vacuum x.min=0 x.max=$contLL y.min=$contH
y.max=$capL
region num=4 material=vacuum x.min=$contRR x.max=$cellwidth
y.min=$contH y.max=$capL
#Anode
region num=5 material=InGaAs x.min=0 x.max=$cellwidth y.min=$anoH
y.max=$anoL
#Cathode
region num=6 material=InGaAs x.min=0 x.max=$cellwidth y.min=$catH
y.max=$catL
#BSF
region num=7 material=InGaAs x.min=0 x.max=$cellwidth y.min=$bsfH
y.max=$bsfL

##Electrodes
electrode name=anode material=Gold x.min=$contLL x.max=$contRR
y.min=$contH y.max=$contL
electrode name=cathode material=Gold x.min=0 x.max=$cellwidth
y.min=$bsfL y.max=$bsfL



#Doping  (In this model there are no specified doping levels, try sev-
eral)
```

```
# Cap
doping uniform region=2 p.type conc=$capdoping
# Anode
doping uniform region=5 p.type conc=$anodedoping
# Cathode
doping uniform region=6 n.type conc=$cathodedoping
# BSF
doping uniform region=7 n.type conc=$bsfdoping


#Material properties
# Vacuum
material material=Vacuum real.index=3.4 imag.index=0
# InGaSb
material material=InGaAs COPT=7e-10
material material=InGaAs EG300=.55 PERMITTIVITY=$perm AFFINITY=$affin
material material=InGaAs NC300=1.15e17 NV300=8.12e18
material material=InGaAs index.file=InGaAs.opt
# Gold
material material=Gold real.index=1.2 imag.index=1.8
# Models
models OPTR print

#Light beams
beam num=1 x.origin=0 y.origin=$lightY angle=90 back.refl
power.file=1300bb.spec wavel.start=0.21 wavel.end=7 wavel.num=50


### SOLVING I-V CURVE

set suns=1
set I=.95*$suns
set a=$I*.75

solve init
method gummel newton maxtraps=10 itlimit=25
solve b1=$a

method newton maxtraps=10 itlimit=100
solve b1=$I

extract name="isc" max(curve(v."anode", i."cathode"))

set isc=$isc*$3D
set i1=$isc/10
set i2=$i1+$isc/10
set i3=$i2+$isc/10
set i4=$i3+$isc/10
set i5=$i4+$isc/10
set i6=$i5+$isc/20
set i7=$i6+$isc/20
set i8=$i7+$isc/20
set i9=$i8+$isc/20
set i10=$i9+$isc/20
set i11=$i10+$isc/40
set i12=$i11+$isc/40
set i13=$i12+$isc/40
set i14=$i13+$isc/40
set i15=$i14+$isc/40
set i16=$i15+$isc/80
set i17=$i16+$isc/80
set i18=$i17+$isc/80
set i19=$i18+$isc/80
set i20=$i19+$isc/80
set i21=$i20+$isc/80
set i22=$i21+$isc/80
set i23=$i22+$isc/80
set i24=$i23+$isc/80
set i25=$i24+$isc/80

contact name=anode current

method newton maxtraps=10 itlimit=100

log outfile=ingaas.log
struct outfile=ingaas.str

solve ianode=0 b1=$I
solve ianode=-$i1 b1=$I
solve ianode=-$i2 b1=$I
solve ianode=-$i3 b1=$I
solve ianode=-$i4 b1=$I
solve ianode=-$i5 b1=$I
solve ianode=-$i6 b1=$I
solve ianode=-$i7 b1=$I
solve ianode=-$i8 b1=$I
solve ianode=-$i9 b1=$I
solve ianode=-$i10 b1=$I
solve ianode=-$i11 b1=$I
solve ianode=-$i12 b1=$I
solve ianode=-$i13 b1=$I
solve ianode=-$i14 b1=$I
solve ianode=-$i15 b1=$I
solve ianode=-$i16 b1=$I
solve ianode=-$i17 b1=$I
solve ianode=-$i18 b1=$I
solve ianode=-$i19 b1=$I
solve ianode=-$i20 b1=$I
solve ianode=-$i21 b1=$I
solve ianode=-$i22 b1=$I
solve ianode=-$i23 b1=$I
solve ianode=-$i24 b1=$I
solve ianode=-$i25 b1=$I

log off

tonyplot ingaas.log -set onecon.set
tonyplot ingaas.str
```

2. Frequency Response

```
go atlas

#############################################
## Parameters
##
## Cell Width (um)
set cellwidth=500
##
## Cap/Contact (%)
set contactpercent=8
##
## Standard # of Divisions
set divs=20
##
## Contact
set contactthickness=.1
##
##
##Molar Concentration of In(1-x)Ga(x)As(x)
set x=.28
set perm=15.1-2.87*$x+.67*$x^2
set affin=4.9-.83*$x
set n=3.51-.21*$x

## Cap  (there is no cap in this model)
set capthickness=.1
set capdoping=3e18
##
## Cathode(N-type)
set cathodethickness=17.000000
set cathodedoping=1e20
##
## Anode(P-type)  (.2-.5um)
set anodethickness=2.22
set anodedoping=1+20
##
## Back Surface Field (BSF)
set bsfthickness=.1
set bsfdoping=1e20
##
#############################################

set cellwdiv=$cellwidth/$divs
set 3D=100e6 /$cellwidth
set capwidth=.01*$contactpercent*$cellwidth
set capwdiv=$capwidth/$divs

set bsfL=0
set bsfH=$bsfL-$bsfthickness
set bsfdivs=$bsfthickness/$divs

set catL=$bsfH
set catH=$catL-$cathodethickness
set catdivs=$cathodethickness/$divs
set anoL=$catH
set anoH=$anoL-$anodethickness
set anodivs=$anodethickness/$divs

set capL=$anoH
set capH=$capL-$capthickness
set capdivs=$capthickness/$divs

set contL=$capH
set contH=$contL-$contactthickness
set contdivs=$contactthickness/$divs
set contcenter=$cellwidth/2
set contRR=$contcenter+$capwidth/2
set contLL=$contcenter-$capwidth/2

#Sets light source 200um above surface (try different heights)
set lightY=$contH-200


mesh width=$3D
#X-Mesh
x.mesh loc=0 spac=$cellwdiv
x.mesh loc=$contLL spac=$capwdiv
x.mesh loc=$contRR spac=$capwdiv
x.mesh loc=$cellwidth spac=$cellwdiv


#Y–Mesh
y.mesh loc=$contH spac=$contdivs
y.mesh loc=$capH spac=$capdivs
y.mesh loc=$catH spac=$catdivs
y.mesh loc=$anoH spac=$anodivs
y.mesh loc=$bsfH spac=$bsfdivs
y.mesh loc=$bsfL spac=$bsfdivs


#Regions
##Contacts
region num=1 material=Gold x.min=$contLL x.max=$contRR y.min=$contH
y.max=$contL
##Cap
region num=2 material=InGaAs x.min=$contLL x.max=$contRR y.min=$capH
y.max=$capL
##Vacuums
region num=3 material=Vacuum x.min=0 x.max=$contLL y.min=$contH
y.max=$capL
region num=4 material=vacuum x.min=$contRR x.max=$cellwidth
y.min=$contH y.max=$capL
#Anode
region num=5 material=InGaAs x.min=0 x.max=$cellwidth y.min=$anoH
y.max=$anoL
#Cathode
region num=6 material=InGaAs x.min=0 x.max=$cellwidth y.min=$catH
y.max=$catL
#BSF
region num=7 material=InGaAs x.min=0 x.max=$cellwidth y.min=$bsfH
y.max=$bsfL
```

```
##Electrodes
electrode name=anode material=Gold x.min=$contLL x.max=$contRR
y.min=$contH y.max=$contL
electrode name=cathode material=Gold x.min=0 x.max=$cellwidth
y.min=$bsfL y.max=$bsfL

#Doping  (In this model there are no specified doping levels, try sev-
eral)
# Cap
doping uniform region=2 p.type conc=$capdoping
# Anode
doping uniform region=5 p.type conc=$anodedoping
# Cathode
doping uniform region=6 n.type conc=$cathodedoping
# BSF
doping uniform region=7 n.type conc=$bsfdoping

#Material properties
# Vacuum
material material=Vacuum real.index=3.4 imag.index=0
# InGaSb
material material=InGaAs COPT=7e-10
material material=InGaAs EG300=.55 PERMITTIVITY=$perm AFFINITY=$affin
material material=InGaAs NC300=1.15e17 NV300=8.12e18
material material=InGaAs index.file=InGaAs.opt
# Gold
material material=Gold real.index=1.2 imag.index=1.8
# Models
models OPTR print

#Light beams
beam num=1 x.origin=0 y.origin=$lightY angle=90 back.refl
power.file=1300bb.spec wavel.start=0.21 wavel.end=5 wavel.num=100

### SOLVING I-V CURVE

set I=.1

solve init
solve b1=$I

extract name="isc" max(curve(v."anode", i."cathode"))

output con.band val.band
solve init
log outfile=freq.log
solve b1=0.1 lambda=0.22
solve b1=0.1 lambda=0.3
solve b1=0.1 lambda=0.4
solve b1=0.1 lambda=0.5
solve b1=0.1 lambda=0.6
solve b1=0.1 lambda=0.7
solve b1=0.1 lambda=0.8
solve b1=0.1 lambda=.82
solve b1=0.1 lambda=.84
solve b1=0.1 lambda=.86
solve b1=0.1 lambda=.88
solve b1=0.1 lambda=0.9
solve b1=0.1 lambda=1.0
solve b1=0.1 lambda=1.1
solve b1=0.1 lambda=1.2
solve b1=0.1 lambda=1.3
solve b1=0.1 lambda=1.4
solve b1=0.1 lambda=1.5
solve b1=0.1 lambda=1.6
solve b1=0.1 lambda=1.7
solve b1=0.1 lambda=1.8
solve b1=0.1 lambda=1.9
solve b1=0.1 lambda=2.0
solve b1=0.1 lambda=2.1
solve b1=0.1 lambda=2.2
solve b1=0.1 lambda=2.3
solve b1=0.1 lambda=2.4
solve b1=0.1 lambda=2.5
solve b1=0.1 lambda=2.6
solve b1=0.1 lambda=2.7
solve b1=0.1 lambda=2.8
solve b1=0.1 lambda=2.9
solve b1=0.1 lambda=3.0
solve b1=0.1 lambda=3.1
solve b1=0.1 lambda=3.2
solve b1=0.1 lambda=3.3
solve b1=0.1 lambda=3.4
solve b1=0.1 lambda=3.5
solve b1=0.1 lambda=3.6
solve b1=0.1 lambda=3.7
solve b1=0.1 lambda=3.8
solve b1=0.1 lambda=3.9
solve b1=0.1 lambda=4.0
solve b1=0.1 lambda=4.1
solve b1=0.1 lambda=4.2
solve b1=0.1 lambda=4.3
solve b1=0.1 lambda=4.4
solve b1=0.1 lambda=4.5
solve b1=0.1 lambda=4.6
solve b1=0.1 lambda=4.7
solve b1=0.1 lambda=4.8
solve b1=0.1 lambda=4.9
solve b1=0.1 lambda=5.0
log off
```

THIS PAGE INTENTIONALLY LEFT BLANK

APPENDIX B: MATLAB CODE

This section contains the Matlab functions that were written and used for this thesis.

A. ATLASARUN.M

```
%atlasrun.m
%
%This program runs iterations of Atlas.  It uses ivmaxp.m to calculate
open %circuit voltage, short circuit current, max power, fill factor,
and efficiency.
%The function filerw.m is called to iterate the ATLAS input deck.  The
function %time.m is called to calculate the time of each iteration in
hours, minutes, and %seconds.
%
%(c) 2004 by B.P. Davenport

close all
clear all
clc

%specifies the number of iterations to perform
iterations=250;
%specifies the range of values to iterate between
old=1.8;ol=old;
final=5;

step=(final-old)/iterations;

k=0;
totalruntime=0;

for(a=ol:step:final)
    tic
    k=k+1;
    fidres=fopen('atres.txt','a')
    filerw('ingaas.in',old,a)
    delete done.log
    delete atlaslog.log

    %Here atlas is called by Matlab to run the specified input deck
    !D:\Silvaco\etc\GuiAppStarter.exe -lib-dir-name deckbuild -exe-name
Deckbld -run ingaas.in -outfile atlaslog.log

    sprintf('Executing run %u\nStandby for results',k)
    xy=-1;

    while(xy==-1)
        xy=fopen('done.log');
        pause(3)
    end

    %Here the *.log file created by ATLAS is read and open-circuit
voltage,
     %short circuit current, max power, fill factor and efficiency are
returned.
    [Voc,Isc,Pmax,FF,Eff]=ivmaxp('ingaas.log');
    data(k,:)=[a Voc Isc Pmax FF Eff];
    %The previously calculated data is written to file.
    fprintf(fidres,'%f %f %f %f %f %f\n',data(k,:));

    %After each iteration, all calculated data is printed to the screen
    %including the time it took to run the iteration.  A plot of effi-
ciency is
    %updated after each iteration.
    clc
    data
    thisruntime=toc;T1=time(toc);
    totalruntime=totalruntime+thisruntime;T2=time(totalruntime);
    averageruntime=totalruntime/k;T3=time(averageruntime);
    estimaterun-
time=averageruntime*(iterations+1);T4=time(estimateruntime);
    sprintf('This run took %s\nTotal run time so far is %s\nAverage run
time is %s\nEstimated total run time is %s',T1,T2,T3,T4)

    old=a;
    fclose('all')
    pause(3)
    plot(data(:,1),data(:,6))
    title('Efficiency')
end


figure(1)
plot(data(:,1),data(:,2))
title('Voc')

figure(2)
plot(data(:,1),data(:,3))
title('Isc')

figure(3)
plot(data(:,1),data(:,4))
title('Pmax')

figure(4)
plot(data(:,1),data(:,5))
title('FF')

figure(5)
plot(data(:,1),data(:,6))
title('Eff')
```

B. FILERW.M

```
function filerw(file,old,new)
%filerw(file,old,new)
%This program opens an infile, "file", and writes over the
%"old" anode thickness with the "new" anodethickness
%file must be in ''
%old and new are the old and new values of anodethickness
%This same function was also used to iterate other variables by replac-
ing %‘anodethickness’ with the name of the variable to be iterated.
%
%(c) 2004 B.P. Davenport

fidr=fopen(file,'r');
a=fscanf(fidr,'%c');
fclose(fidr);
fidw=fopen(file,'w');
a=strrep(a,sprintf('anodethickness=%f',old),sprintf('anodethickness=%f'
,new));
fwrite(fidw,a);
fclose(fidw);
```

C. IVMAXP.M

```
function [Voc,Isc,Pmax,FF,Eff]=ivmaxp(varargin)
%[Voc,Isc,Pmax,FF,Eff]=ivmaxp(file,type)
%Finds Voc, Isc, Pmax, FF, and Efficiency from an Atlas *.log file
%file and type must be in ''
%Type is the doping of the top layer, n or p
%
%(c) 2004 B.P. Davenport

if(nargin==1)
    file=char(varargin(1));
    type='P';
elseif(nargin==2)
    file=char(varargin(1))
    type=char(varargin(2))
else
    'Type mus be either "N", "n", "P", or "p"'
    Voc=NaN;
    Isc=NaN;
    Pmax=NaN;
    FF=NaN;
    return
end

if(type=='N'|type=='n')
    [I  V]=textread(file,'%*s  %*f  %*f  %*f  %*f  %*f  %*f  %f  %f  %*f
%*f','headerlines',20);
elseif(type=='P'|type=='p')
```

```
    [V  I]=textread(file,'%*s  %*f  %*f  %*f  %*f  %f  %*f  %*f  %*f  %*f
%f','headerlines',20);
else
    'Type mus be either "N", "n", "P", or "p"'
    Voc=NaN;
    Isc=NaN;
    Pmax=NaN;
    FF=NaN;
    return
end
P=I.*V;
[a b]=max(P);
Pmax=V(b)*I(b);
Voc=max(V);
Isc=max(I);
FF=Pmax/(Voc*Isc);
Eff=100*Pmax/(.1353);


x=1.1*Voc;
y=1.1*Isc;
plot(V,I,V(b),I(b),'rh')
xlabel('Voltage (V)')
ylabel('Current (A)')
title('I-V Curve')
axis([0 x 0 y])
```

D. BLACKBODY.M

```
function [Lx,Sx]=blackbody(spec)

%[Lx,Sx]=blackbody(spec)
%This program calculates the spectrum a 5800K blackbody which repre-
sents AM0 and
%the spectrum from any other temperature body specified by ‘T’.  The
wavelength %and radiance are returned for the desired spectrum.  The
spectrum of the %blackbody source is written to a *.spec file formatted
for ATLAS and the %results are plotted.
%
%(c) 2004 B.P. Davenport


spec=char(spec);
Tsun=5800;
T=1300;

%constants definition
h=6.6260693e-34;
c=299792458;
k=1.386505e-23;

%scaling factor to account for the distance from the sun
dilution=1/46200;
```

```
%the number of evenly spaced points to calculate
points=3000;
L=linspace(1e-18,11e-6,points)*10^6;

Ssun=(2.*pi.*c.^2.*h)./((L*10^-6).^5.*(exp(h.*c./((L*10^-6).*k.*Tsun))-
1))*1e-10*dilution;
[xsun,ysun]=max(Ssun);
S=(2.*pi.*c.^2.*h)./((L*10^-6).^5.*(exp(h.*c./((L*10^-6).*k.*T))-
1))*1e-10;
[xother,yother]=max(S);

fid=fopen('1300BB.spec','w');
fprintf(fid,'%u\n',length(S))
for(x=1:points)
    fprintf(fid,'%f %f\n',L(x),S(x));
end
fclose(fid)
plot(L,Ssun,'b',L,S,'g')
title('Optical File')
xlabel('Wavelength (um)')
ylabel('Power Density (W/cm^2/um)')


figure(2)
plot(L,Ssun,'b')
title('Sun Optical File')
xlabel('Wavelength (um)')
ylabel('Power Density (W/cm^2/um)')

psun=0;
pother=0;
for(x=1:(points-1))
    psun=psun+(L(x+1)-L(x))*Ssun(x);
    pother=pother+(L(x+1)-L(x))*S(x);
end
pother
psun
pother
ps=sprintf('Total power is:\n%f Watts/cm^2\nThe peak is:\n%f
Watts/cm^2\nAt L=%f um',pother,xother,L(yother));
ps2=sprintf('Total power is:\n%f Watts/cm^2\nThe peak is:\n%f
Watts/cm^2\nAt L=%f um',psun,xsun,L(ysun));


figure(3)
plot(L,S,'g')
title('1300 Blackbody Radiance')
xlabel('Wavelength (um)')
ylabel('Power Density (W/cm^2/um)')
text(1.5,1,ps)

figure(2)
text(2,.1,ps2)

Lx=L';
if(strcmp(spec,'BB')|strcmp(spec,'bb'))
    Sx=S';
```

```
end
if(strcmp(spec,'Sun')|strcmp(spec,'sun'))
    Sx=Ssun';
end
```

E. FREQRESP.M

```
function [L,photo]=freqresp(varargin)
%
%[L,photo]=freqresp(varargin)
%This program reads in data a specified file and returns and plots the
frequency %response from a cell.
%
%(c) 2004 B.P. Davenport

%If there is only one input, the cell is assumed to be P on N.
if(nargin==1)
    file=char(varargin(1));
    type='P';
elseif(nargin==2)
    file=char(varargin(1));
    type=char(varargin(2));
elseif(nargin==3)
    file=char(varargin(1));
    type==char(varargin(2));
else
    'Type mus be either "N", "n", "P", or "p"'
    L=NaN;
    photo=NaN;
    return
end

%This function can accept data in two different forms from ATLAS or
from a file %containing wavelength radiance pairs.
if(type=='N'|type=='n')
    [L photo]=textread(file,'%*s %*f %*f %*f %f %*f %*f %f %*f %*f
%*f','headerlines',20);
elseif(type=='P'|type=='p')
     [L photo]=textread(file,'%*s %*f %*f %*f %f %*f %*f  %*f %*f %*f
%f','headerlines',20);
elseif(type=='x'|type=='X')
    [L photo]=textread(file,'%f%f','delimiter','\t');
else
    'Type mus be either "N", "n", "P", or "p"'
    L=NaN;
    photo=NaN;
    return
end

[L2,R2]=textread('am01.txt','%f%f','headerlines',1);


[a b]=max(photo);
```

```
R2norm=R2/max(R2);
photonorm=photo/a;
plot(L,photonorm,L2,R2norm,L(b),photonorm(b),'rh')
title('Frequency Response vs. AM0')
xlabel('Wavelength(um)')
ylabel('Normalized Photogeneration')
axis([.22,3,0,1.1])
legend('Frequency Response','AM0')
L(b)
```

F. TIME.M

```
function [T]=time(s)
%This funcion takes an input time, 's',
%in seconds and returns time in the format
%of hr:min:sec
%
%(c) 2004 B.P. Davenport

hr=floor(s/3600);
min=floor(s/60-hr*60);
sec=floor(s-min*60-hr*3600);

if(hr<10)
    hr=sprintf('0%u',hr);
else
    hr=sprintf('%u',hr);
end

if(min<10)
    min=sprintf('0%u',min);
else
    min=sprintf('%u',min);
end

if(sec<10)
    sec=sprintf('0%u',sec);
else
    sec=sprintf('%u',sec);
end

T=sprintf('%s:%s:%s',hr,min,sec);
```

THIS PAGE INTENTIONALLY LEFT BLANK

LIST OF REFERENCES

1. *Solar Cells* Webpage, (http://www.solarbotics.net/starting/200202_solar_cells/ 200202_solar_cells.html), last accessed June 2004.

2. R. Pierret, *Semiconductor Device Fundamentals*, Addison Wesley, Inc., Reading, MA, 1996.

3. Sherif Michael, EC3230 Lecture Notes, Naval Postgraduate School, Winter 2004, (unpublished).

4. *National Renewable Energy Laboratory, Renewable Resource Data Center* Webpage, (http://rredc.nrel.gov/solar/spectra/am0/NewAM0.xls), last accessed June 2004.

5. M. Green, "Photovoltaics: Coming of Age", *Proc. 21st IEEE Photovoltaic Specialists Conference*, pp. 1-8, Kissimmee FL,1990.

6. *State-of-the-Art Solar Cells* Webpage (http://www.ece.umr.edu/links/power/ Energy_Course/energy/ Renewables/pv/French_site/pvart01.html), last accessed May 2004.

7. R. Nelson, *A Brief History of Thermophotovoltaic Development* Webpage, (http://www.iop.org/EJ/article/0268-1242/18/5/301/s30501.html), last accessed June 2004.

8. F. Incropera and D. DeWitt, *Fundamentals of Heat and Mass Transfer, Fifth Edition*, John Wiley & Sons, Inc., New York, 2002.

9. S. Malvadkar and E. Parsons, *Analysis of Potential Power Sources for Inspection Robots in Natural Gas Transmission Pipelines* Webpage, (http://www.netl.doe.gov/ scng/publications/t&d/parsons%20malvadkar%20report.pdf), last accessed June 2004.

10. H. Sai, H. Yugami, Y. Akiyama, Y. Kanamori, and K. Hane, "Surface microstructured selective emitters for TPV systems**",** *Proc. 28th IEEE Photovoltaic Specialists Conference*, pp. 1016-1019, Kissimmee FL, 2000.

11. W. Horne, M. Morgan, and V. Sundaram, "Integrated Bandpass Filter Contacts For Radioisotope Thermophotovoltaic Cells," *Proc. of the 31st Intersociety IEEE Energy Conversion Engineering Conference*, Volume: 2 , 11-16 Aug. 1996.

12. *Thomas Johann Seebeck* Webpage, (http://chem.ch.huji.ac.il/~eugeniik/history/ seebeck.html), last accessed June 2004.

13. *Office of Space & Defense Power Systems: History* Webpage (http://www.ne.doe.gov/space/space-history.html), last accessed June 2004.

14. S. Wojtczuk, P. Colter, G. Charache, and B. Campbell, “Production Data On 0.55 eV InGaAs Thermophotovoltaic Cells”, *Proc. 25th IEEE Photovoltaic Specialists Conference*, pp. 77-80, Washington, D.C., 1996.

15. V. Friedensen, “Protest Space: A Study of Technology Choice, Perception of Risk, and Space Exploration”, Masters Thesis, Virginia Polytechnic Institute and State University, 1999.

16. *NASA JPL Images* Webpage (http://saturn.jpl.nasa.gov/spacecraft/images/ rtgcut-out.jpg), last accessed May 2004.

17. “Nuclear Power in Space”, United States Department of Energy Office of Nuclear Energy, Science, and Technology, Washington, D.C..

18. *Atomic Insights: RTG Heat Sources* Webpage (http://www.atomicinsights.com/sep96/materials.html), last accessed June 2004.

19. *Office of Space & Defense Power Systems: General Purpose Heat Source* Webpage (http://www.ne.doe.gov/space/gphs.html), last accessed May 2004.

20. *How Stuff Works: The Stirling Engine* Webpage (http://travel.howstuffworks.com/ stirling-engine1.htm), last accessed May 2004.

21. NASA Glenn Research Center, *Thermo-Mechanical Systems Branch: Stirling Radioisotope Power for Deep Space* Webpage (http://www.grc.nasa.gov/ WWW/tmsb/stirling/doc/stirl_radisotope.html), last accessed May 2004.

22. M. Todorovi, S. Mentus, F. Kosi, and G. Kold, “Decentralized Energy Supply By the Cogeneration and Hybridization With Concentrated Solar Radiation”, Laboratory for Thermodynamics and Thermotechnics of the Division for Energy Efficiency and Renewable Energy Sources, University of Belgrade, web (http://www.rcub.bg.ac.yu/~todorom/tutorials/rad23.html), last accessed June 2004.

23. *ATLAS User’s Manual*, vols. 1-2, SILVACO International, Sunnyvale, CA, 2003.

24. A. Bett, S. Keser, G. Stollwerck, O. Sulima, and W. Wettling, “GaSb-Based (Thermo)Photovoltaic Cells With Zn Diffused Emitters”, *Proc. 25th IEEE Photovoltaic Specialists Conference*, pp. 133-136, Washington, D.C., 1996.

25. V. Andreev, V. Khvostikov, E. Paleeva, S. Sorokina, M. Shvarts, V. Vasil’ev, and A. Vlasov, “Tandem GaSb/InGaAsSb Thermophotovoltaic Cells”, *Proc. 26th IEEE Photovoltaic Specialists Conference*, pp. 935-938, Anaheim CA, 1997.

26. D. Wilt, D. Brinker, N. Fatemi, R. Hoffman, P. Jenkins, and R. Lowe, "Lattice Mismatched InGaAs Photovoltaic Devdes For Thermophotovoltaic Power Systems", *Proc. First IEEE World Conference On Photovoltaic Energy Conversion*, pp. 1738-1741, Hawaii, 1994.

27. M. Green, "The verification of Silvaco as a solar cell simulation tool and the design and optimization of a four-junction solar cell", Master Thesis, Naval Postgraduate School, 2003.

28. P. Michalopoulos, "A novel approach for the development and optimization of state-of-the-art photovoltaic devices using Silvaco", Masters Thesis, Naval Postgraduate School, 2002.

29. D. Neamen, *Semiconductor Physics and Devices: Basic Principles – 3rd Edition*, McGraw-Hill, New York, 2003.

30. W. Callister, *Materials Science and Engineering – An Introduction, 6th Edition*, John Wiley & Sons, Inc., New York, 2003.

31. V. Andreev, V. Khvostikov, E. Paleeva, S. Sorokina, and M. Shvarts, "GaAs and GaSb Based Solar Cells For Concentrator and Thermophotovoltaic Applications", *Proc. 25th IEEE Photovoltaic Specialists Conference*, pp. 143-146, Washington, D.C., 1996.

32. V. Andreev, V. Khvostikov, V. Rumyantsev, S. Sorokina, M. Shvarts, "Single-Junction GaSb and Tandem GaSb/InGaAsSb & AlGaAsSb/GaSb Thermophotovoltaic Cells", *Proc. 28th IEEE Photovoltaic Specialists Conference*, pp. 1265-1268, Anchorage, 2000.

33. F. Becker, E. Doyle, R. Mastronardi, and K. Shukla, "Development of a 500 Watt Portable Thermophotovoltaic Power Generator", *Proc. 25th IEEE Photovoltaic Specialists Conference*, pp. 1413-1416, Washington, D.C., 1996.

34. G. Charache, J. Egley, L. Danielson, D. DePoy, P. Baldasaro, and B. Campbell, "Current Satus of Low-Temperature Radiator Thermophotovoltsic Devices", *Proc. 25th IEEE Photovoltaic Specialists Conference*, pp. 137-140, Washington, D.C., 1996.

35. T. Coutts, M. Wanlass, J. Ward, and S. Johnson, "A Review of Recent Advances In Thermophotovoltaics", *Proc. 25th IEEE Photovoltaic Specialists Conference*, Washington, D.C., pp. 25-30, Washington, D.C., 1996.

36. A. Day, W. Horne, and M. Morgan, "Application of the GaSb Solar Cell In Isotope-Heated Power Systems", *Proc. 21st IEEE Photovoltaic Specialists Conference*, pp. 1320-1325, Kissimmee FL, 1990.

37. A. Et-Husseini, and J. Gray, "Numerical Modeling of Thermophotovoltaic Cells and Systems", *Proc. 26th IEEE Photovoltaic Specialists Conference*, pp. 959-962, Anaheim CA, 1997.

38. L. Fraas, J. Avery, P. Gruenbaum, and V. Sundaram, "Fundamental Characterization Studies of GaSb Solar Cells", *Proc. 22nd IEEE Photovoltaic Specialists Conference*, pp. 80-84, Las Vegas, 1991.

39. P. Iles and C. Chu, "Design and Fabrication of Thermophotovoltaic Cells", *Proc. First World Photovoltaic Energy Conversion*, pp. 1750-1753, Hawaii, 1994.

40. P. Iles, "Non-Solar Photovoltaic Cells", *Proc. 21st IEEE Photovoltaic Specialists Conference*, pp. 420-425, Kissimmee FL, 1990.

41. L. Karlina, B. Ber, M. Kulagina, A. Kovarsky, D. Brinker, and D. Scheiman, "Simultaneous Diffusion of Zn and P In InGaAs and GaSb Cells For Solar and Thermophotovoltaic Space Applications", *Proc. 28th IEEE Photovoltaic Specialists Conference*, pp. 1230-1233, Anaheim CA, 2000.

42. M. Mauk, Z. Shellengarger, J. Cox, A. Tata, T. Warden, and L. DiNetta, "Advances In Low-Bandgap InAsSbP/InAs and GaInAsSb/GaSb Thermophotovoltaics", *Proc. 28th IEEE Photovoltaic Specialists Conference*, pp. 1028-1031, Kissimmee FL, 2000.

43. Z. Shellengarger M. Mauk, and L. DiNetta, "Recent Progress In InGaAsSb/GaSb TPV Devices", *Proc. 25th IEEE Photovoltaic Specialists Conference*, pp. 81-84, Washington, D.C., 1996.

44. K. Stone, R. Drubka, S. Kusek, "A Space Solar Thermophotovoltaic Power System", *Proc. 31st IEEE Intersociety Energy Conversion Engineering Conference*,Volume: 2 , 11 Aug. 1996.

45. O. Sulima, A. Bett, P. Dutta, M. Mauk, and R. Mueller, "GaSb-, InGaAsSb-, InGaSb-, InAsSbP- and Ge- TPV Cells With Diffused Emitters", *Proc. 29th IEEE Photovoltaic Specialists Conference*, New Orleans, 2002.

46. M. Wanlass, J. Ward, K. Emery, and T. Coutts, "$Ga_xIn_{1-x}As$ Thermophotovoltaic Converters", *Proc. First IEEE World Photovoltaic Energy Conversion*, pp. 1685-1691, Hawaii, 1994.

47. D. Wilt, N. Fatemi, P. Jenkins, R. Hoffman, G. Landis, and R. Jain, "Monolithically Interconnected InGaAs TPV Module Development", *Proc. 25th IEEE Photovoltaic Specialists Conference*, pp. 43-48, Washington, D.C., 1996.

48. B. Davenport and S. Michael, "Advanced Thermophotovoltaic Cells Modeling, Optimized for Use in Radioisotope Thermoelectric Generators (RTGs) for Mars and

Deep Space Missions*”*, *Proc. 22nd AIAA International Communications Satellite Systems Conference & Exhibit*, Monterey, 2004.

THIS PAGE INTENTIONALLY LEFT BLANK

INITIAL DISTRIBUTION LIST

1. Defense Technical Information Center
   Ft. Belvoir, Virginia

2. Dudley Knox Library
   Naval Postgraduate School
   Monterey, California

3. Chairman, Code EC
   Department of Electrical and Computer Engineering
   Naval Postgraduate School
   Monterey, California

4. Dr. Sherif Michael, Code ECMI
   Department of Electrical and Computer Engineering
   Naval Postgraduate School
   Monterey, California

5. Gamani Karunasiri, Code PHKG
   Department of Physics
   Naval Postgraduate School
   Monterey, California

6. Brad Davenport
   United States Navy
   Pacific Grove, California